From: <George.Beck@exeloncorp.com>
To: <dja1@nrc.gov>, <rkm@nrc.gov>
Date: 04/05/2006 5:15:19 PM
Subject: RE: Audit Q & A (Question Numbers AMP-141, 210, 356)

Attached is third part of AMP-210. (third of three)

<<Pages from AMP-210-2.pdf>>

> -----Original Message-----
> From: Beck, George
> Sent: Wednesday, April 05, 2006 5:02 PM
> To: Donnie Ashley (E-mail); 'Roy Mathew (E-mail) ' (E-mail)
> Cc: Ouaou, Ahmed; Hufnagel Jr, John G; Warfel Sr, Donald B; Polaski, Frederick W
> Subject: FW: Audit Q & A (Question Numbers AMP-141, 210, 356)
>
> Note: As originally transmitted this email was undeliverable to the NRC; it exceeded the size limit. It is being retransmitted without the AMP-210.pdf. This file will be reconstituted and sent in smaller ".pdf"s; the first 11 pages are attached.
>
> George
>
> -----Original Message-----
> From: Beck, George
> Sent: Wednesday, April 05, 2006 4:39 PM
> To: Donnie Ashley (E-mail); 'Roy Mathew (E-mail) ' (E-mail)
> Cc: Ouaou, Ahmed; Hufnagel Jr, John G; Warfel Sr, Donald B; Polaski, Frederick W
> Subject: Audit Q & A (Question Numbers AMP-141, 210, 356)
>
> Donnie/Roy,
>
> Attached are the responses to AMP-210 and AMP-356 in an updated version of the reports from the AMP/AMR Audit database. Also included is a revised version of AMP-141. These answers have been reviewed and approved by Technical Lead, Don Warfel.
>
> Regarding AMP-210, please note:
> As pointed out in our response to NRC Question AMP-210, (8a)(1), "The 0.806" minimum average thickness verbally discussed with the Staff during the AMP audit was recorded in location 19A in 1994. Additional reviews after the audit noted that lower minimum average thickness values were recorded at the same location in 1991 (0.803") and in September 1992 (0.800"). However, the three values are within the tolerance of +/- 0.010" discussed with the Staff."
>
> Regarding AMP-141, please note:
> Our response to AMP-141 has been revised to reflect additional information developed during the ongoing preparation of RAI responses.
>
> Please let John Hufnagel or me know if you have any questions.
>
> George
>
>
>
> << File: Pages from AMP-210-2.pdf >>

> << File: Pages from AMP-210.pdf >>
>
> << File: AMP-141.pdf >>
>
> << File: AMP-356.pdf >>

****
This e-mail and any of its attachments may contain Exelon Corporation proprietary information, which is privileged, confidential, or subject to copyright belonging to the Exelon Corporation family of Companies. This e-mail is intended solely for the use of the individual or entity to which it is addressed. If you are not the intended recipient of this e-mail, you are hereby notified that any dissemination, distribution, copying, or action taken in relation to the contents of and attachments to this e-mail is strictly prohibited and may be unlawful. If you have received this e-mail in error, please notify the sender immediately and permanently delete the original and any copy of this e-mail and any printout. Thank You.
****

CC: <ahmed.ouaou@exeloncorp.com>, <john.hufnagel@exeloncorp.com>, <donald.warfel@exeloncorp.com>, <fred.polaski@exeloncorp.com>

Mail Envelope Properties (44343353.D56 : 16 : 7510)

Subject: RE: Audit Q & A (Question Numbers AMP-141, 210, 356)
Creation Date: 04/05/2006 5:14:15 PM
From: <George.Beck@exeloncorp.com>

Created By: George.Beck@exeloncorp.com

Recipients
nrc.gov
OWGWPO01.HQGWDO01
DJA1 (D. Ashley)

nrc.gov
TWGWPO01.HQGWDO01
RKM (Roy Mathew)

exeloncorp.com
fred.polaski CC
donald.warfel CC
john.hufnagel CC
ahmed.ouaou CC

Post Office	Route
OWGWPO01.HQGWDO01	nrc.gov
TWGWPO01.HQGWDO01	nrc.gov
	exeloncorp.com

Files	Size	Date & Time
MESSAGE	3191	05 April, 2006 5:14:15 PM
TEXT.htm	6929	
Pages from AMP-210-2.pdf	4635176	
Mime.822	6356158	

Options
Expiration Date: None
Priority: Standard
Reply Requested: No
Return Notification: None

Concealed Subject: No
Security: Standard

Attachment 2

OYSTER CREEK NUCLEAR LICENSING

REGULATORY CORRESPONDENCE DISTRIBUTION SHEET

OC FILE NO: 83611 CORRESPONDENCE NO: 5000-92-2093 C321-92-2008 LETTER DATE: 1-16-92

SUBJECT: Oyster Creek Drywell Corrosion - Revision to Stability Calculations

COGNIZANT LICENSING ENGR: R. ZAK ACTION ASSIGNED TO: N/A

DISTRIBUTION: TO ED&CC ON: 1-17-92 ED&CC DIST'D ON: 1/17/92

ED&CC FILING INSTRUCTIONS: GENERAL ⊗ = w/o Attachments Use 2-sided copy for Attachments

Note: Revisions to Reports filed as DCNs 081629 & 081630.

OFFICE OF THE PRESIDENT

P. Clark	Bldg E	X
J. Wilson	Bldg E	
M. A. Kunz	Bldg 12/FR	X
K. Bromery	Bldg 12/FR	X

OYSTER CREEK

J. Barton	MOB	X
S. Levin	MOB	X
R. Barrett	MOB	X
R. Brown	MOB	
N. Chrissotimos	MOB	
K. Bass	PEB	
M. Budaj	MOB	X
P. Cervenka/TSCR	PEB	
J. DeBlasio	PEB	
L. Lammers	NMB	
D. Ranft	PEB	
W. Stewart	PEB	
T. Quintenz	NMB	
T. Dempsey	PEB	
P. Scallon	MOB	
W. Garvey	MOB	
R. Baran	MOB	X
R. Booth	PEB	

INDEPENDENT REVIEW

J. Sullivan	Bldg E	X
E. Roessler	Trl 256	X

NUCLEAR ASSURANCE

P. Fiedler	Bldg E	
T. Murphy	Bldg E	
C. Mascari	Bldg E	
M. Slobodien	Bldg 3	
R. Tilton	SEB	
J. Kowalski	Bldg 12/FR	
R. Markowski	Bldg E	
S. Rice	Bldg E	
B. Alatary	Bldg E	
G. Cropper	Bldg 12/FR	
P. Thompson	SEB	
R. Sullivan	Bldg 12/FR	
G. Young	Bldg 12/FR	

CORPORATE SERVICES

R. L. Long	Bldg E	
J. Knubel	Bldg E	⊗
M. Laggart	Bldg E	⊗
G. Busch	SEB	X
R. Rogan	TMI	
E. O'Donnell	Bldg E	
C. Gomulka (3)	SEB	X
R. ZAK	Bldg E	⊗

SITE SERVICES

I. Finfrock	Bldg E	
T. Brownridge	Trl 300	

TECH FUNCTIONS

J. Devine	Bldg F	⊗
D. Slear	Bldg F	⊗
B. Behrle	Trl 250	
J. Camire	SEB	
W. Popow	Bldg F	
J. Flynn	Bldg E	⊗
J. Colitz	Bldg E	⊗
M. Yekta	Bldg F	X

ADMIN & FINANCE

D. Myers	Bldg F	
R.C. Cutler	Bldg E	

EXTERNAL DISTRIBUTION

NJBNE/K. Tosch		X
SPPT/Blake		X
INPO		
ANI/R. Oliveira		
BPU/R. Chilton		
BPU/T. Gould		
GE/J. Miller		

OTHER

M. Yacabonis	HQ	
M. Fillipone	MGO	
ED&CC	PPY	X
B. Moroney, NSCC	270	X
S. C. Tummwelli	Bldg F	⊗

WP51/DISTGEN

Nuclear

GPU Nuclear Corporation
One Upper Pond Road
Parsippany, New Jersey 07054
201-316-7000
TELEX 136-482
Writer's Direct Dial Number

January 16, 1992
5000-92-2093
C321-92-2008

U. S. Nuclear Regulatory Commission
Attn: Document Control Desk
Washington, DC 20555

Gentlemen:

Subject: Oyster Creek Nuclear Generating Station (OCNGS)
Docket No. 50-219
Facility Operating License No. DPR-16
Oyster Creek Drywell Containment

References: (1) GPU Nuclear Letter dated 12/5/90 - Oyster Creek Drywell Stress and Stability Analyses (With Sand), GE Reports Index No. 9-1 and 9-2.

(2) GPU Nuclear Letter dated 3/4/91 - Oyster Creek Drywell Stress and Stability Analyses (Without Sand), GE Reports Index No. 9-3 and 9-4.

The referenced letters provided GPU Nuclear's ASME Section VIII evaluations of the Oyster Creek Drywell for with and without sand stability analyses, GE Report Indices 9-2 and 9-4. This letter provides you with Revision 1 to these evaluations.

This revision incorporates changes resulting from an internal audit which identified an error in calculating the Z_c factor, see Figure 2-3 of Reports 9-2 and 9-4. The calculated stress assumed a cylindrical shape rather than the more appropriate spherical shape. The calculated capacities are still in compliance with all required ASME Code provisions, however, the margins beyond those capacities are reduced. The revisions to the effected pages are indicated by vertical lines in the right hand margin.

321920C8.LET

If you have any questions or comments on this submittal or the overall drywell corrosion program, please contact Mr. Michael Laggart, Manager, Corporate Nuclear Licensing at (201) 316-7968.

Very truly yours,

E J O'Connor

for J. C. DeVine
Vice President and Director
Technical Functions

JCD/RZ/plp

cc: Administrator, Region 1
Senior Resident Inspector
Oyster Creek NRC Project Manager

DRF# 00664
INDEX 9-2, REV. 0

AN ASME SECTION VIII EVALUATION OF THE OYSTER CREEK DRYWELL

PART 2
STABILITY ANALYSIS

November 1990

prepared for

GPU Nuclear Corporation
Parsippany, New Jersey

prepared by

GE Nuclear Energy
San Jose, California

AN ASME SECTION VIII EVALUATION OF THE OYSTER CREEK DRYWELL

PART 2
STABILITY ANALYSIS

Prepared by: C D Frederickson
C.D. Frederickson, Senior Engineer
Materials Monitoring &
Structural Analysis Services

Reviewed by: H S Mehta
H. S. Mehta, Principal Engineer
Materials Monitoring &
Structural Analysis Services

Approved by: S Ranganath
S. Ranganath, Manager
Materials Monitoring &
Structural Analysis Services

TABLE OF CONTENTS

	Page
1. INTRODUCTION	1-1
1.1 General	1-1
1.2 Report Outline	1-1
1.3 References	1-1
2. BUCKLING ANALYSIS METHODOLOGY	2-1
2.1 Basic Approach	2-1
2.2 Determination of Capacity Reduction Factor	2-2
2.3 Modification of Capacity Reduction Factor for Hoop Stress	2-3
2.4 Determination of Plasticity Reduction Factor	2-5
2.5 References	2-5
3. FINITE ELEMENT MODELING AND ANALYSIS	3-1
3.1 Finite Element Buckling Analysis Methodology	3-1
3.2 Finite Element Model	3-2
3.3 Drywell Materials	3-3
3.4 Boundary Conditions	3-3
3.5 Loads	3-4
3.6 Stress Results	3-7
3.7 Theoretical Elastic Buckling Stress Results	3-9
3.8 References	3-10
4. ALLOWABLE BUCKLING STRESS EVALUATION	4-1
5. SUMMARY AND CONCLUSIONS	5-1

LIST OF FIGURES

Figure No.	Title	Page No.
1-1	Drywell Configuration	1-2
2-1	Capacity Reduction Factors for Local Buckling of Stiffened and Unstiffened Spherical Shells	2-8
2-2	Experimental Data Showing Increase in Compressive Buckling Stress Due to Internal Pressure (Reference 2-6)	2-9
2-3	Design Curve to Account for Increase in Compressive Buckling Stress Due to Internal Pressure (Reference 2-11)	2-10
2-4	Plasticity Reduction Factors for Inelastic Buckling	2-11
3-1	Oyster Creek Drywell Geometry	3-21
3-2	Oyster Creek Drywell 3-D Finite Element Model	3-22
3-3	Closeup of Lower Drywell Section of FEM (Outside View)	3-23
3-4	Closeup of Lower Drywell Section of FEM (Inside View)	3-24
3-5	Boundary Conditions of Finite Element Model	3-25
3-6	Application of Loading to Simulate Seismic Bending	3-26
3-7	Meridional Stresses - Refueling Case	3-27
3-8	Lower Drywell Meridional Stresses - Refueling Case	3-28
3-9	Circumferential Stresses - Refueling Case	3-29

LIST OF FIGURES

Figure No.	Title	Page No.
3-10	Lower Drywell Circumferential Stresses - Refueling Case	3-30
3-11	Meridional Stresses - Post-Accident Case	3-31
3-12	Lower Drywell Meridional Stresses - Post-Accident Case	3-32
3-13	Circumferential Stresses - Post-Accident Case	3-33
3-14	Lower Drywell Circumferential Stresses - Post-Accident Case	3-34
3-15	Symmetric and Anti-Symmetric Buckling Modes	3-35
3-16	Symmetric Buckling Mode Shape - Refueling Case	3-36
3-17	Anti-Symmetric Buckling Mode Shape - Refueling Case	3-37
3-18	Buckling Mode Shape - Post-Accident Case	3-38

1. INTRODUCTION

1.1 General

To address local wall thinning of the Oyster Creek drywell, GPUN has planned to prepare a supplementary report to the Code stress report of record [1-1]. For convenience, the supplementary report is divided into two parts. Part 1 of the supplementary report [1-2] includes all of the Code stress analysis results other than the buckling capability for the drywell shell. This report addresses the buckling capability of the drywell shell shown in Figure 1-1 and constitutes the second part of the supplementary report. Buckling of the entire drywell shell is considered in this analysis with the sandbed region being the area of primary concern.

1.2 Report Outline

Section 2 of this report outlines the methodology used in the buckling capability evaluation. Finite element modeling, analysis and results are described in section 3. Evaluation of the allowable compressive buckling stresses and comparisons with the calculated compressive stresses for the limiting load combinations are covered in section 4. Section 5 presents the summary of results and conclusions.

1.3 References

1-1 "Structural Design of the Pressure Suppression Containment Vessels," by Chicago Bridge & Iron Co.,Contract # 9-0971, 1965.

1-2 "An ASME Section VIII Evaluation of the Oyster Creek Drywell," GE Report No. 9-1, DRF# 00664, November 1990, prepared for GPUN.

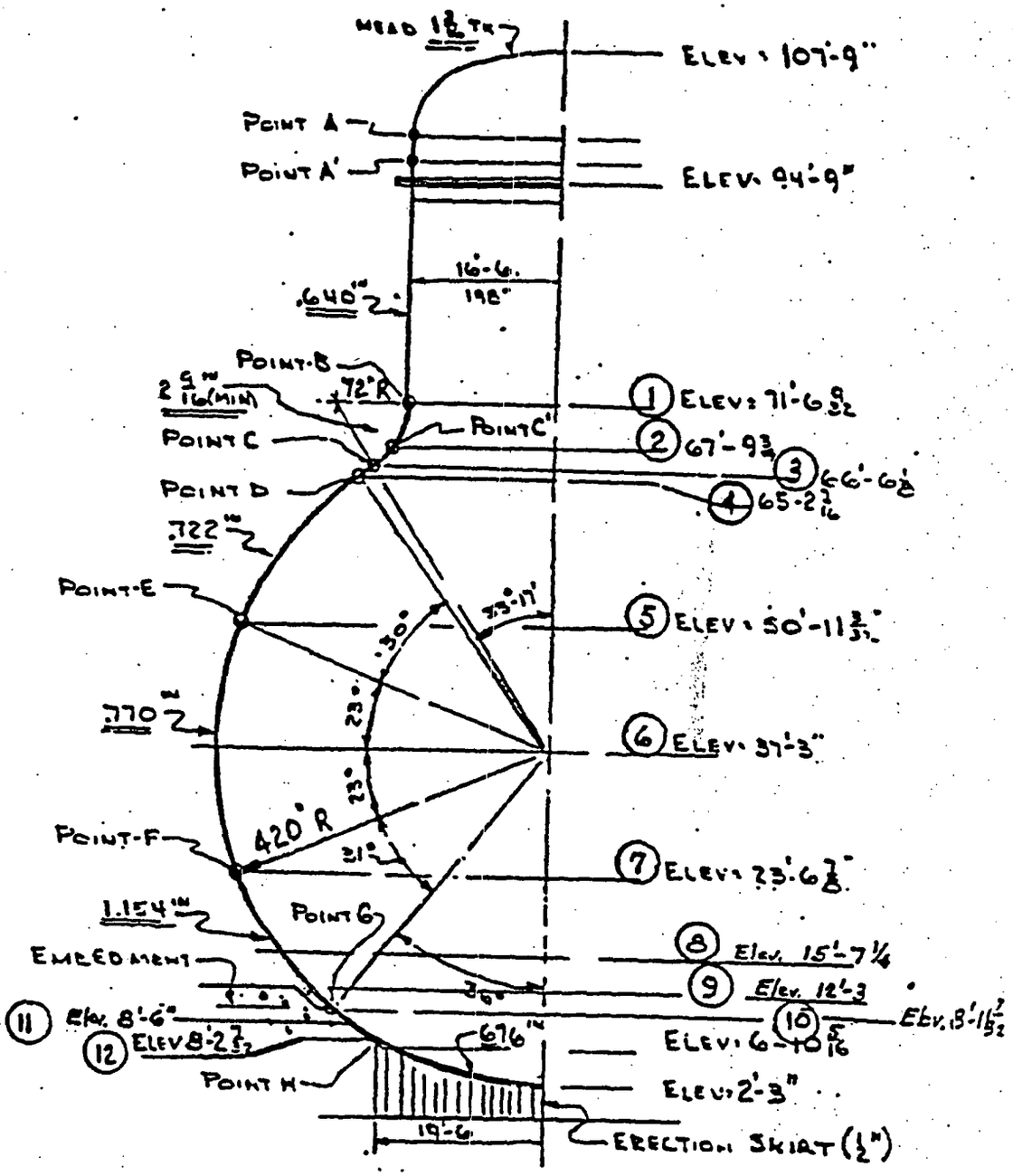

Figure 1-1. Drywell Configuration

2. BUCKLING ANALYSIS METHODOLOGY

2.1 Basic Approach

The basic approach used in the buckling evaluation follows the methodology outlined in the ASME Code Case N-284 [References 2-1, 2-2]. Following the procedure of this Code Case, the allowable compressive stress is evaluated in three steps.

In the first step, a theoretical elastic buckling stress, σ_{ie}, is determined. This value may be calculated either by classical buckling equations or by finite element analysis. Since the drywell shell geometry is complex, a three dimensional finite element analysis approach is followed using the eigenvalue extraction technique. More details on the eigenvalue determination are given in Section 3.

In the second step, the theoretical elastic buckling stress is modified by the appropriate capacity and plasticity reduction factors. The capacity reduction factor, α_i, accounts for the difference between classical buckling theory and actual tested buckling stresses for fabricated shells. This difference is due to imperfections inherent in fabricated shells, not accounted for in classical buckling theory, which can cause significant reductions in the critical buckling stress. Thus, the elastic buckling stress for fabricated shells is given by the product of the theoretical elastic buckling stress and the capacity reduction factor, i.e., $\sigma_{ie}\alpha_i$. When the elastic buckling stress exceeds the proportional limit of the material, a plasticity reduction factor, η_i, is used to account for non-linear material behavior. The inelastic buckling stress for fabricated shells is given by $\eta_i\alpha_i\sigma_{ie}$.

In the final step, the allowable compressive stress is obtained by dividing the buckling stress calculated in the second step by the safety factor, FS:

$$\text{Allowable Compressive Stress} = \eta_i\alpha_i\sigma_{ie}/FS$$

In Reference 2-1, the safety factor for the Design and Level A & B service conditions is specified as 2.0. A safety factor of 1.67 is specified for Level C service conditions (such as the post-accident flooded condition).

The Determination of appropriate values for capacity and plasticity reduction factors is discussed next.

2.2 Determination of Capacity Reduction Factor

The capacity reduction factor, α_i, is used to account for reductions in actual buckling strength due to the existence of geometric imperfections. The capacity reduction factors given in Reference 2-1 are based on extensive data compiled by Miller [2-3]. The factors appropriate for a spherical shell geometry such as that of the drywell in the sandbed region, are shown in Figure 2-1 (Figure 1512-1 of Reference 2-1). The tail (flat) end of the curves are used for unstiffened shells. The curve marked 'Uniaxial compression' is applicable since the stress state in the sandbed region is compressive in the meridional direction but tensile in the circumferential direction. From this curve, α_i is determined to be 0.207.

The preceding value of the capacity reduction factor is very conservative for two reasons. First, it is based on the assumption that the spherical shell has a uniform thickness equal to the reduced thickness. However, the drywell shell has a greater thickness above the sandbed region which would reinforce the sandbed region. Second, it is assumed that the circumferential stress is zero. The tensile circumferential stress has the effect of rounding the shell and reducing the effect of imperfections introduced during the fabrication and construction phase. A modification of the α_i value to account for the presence of tensile circumferential stress is discussed in Subsection 2.3.

The capacity reduction factor values given in Reference 2-1 are applicable to shells which meet the tolerance requirements of NE-4220

of Section III [2-4]. Appendix A of Reference 2-5 compares the tolerance requirements of NE-4220 to the requirements to which the Oyster Creek drywell shell was fabricated. The comparison shows that the Oyster Creek drywell shell was erected to the tolerance requirements of NE-4220. Therefore, although the Oyster Creek drywell is not a Section III, NE vessel, it is justified to use the approach outlined in Code Case N-284.

2.3 Modification of Capacity Reduction Factor for Hoop Stress

The orthogonal tensile stress has the effect of rounding fabricated shells and reducing the effect of imperfections on the buckling strength. The Code Case N-284 [2-1 and 2-2] notes in the last paragraph of Article 1500 that, "The influence of internal pressure on a shell structure may reduce the initial imperfections and therefore higher values of capacity reduction factors may be acceptable. Justification for higher values of α_i must be given in the Design report."

The effect of hoop tensile stress on the buckling strength of cylinders has been extensivelly documented [2-6 through 2-11]. Since the methods used in accounting for the effect of tensile hoop stress for the cylinders and spheres are similar, the test data and the methods for the cylinders are first reviewed. Harris, et al [2-6] presented a comprehensive set of test data, including those from References 2-7 and 2-8, which clearly showed that internal pressure in the form of hoop tension, increases the axial buckling stress of cylinders. Figure 2-2 shows a plot of the test data showing the increase in buckling stress as a function of nondimensional pressure. This increase in buckling capacity is accounted for by defining a separate reduction factor, α_p. The capacity reduction factor α_i can then be modified as follows:

$$\alpha_{i,mod} = \alpha_i + \alpha_p \quad .$$

The buckling stress in uniaxial compression for a cylinder or a sphere of uniform thickness with no internal pressure is given by the following:

$$S_c = (0.605)(\alpha_i)Et/R$$
$$= (0.605)(0.207)\ Et/R$$

Where, 0.605 is a constant, 0.207 is the capacity reduction factor, α_i, and E,t and R are Young's Modulus, wall thickness and radius, respectively. In the presence of a tensile stress such as that produced by an internal pressure, the buckling stress is given as follows:

$$S_{c,mod} = (0.605)(\alpha_i + \alpha_p)Et/R$$
$$= (0.605)(0.207 + \alpha_p)Et/R$$
$$= [(0.605)(0.207) + \Delta C]\ Et/R$$

Where ΔC is $\alpha_p/0.605$ and is given for cylindrical geometries in the graphical form in Figure 2-3. As can be seen in Figure 2-3, ΔC is a function of the parameter $X=(p/4E)(2R/t)^2$, where ,p, is the internal pressure. Miller [2-12] gives the following equation that fits the graphical relationship between X and ΔC shown in Figure 2-3:

$$\Delta C = \alpha_p/0.605 = 1.25/(5+1/X)$$

The preceding approach pertains to cylinders. Along the similar lines, Miller [2-13] has developed an approach for spheres as described next.

The non-dimensional parameter X is essentially $(\sigma_\theta/E)(R/t)$. Since in the case of a sphere, the hoop stress is one-half of that in the cylinder, the parameter X is redefined for spheres as follows:

$$X_{(sphere)} = (p/8E)(2R/t)^2$$

When the tensile stress magnitude, S, is known, the equivalent internal pressure can be calculated using the expression:

$$p = 2tS/R$$

Based on a review of spherical shell buckling data [2-14, 2-15], Miller [2-13] proposed the following equation for ΔC:

$$\Delta C_{(sphere)} = 1.06/(3.24 + 1/X)$$

The modified capacity reduction factor, $\alpha_{i,mod}$, for the drywell geometry was obtained as follows:

$$\alpha_{i,mod} = 0.207 + \Delta C_{(sphere)}/0.605$$

2.4 Determination of Plasticity Reduction Factor

When the elastic buckling stress exceeds the proportional limit of the material, a plasticity reduction factor, η_i, is used to account for the non-linear material behavior. The inelastic buckling stress for fabricated shells is given by $\eta_i \alpha_i \sigma_{ie}$. Reference 2-2 gives the mathematical expressions shown below [Article -1611 (a)] to calculate the plasticity reduction factor for the meridional direction elastic buckling stress. Δ is equal to $\alpha_i \sigma_{ie}/\sigma_y$ and σ_y is the material yield strength. Figure 2-4 shows the relationship in graphical form.

$$\begin{aligned} \eta_i &= 1.0 && \text{if } \Delta \le 0.55 \\ &= (0.45/\Delta) + 0.18 && \text{if } 0.55 < \Delta \le 1.6 \\ &= 1.31/(1+1.15\Delta) && \text{if } 1.6 < \Delta \le 6.25 \\ &= 1/\Delta && \text{if } \Delta > 6.25 \end{aligned}$$

2.5 References

2-1 ASME Boiler and Pressure Vessel Code Case N-284, "Metal Containment Shell Buckling Design Methods, Section III, Division 1, Class MC", Approved August 25, 1980.

2-2 Letter (1985) from C.D. Miller to P. Raju; Subject: Recommended Revisions to ASME Code Case N-284.

2-3 Miller, C.D., "Commentary on the Metal Containment Shell Buckling Design Methods of the ASME Boiler and Pressure Vessel Code," December 1979.

2-4 ASME Boiler & Pressure Vessel Code, Section III, Nuclear Power Plant Components.

2-5 "Justification for Use of Section III, Subsection NE, Guidance in Evaluating the Oyster Creek Drywell," Appendix A to letter dated December 21, 1990 from H.S. Mehta of GE to S.C. Tumminelli of GPUN.

2-6 Harris, L.A., et al, "The Stability of Thin-Walled Unstiffened Circular Cylinders Under Axial Compression Including the Effects of Internal Pressure," Journal of the Aeronautical Sciences, Vol. 24, No. 8 (August 1957), pp. 587-596.

2-7 Lo, H., Crate, H., and Schwartz, E.B., "Buckling of Thin-Walled Cylinder Under Axial Compression and Internal Pressure," NACA TN 2021, January 1950.

2-8 Fung, Y.C., and Sechler, E.E., "Buckling of Thin-Walled Circular Cylinders Under Axial Compression and Internal Pressure," Journal of the Aeronautical Sciences, Vol. 24, No. 5, pp. 351-356, May 1957.

2-9 Baker, E.H., et al., "Shell Analysis Manual," NASA, CR-912 (April 1968).

2-10 Bushnell, D., "Computerized Buckling Analysis of Shells," Kluwer Academic Publishers, 1989 (Chapter 5).

2-11 Johnson, B.G., "Guide to Stability Design Criteria for Metal Structures," Third Edition (1976), John Wiley & Sons.

2-12 Miller, C.D., "Effects of Internal Pressure on Axial Compression Strength of Cylinders," CBI Technical Report No. 022891, February 1991.

2-13 Miller, C.D., "Evaluation of Stability Analysis Methods Used for the Oyster Creek Drywell," CBI Technical Report Prepared for GPU Nuclear Corporation, September 1991.

2-14 Odland, J., "Theoretical and Experimental Buckling Loads of Imperfect Spherical Shell Segments," Journal of Ship Research, Vol. 25, No.3, September 1981, pp. 201-218.

2-15 Yao, J.C., "Buckling of a Truncated Hemisphere Under Axial Tension," AIAA Journal, Vol. 1, No. 10, October 1963, pp. 2316-2319.

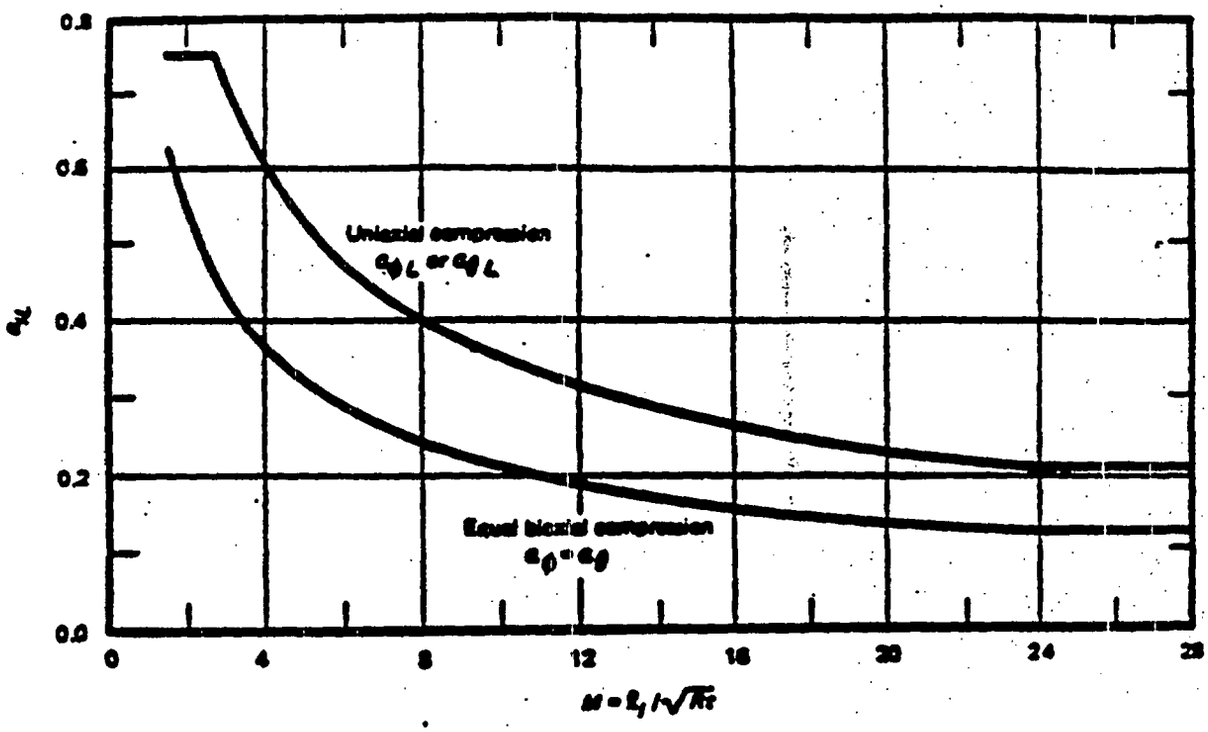

Figure 2-1 Capacity Reduction Factors for Local Buckling of Stiffened and Unstiffened Spherical Shells

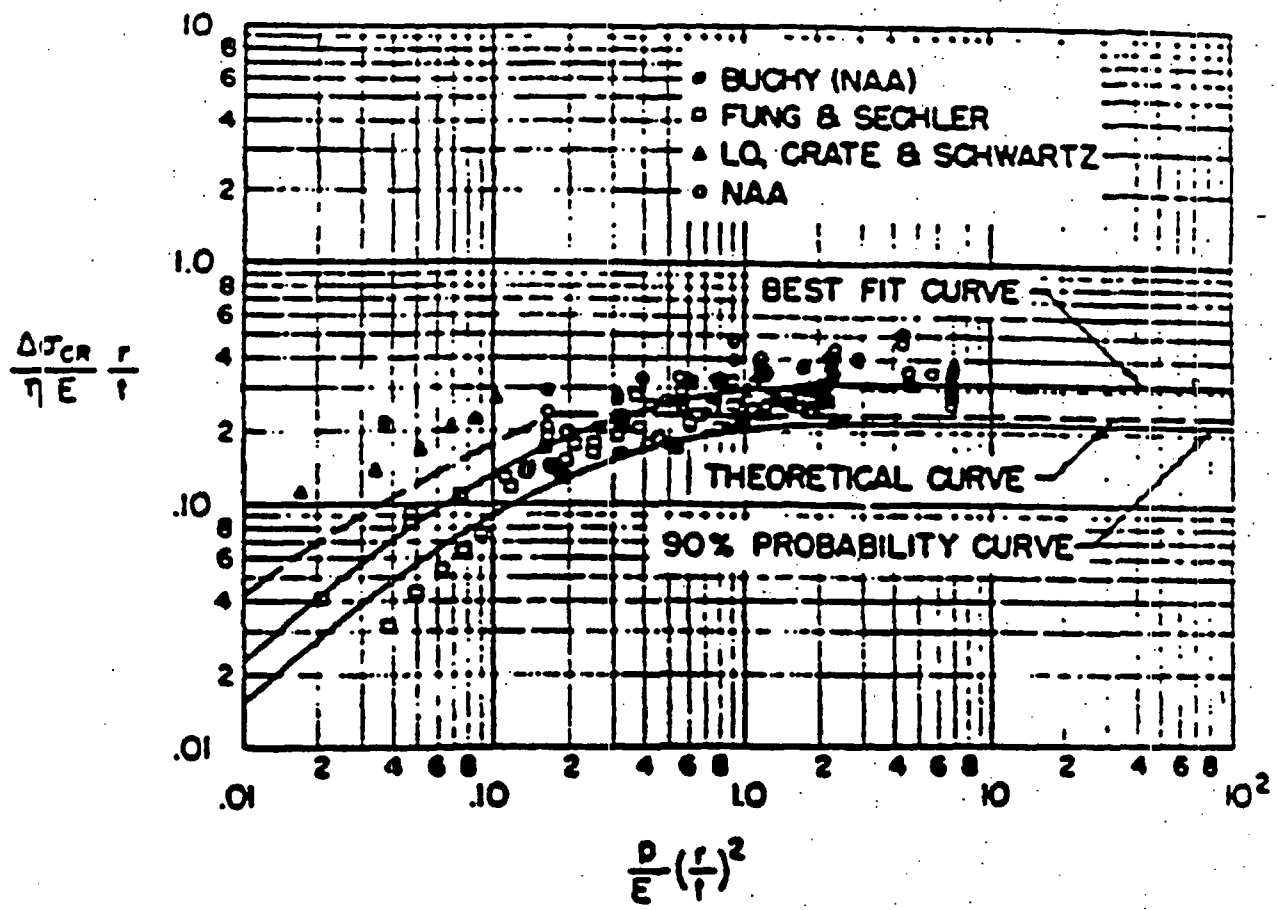

Figure 2-2 Experimental Data Showing Increase in Compressive Buckling Stress Due to Internal Pressure (Reference 2-6)

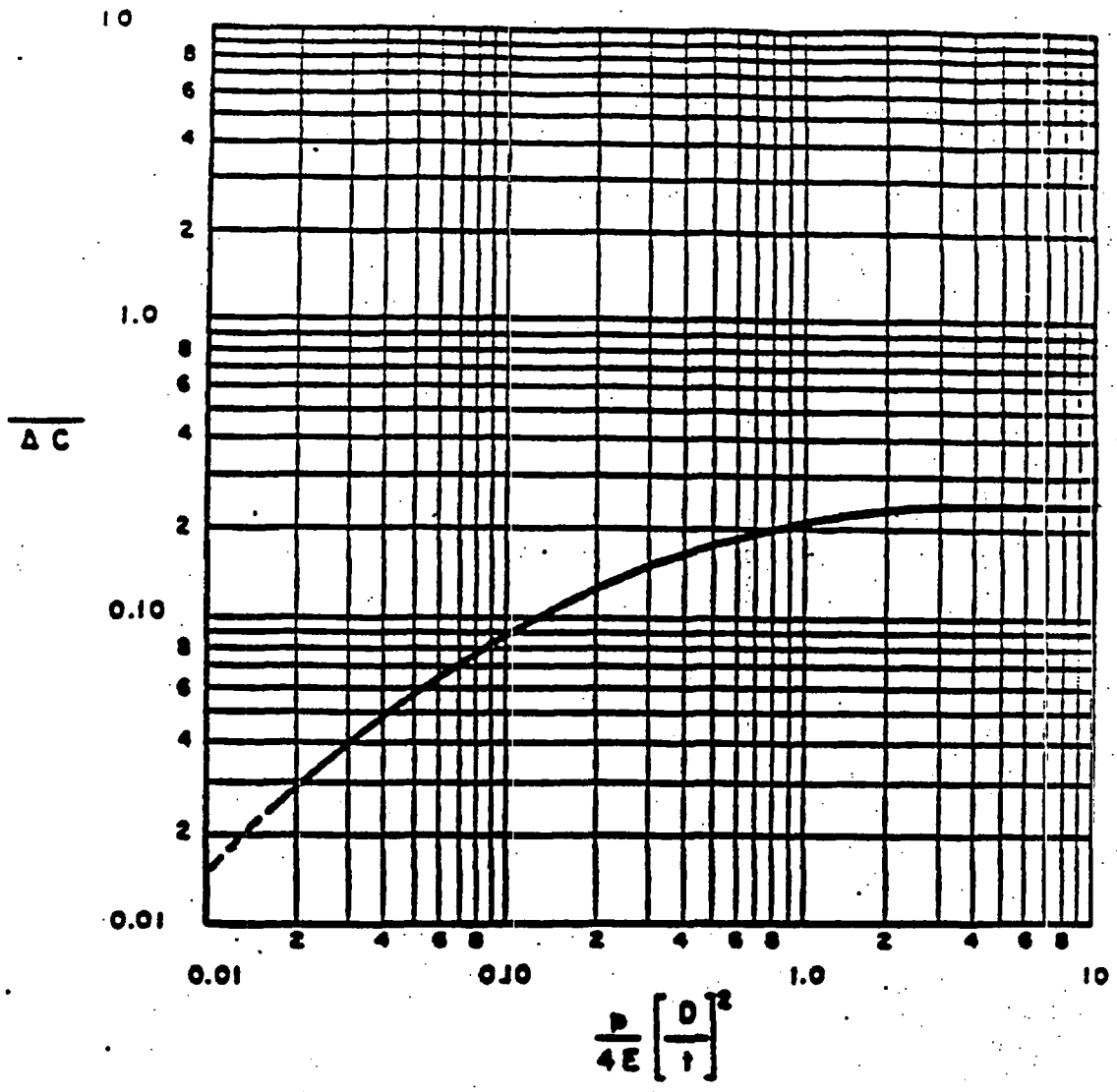

Figure 2-3 Design Curve to Account for Increase in Compressive Buckling Stress Due to Internal Pressure (Reference 2-11)

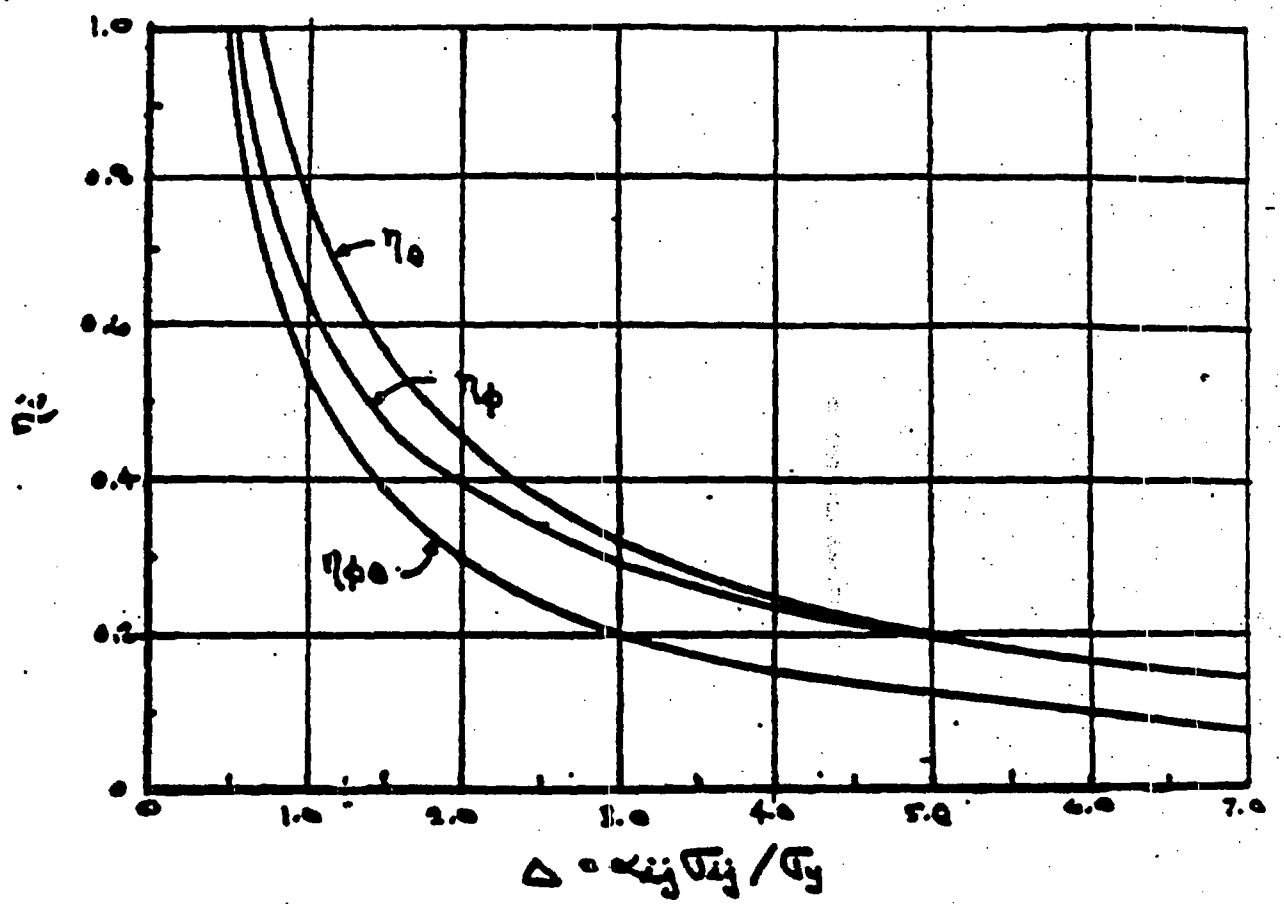

Figure 2-4 Plasticity Reduction Factors for Inelastic Buckling

3. FINITE ELEMENT MODELING AND ANALYSIS

3.1 Finite Element Buckling Analysis Methodology

This evaluation of the Oyster Creek Drywell buckling capability uses the Finite Element Analysis (FEA) program ANSYS [Reference 3-1]. The ANSYS program uses a two step eigenvalue formulation procedure to perform linear elastic buckling analysis. The first step is a static analysis of the structure with all anticipated loads applied. The structural stiffness matrix, [K], the stress stiffness matrix, [S], and the applied stresses, σ_{ap}, are developed and saved from this static analysis. A buckling pass is then run to solve for the eigenvalue or load factor, λ, for which elastic buckling is predicted using the equation:

$$([K] + \lambda [S]) \{u\} = 0$$

where: λ is the eigenvalue or load factor.
$\{u\}$ is the eigenvector representing the buckled shape of the structure.

This load factor is a multiplier for the applied stress state at which the onset of elastic buckling will theoretically occur. All applied loads (pressures, forces, gravity, etc...) are scaled equally. For example, a load factor of 4 would indicate that the structure would buckle for a load condition four times that defined in the stress pass. The critical stress, σ_{cr}, at a certain location of the structure is thus calculated as:

$$\sigma_{cr} = \lambda \sigma_{ap}$$

This theoretical elastic buckling stress is then modified by the capacity and plasticity reduction factors to determine the predicted buckling stress of the fabricated structure as discussed in Section 2. This stress is further reduced by a factor of safety to determine the allowable compressive stress.

3.2 Finite Element Model

The Oyster Creek drywell has been previously analyzed using a simplified axisymmetric model to evaluate the buckling capability in the sandbed region [Reference 3-2]. This type of analysis conservatively neglects the vents and reinforcements around the vents which significantly increase the stiffness of the shell near the sandbed region. In order to more accurately determine the buckling capability of the drywell, a three dimensional finite element model is developed.

The geometry of the Oyster Creek drywell is shown in Figure 3-1. Taking advantage of symmetry of the drywell with 10 vents, a 36° section is modeled. Figure 3-2 illustrates the finite element model of the drywell. This model includes the drywell shell from the base of the sandbed region to the top of the elliptical head and the vent and vent header. The torus is not included in this model because the bellows provide a very flexible connection which does not allow significant structural interaction between the drywell and torus.

Figure 3-3 shows a more detailed view of the lower section of the drywell model. The various colors on Figures 3-2 and 3-3 represent the different shell thicknesses of the drywell and vent. Nominal or as-designed thicknesses, summarized in Table 3-1, are used for the drywell shell for all regions other than the sandbed region. The sandbed region shown in blue in Figure 3-3 is considered to have a thickness of 0.700 inch. This is less than the 95% confidence projected thickness for outage 14R. Figure 3-4 shows the view from the inside of the drywell with the gussets and the vent jet deflector.

The drywell and vent shell is modeled using the 3-dimensional plastic quadrilateral shell (STIF43) element. Although this element has plastic capabilities, this analysis is conducted using only elastic behavior. This element type was chosen over the elastic quadrilateral shell (STIF63) element because it is better suited for modeling curved surfaces.

At a distance of 76 inches from the drywell shell, the vent is simplified using beam elements. The transition from shell to beam elements is made by extending rigid beam elements from a node along the centerline of the vent radially outward to each of the shell nodes of the vent. ANSYS STIF4 beam elements are then connected to this centerline node to model the axial and bending stiffness of the vent and header. Spring (STIF14) elements are used to model the vertical header supports inside the torus. ANSYS STIF4 beam elements are also used to model the stiffeners in the cylindrical region of the upper drywell. The section properties of these stiffeners are summarized in Table 3-2.

The sandbed region at the base of the drywell was designed to provide a smooth transition to reduce thermal and mechanical discontinuities. The sand provides lateral support to the drywell sphere in this region. The foundation stiffness for the sandbed is considered to be 366 psi/in per Reference 2.4.10 of Reference 3-2. ANSYS STIF14 spring elements are extended radially outward from each node of the shell in the sandbed region to model the sand support as shown in Figure 3-3. The stiffness for each of these sand spring elements is calculated by multiplying the foundation stiffness of the sand by the contributory area of each node in the sandbed region.

3.3 Drywell Materials

The drywell shell is fabricated from SA-212B FBX steel. The mechanical properties for this material at room temperature are shown in Table 3-3. These are the properties used in the finite element analysis. For the perforated vent jet deflector, the material properties were modified to account for the reduction in stiffness due to the perforations.

3.4 Boundary Conditions

Symmetric boundary conditions are defined for both edges of the 36° drywell model for the static stress analysis as shown on Figure 3-5. This allows the nodes at this boundary to expand radially outward from

the drywell centerline and vertically, but not in the circumferential direction. Rotations are also fixed in two directions to prevent the boundary from rotating out of the plane of symmetry. Nodes at the bottom edge of the drywell are fixed in all directions to simulate the fixity of the shell within the concrete foundation. Nodes at the ends of the sand spring elements and the header support spring elements are also fixed.

3.5 Loads

The loads are applied to the drywell finite element model in the manner which most accurately represents the actual loads anticipated on the drywell. Details on the application of loads are discussed in the following paragraphs.

3.5.1 Load Combinations

All load combinations to be considered on the drywell are summarized on Table 3-4. The most limiting load combinations in terms of possible buckling are those which cause the most compressive stresses in the sandbed region. Many of the design basis load combinations include high internal pressures which would create tensile stresses in the shell and help prevent buckling. The most severe design load combination identified for the buckling analysis of the drywell is the refueling condition (Case IV). This load combination consists of the following loads:

- Dead weight of vessel, penetrations, compressible material, equipment supports and welding pads.
- Live loads of welding pads and equipment door
- Weight of refueling water
- External Pressure of 2 psig
- Seismic inertia and deflection loads for unflooded condition

The normal operation condition with seismic is very similar to this condition, however, it will be less severe due to the absence of the refueling water and equipment door weight.

The most severe load combination for the emergency condition is for the post-accident (Case VI) load combination including:

- Dead weight of vessel, penetrations, compressible material and equipment supports
- Live load of personnel lock
- Hydrostatic Pressure of Water for Drywell Flooded to 74'-6"
- External Pressure of 2 psig
- Seismic inertia and deflection loads for flooded condition

The application of these loads is described in more detail in the following sections.

3.5.2 Gravity Loads

The gravity loads include dead weight loads of the drywell shell, weight of the compressible material and penetrations and live loads. The drywell shell loads are imposed on the model by defining the weight density of the shell material and applying a vertical acceleration of 1.0 g to simulate gravity. The ANSYS program automatically distributes the loads consistent with the mass and acceleration. The compressible material weight of 10 lb/ft^2 is added by adjusting the weight density of the shell to also include the compressible material. The adjusted weight densities for the various shell thicknesses are summarized on Table 3-5. The compressible material is assumed to cover the entire drywell shell (not including the vent) up to the elevation of the flange.

The additional dead weights, penetration weights and live loads are applied as additional nodal masses to the model. As shown on Table 3-6 for the refueling case, the total additional mass is summed for each 5 foot elevation of the drywell. The total is then divided by 10 for the 36° section assuming that the mass is evenly distributed around the perimeter of the drywell. The resulting mass is then applied uniformly to a set of nodes at the desired elevation as shown on Table 3-6. These applied masses automatically impose gravity loads on the drywell model with the defined acceleration of 1g. The same

method is used to apply the additional masses to the model for the post-accident, flooded case as summarized in Table 3-7.

3.5.3 Pressure Loads

The 2 psi external pressure load for the refueling case is applied to the external faces of all of the drywell and vent shell elements. The compressive axial stress at the transition from vent shell to beam elements is simulated by applying equivalent axial forces to the nodes of the shell elements.

Considering the post-accident, flooded case, the drywell is assumed to be flooded to elevation 74'-6" (894 inches). Using a water density of 62.3 lb/ft^3 (0.0361 lb/in^3), the pressure gradient versus elevation is calculated as shown in Table 3-8. The hydrostatic pressure at the bottom of the sandbed region is calculated to be 28.3 psi. According to the elevation of the element centerline, the appropriate pressures are applied to the inside surface of the shell elements.

3.5.4 Seismic Loads

Seismic stresses have been calculated for the Oyster Creek Drywell in Part 1 of this report, Reference 3-3. Meridional stresses are imposed on the drywell during a seismic event due to a 0.058" deflection of the reactor building and due to horizontal and vertical inertial loads on the drywell.

The meridional stresses due to a seismic event are imposed on the 3-D drywell model by applying downward forces at four elevations of the model (A: 23'-7",B: 37'-3",C: 50'-11" and D: 88'-9") as shown on Figure 3-6. Using this method, the meridional stresses calculated in Reference 3-3 are duplicated at four sections of the drywell including 1) the mid-elevation of the sandbed region, 2) 17.25° below the equator, 3) 5.75° above the equator and 4) just above the knuckle region. These four sections were chosen to most accurately represent the load distribution in the lower drywell while also providing a reasonably accurate stress distribution in the upper drywell.

To find the correct loads to match the seismic stresses, the total seismic stress (due to reactor building deflection and horizontal and vertical inertia) are obtained from Reference 3-3 at the four sections of interest. The four sections and the corresponding meridional stresses for the refueling (unflooded) and post-accident (flooded) seismic cases are summarized in Table 3-9.

Unit loads are then applied to the 3-D model in separate load steps at each elevation shown in Figure 3-6. The resulting stresses at the four sections of interest are then averaged for each of the applied unit loads. By solving four equations with four unknowns, the correct loads are determined to match the stresses shown in Table 3-9 at the four sections. The calculation for the correct loads are shown on Tables 3-10 and 3-11 for the refueling and post-accident cases, respectively.

3.6 Stress Results

The resulting stresses for the two load combinations described in section 3.5 are summarized in this section.

3.6.1 Refueling Condition Stress Results

The resulting stress distributions for the refueling condition are shown in Figures 3-7 through 3-10. The red colors represent the most tensile stresses and the blue colors, the most compressive. Figures 3-7 and 3-8 show the meridional stresses for the entire drywell and lower drywell. The circumferential stresses for the same areas are shown on Figures 3-9 and 3-10. The resulting average meridional stress at the mid-elevation of the sandbed region was found to be;

$$\sigma_{Rm} = -7097 \text{ psi}$$

The circumferential stress averaged from the bottom to the top of the sandbed region is;

$$\sigma_{Rc} = -277 \text{ psi}$$

3.6.2 Post-Accident Condition Stress Results

The application of all of the loads described for the post-accident condition results in the stress distributions shown in Figures 3-11 through 3-14. The red colors represent the most tensile stresses and the blue colors, the most compressive. Figures 3-11 and 3-12 show the meridional stresses for the entire drywell and lower drywell. The circumferential stresses for the same areas are shown on Figures 3-13 and 3-14. The resulting average meridional stress at mid-elevation of the sandbed region was found to be;

$$\sigma_{PAm} = -9693 \text{ psi}$$

The circumferential stress averaged from the bottom to the top of the sandbed region is;

$$\sigma_{PAc} = +4049 \text{ psi}$$

3.7 Theoretical Elastic Buckling Stress Results

After completion of the stress runs for the Refueling and Post-Accident load combinations, the eigenvalue buckling runs are made as described in Section 3.1. This analysis determines the theoretical elastic buckling loads and buckling mode shapes.

3.7.1 Refueling Condition Buckling Results

As shown on Figure 3-15, it is possible for the drywell to buckle in two different modes. In the case of symmetric buckling shown on Figure 3-15, each edge of the 36° drywell model experiences radial displacement with no rotation. This mode is simulated by applying symmetry boundary conditions to the 3-D model the same as used for the stress run. Using these boundary conditions for the refueling case, the critical load factor was found to be 14.32 with the critical buckling occurring in the sandbed region. The critical buckling mode shape is shown in Figure 3-16 for applied symmetry boundary conditions. The red color indicates sections of the shell which displace radially outward and the blue, those areas which displace inward.

The first four buckling modes were solved for in this eigenvalue buckling analysis with no buckling modes found outside the sandbed region for a load factor as high as 16.32. Therefore, buckling is not a concern outside of the sandbed region.

It is also possible for the drywell to buckle in the anti-symmetric manner shown in Figure 3-15. For this mode, the edges of the 3-D model are allowed to rotate but are restrained from expanding radially. This case is considered by applying anti-symmetric boundary conditions at the edges of the 3-D model. With the two pass approach used by ANSYS, it is possible to study anti-symmetric buckling of the drywell when the stresses are found based on symmetry boundary conditions. The resulting load factor found using anti-symmetric boundary conditions is 16.81. The mode shape for this case is shown on Figure 3-17.

Because the load factor is lower for symmetry boundary conditions with the same applied stress, the symmetric buckling condition is more limiting. Multiplying the load factor of 14.32 by the average meridional stress from section 3.6.1, the theoretical elastic buckling stress is found to be;

$$\sigma_{Rie} = 14.32 \times (7097 \text{ psi}) = 101{,}650 \text{ psi}$$

3.7.2 Post-Accident Condition Buckling Results

Considering the post-accident case with symmetry boundary conditions, the load factor was calculated as 9.91. Multiplying this load factor by the applied stress from section 3.6.2 results in a theoretical elastic buckling stress of

$$\sigma_{PAie} = 9.91 \times (9693 \text{ psi}) = 96{,}060 \text{ psi}$$

The critical mode shape for this condition is shown in Figure 3-18. Again, the critical buckling mode is in the sandbed region.

3.8 References

3-1 DeSalvo, G.J., Ph.D, and Gorman, R.W., "ANSYS Engineering Analysis System User's Manual, Revision 4.4," Swanson Analysis Systems, Inc., May 1, 1989.

3-2 GPUN Specification SP-1302-53-044, Technical Specification for Primary Containment Analysis - Oyster Creek Nuclear Generating Station; Rev. 2, October 1990.

3-3 "An ASME Section VIII Evaluation of the Oyster Creek Drywell - Part 1 Stress Analysis," GE Report No. 9-1, DRF # 00664, November 1990, prepared for GPUN.

Table 3-1

Oyster Creek Drywell Shell Thicknesses

Section	Thickness (in.)
Sandbed Region	0.700
Lower Sphere	1.154
Mid Sphere	0.770
Upper Sphere	0.722
Knuckle	2.5625
Cylinder	0.640
Reinforcement Below Flange	1.250
Reinforcement Above Flange	1.500
Elliptical Head	1.1875
Ventline Reinforcement	2.875
Gussets	0.875
Vent Jet Deflector	2.500
Ventline Connection	2.500
Upper Ventline	0.4375
Lower Ventline	0.250

Table 3-2

Cylinder Stiffener Locations and Section Properties

Elevation (in)	Height (in)	Width (in)	Area (in^2)	Bending Inertia (in^4) Horizontal	Vertical
966.3	0.75	6.0	4.5	13.5	0.211
1019.8	0.75	6.0	4.5	13.5	0.211
1064.5	0.50	6.0	3.0	9.0	0.063
1113.0(1)	2.75 1.00	7.0 7.38	26.6	387.5	12.75
1131.0	1.0	12.0	12.0	144.0	1.000

(1) - This stiffener is made up of a 2 beam sections, one 2.75x7" and one 1.0x7.375"

Table 3-3

Material Properties for FBX-212B Steel

Material Property	Value
Young's Modulus	29.6×10^6 psi
Yield Strength	38000 psi
Poisson's Ratio	0.3
Density	0.283 lb/in^3

Table 3-4

Oyster Creek Drywell Load Combinations

CASE I - INITIAL TEST CONDITION
Deadweight + Design Pressure (62 psi) + Seismic (2 x DBE)

CASE II - FINAL TEST CONDITION
Deadweight + Design Pressure (35 psi) + Seismic (2 x DBE)

CASE III - NORMAL OPERATING CONDITION
Deadweight + Pressure (2 psi external) + Seismic (2 x DBE)

CASE IV - REFUELING CONDITION
Deadweight + Pressure (2 psi external) + Water Load + Seismic (2 x DBE)

CASE V - ACCIDENT CONDITION
Deadweight + Pressure(62 psi @ 175°F or 35 psi @ 281°F) + Seismic (2 x DBE)

CASE VI - POST ACCIDENT CONDITION
Deadweight + Water Load @ 74'6" + Seismic (2 x DBE)

Table 3-5

Adjusted Weight Densities of Shell to Account for

Compressible Material Weight

Shell Thickness (in.)	Adjusted Weight Density (lb/in^3)
1.154	0.343
0.770	0.373
0.722	0.379
2.563	0.310
0.640	0.392
1.250	0.339

Table 3-6

Oyster Creek Drywell Additional Weights - Refueling Condition

ELEVATION (feet)	DEAD WEIGHT (lbf)	PENETR. WEIGHT (lbf)	& MISC. LOADS (lbf)	TOTAL LOAD (lbf)	5 FOOT RANGE LOAD	LOAD PER 36 DEG. (lbf)	# OF ELEMENTS	NODES OF APPLICATION	LOAD PER FULL NODE (lbf)	LOAD PER HALF NODE (lbf)
15.56	50000			50000						
16		168100		168100						
20		11200		11200						
*' 15-20					229300	22930	6	116-119	3822	1911
22#	556000			556000						
*' 21-25#					556000	55600	8	161-169	6950	3475
26		11100		11100						
30	64100	51500		115600						
30.25	105000		100000	205000						
*' 26-30					331700	33170	8	179-187	4146	2073
31		16500		16500						
32		750		750						
33		15450		15450						
34		28050		28050						
35		1500		1500						
*' 31-35					62250	6225	8	188-196	778	389
36		1550		1550						
40	41000	43350		84350						
*' 36-40					85900	8590	8	197-205	1074	537
50#	1102000			1102000						
*' 45-50#					1102000	110200	8	418-426	13775	6888
54		7850		7850						
*' 51-55					7850	785	8	436-444	93	49
56	56400		24000	80400						
60	95200	700	20000	115900						
*' 56-60					196300	19630	8	454-462	2454	1227
65	52000		20000	72000						
*' 61-65					72000	7200	8	472-480	900	450
70		5750		5750						
*' 66-70					5750	575	8	508-516	72	36
73		8850		8850						
*' 71-75					8850	885	8	526-534	111	55
82.17	21650			21650						
*' 81-85					21650	2165	8	553-561	271	135
87		1000		1000						
90		15000		15000						
*' 86-90					16000	1600	8	571-579	200	100
93.75	20700			20700						
94.75#			698000	698000						
95.75	20100			20100						
*' 91-96					738800	73880	8	589-597	9235	4618
TOTALS:	2184150	388200	862000	3434350	3434350	343435				

- LOAD TO BE APPLIED IN VERTICAL DIRECTION ONLY.
& - MISCELLANEOUS LOADS INCLUDE 698000 LB WATER WEIGHT AT 94.75 FT. ELEVATION 100000 LB EQUIPMENT DOOR WEIGHT AT 30.25 FT. ELEVATION AND WELD PAD LIVE LOADS OF 24000, 20000 AND 20000 AT 56, 60 AND 65 FT. ELEVATIONS

REFWGT.WK1

Table 3-7

Oyster Creek Drywell Additional Weights - Post-Accident Condition

ELEVATION (feet)	DEAD WEIGHT (lbf)	PENETR. WEIGHT (lbf)	& MISC. LOADS (lbf)	TOTAL LOAD (lbf)	5 FOOT RANGE LOAD	LOAD PER 36 DEG. (lbf)	# OF ELEMENTS	NODES OF APPLICATION	LOAD PER FULL NODE (lbf)	LOAD PER HALF NODE (lbf)
15.56	50000			50000						
16		168100		168100						
20		11200		11200						
** 15-20					229300	22930	6	116-119	3822	1911
22#	556000			556000						
** 21-25#					556000	55600	8	161-169	6950	3475
26		11100		11100						
30	64100	51500		115600						
30.25	105000			105000						
** 26-30					231700	23170	8	179-187	2896	1448
31		16500		16500						
32		750		750						
33		15450		15450						
34		28050		28050						
35		1500		1500						
** 31-35					62250	6225	8	188-196	778	389
36		1550		1550						
40	41000	43350		84350						
** 36-40					85900	8590	8	197-205	1074	537
50#	1102000			1102000						
** 45-50#					1102000	110200	8	418-426	13775	6888
54		7850		7850						
** 51-55					7850	785	8	436-444	98	49
56	56400			56400						
60	95200	700		95900						
** 56-60					152300	15230	8	454-462	1904	952
65	52000			52000						
** 61-65					52000	5200	8	472-480	650	325
70		5750		5750						
** 66-70					5750	575	8	508-516	72	36
73		8850		8850						
** 71-75					8850	885	8	526-534	111	55
82.17	21650			21650						
** 81-85					21650	2165	8	553-561	271	135
87		1000		1000						
90		15000		15000						
** 86-90					16000	1600	8	571-579	200	100
93.75	20700			20700						
95.75	20100			20100						
** 91-96					40800	4080	8	589-597	510	255
TOTALS:	2184150	388200	0	2572350	2572350	257235				

- LOAD TO BE APPLIED IN VERTICAL DIRECTION ONLY.
& - NO MISCELLANEOUS LOADS FOR THIS CONDITION.

FLOODWGT.WK1

Table 3-8

Hydrostatic Pressures for Post-Accident, Flooded Condition

WATER DENSITY: 62.32 lb/ft3
0.03606 lb/in3

FLOODED ELEV: 74.5 ft
894 inches

ELEMENTS ABOVE NODES	ANGLE ABOVE EQUATOR (degrees)	ELEVATION (inch)	DEPTH (inch)	PRESSURE (psi)	ELEMENTS
27	-53.32	110.2	783.8	28.3	1-12
40	-51.97	116.2	777.8	28.1	13-24
53	-50.62	122.4	771.6	27.8	25-36
66	-49.27	128.8	765.2	27.6	37-48
79	-47.50	137.3	756.7	27.3	49-51, 61-66 ,55-57
92	-46.20	143.9	750.1	27.1	52-54, 138-141 ,58-60
102	-44.35	153.4	740.6	26.7	142-147, 240-242, 257-259
108	-41.89	166.6	727.4	26.2	148-151, 243, 256
112	-39.43	180.2	713.8	25.7	152-155, 244, 255
116	-36.93	194.6	699.4	25.2	156-159, 245, 254
120	-34.40	209.7	684.3	24.7	160-165, 246, 253
124	-31.87	225.2	668.8	24.1	166-173, 247, 252
130	-29.33	241.3	652.7	23.5	174-183, 248-251
138	-26.80	257.6	636.4	23.0	184-195
148	-24.27	274.4	619.6	22.3	196-207
161	-20.13	302.5	591.5	21.3	208-215
170	-14.38	342.7	551.3	19.9	216-223
179	-8.63	384.0	510.0	18.4	224-231
188	-2.88	425.9	468.1	16.9	232-239
197	2.88	468.1	425.9	15.4	430-437
400	8.63	510.0	384.0	13.8	438-445
409	14.38	551.3	342.7	12.4	446-453
418	20.13	591.5	302.5	10.9	454-461
427	25.50	627.8	266.2	9.6	462-469
436	30.50	660.2	233.8	8.4	470-477
445	35.50	690.9	203.1	7.3	478-485
454	40.50	719.8	174.2	6.3	486-493
463	45.50	746.6	147.4	5.3	494-501
472	50.50	771.1	122.9	4.4	502-509
481	54.86	790.5	103.5	3.7	510-517
490	-	805.6	88.4	3.2	518-525
499	-	820.7	73.3	2.6	526-533
508	-	835.7	58.3	2.1	534-541
517	-	850.8	43.2	1.6	542-549
526	-	885.3	8.7	0.3	550-557
-	-	187.3	706.7	25.5	340-399 (Ventline)

FLOODP.WK1

Table 3-9

Meridional Seismic Stresses at Four Sections

Section	Elevation (inches)	2-D Shell Model Node	Meridional Stresses Refueling (psi)	Meridional Stresses Post-Accident (psi)
A) Middle of Sandbed	119	32	1258	1288
B) 17.25° Below Equator	323	302	295	585
C) 5.75° Above Equator	489	461	214	616
D) Above Knuckle	1037	1037	216	808

Table 3-10

Application of Loads to Match Seismic Stresses - Refueling Case

COMPRESSIVE STRESSES FROM 2-D ANALYSIS	2-D SEISMIC STRESSES AT SECTION (psi)			
SECTION:	1	2	3	4
2-D NODE:	32	302	461	1037
ELEV:	119.3"	322.5"	489.1"	912.3"
0.058" SEISMIC DEFLECTION:	788.67	155.54	103.46	85.31
HORIZ. PLUS VERTICAL SEISMIC INERTIA:	469.55	139.44	110.13	130.21
TOTAL SEISMIC COMPRESSIVE STRESSES:	1258.22	294.98	213.59	215.52

3-D INPUT LOAD SECTION	INPUT 3-D UNIT LOAD DESCRIPTION	3-D STRESSES AT SECTION (psi)			
	SECTION:	1	2	3	4
	3-D NODES:	53-65	170-178	400-408	526-534
	ELEV:	119.3"	322.5"	489.1"	912.3"
A	1000 lbs at nodes 563 through 569	85.43	37.94	34.94	55.23
B	500 lbs at 427&435, 1000 lbs at 428-434	89.88	39.92	36.76	0.00
C	500 lbs at 197&205, 1000 lbs at 198-204	97.64	43.37	0.00	0.00
D	500 lbs at 161&169, 1000 lbs at 162-168	89.85	0.00	0.00	0.00
	DESIRED COMPRESSIVE STRESSES (psi):	1258.22	294.98	213.59	215.52

3-D INPUT LOAD SECTION	LOAD TO BE APPLIED TO MATCH 2-D STRESSES	RESULTING STRESSES AT SECTION (psi)			
A	3902.2	333.37	148.05	136.34	215.52
B	2101.4	188.87	83.89	77.25	0.00
C	1453.6	141.93	63.04	0.00	0.00
D	6611.6	594.05	0.00	0.00	0.00
	SUM:	1258.22	294.98	213.59	215.52

SEISUNFL.WK1

Table 3-11

Application of Loads to Match Seismic Stresses - Post-Accident Case

COMPRESSIVE STRESSES FROM 2-D ANALYSIS	2-D SEISMIC STRESSES AT SECTION (psi)			
SECTION:	1	2	3	4
2-D NODE:	32	302	461	1037
ELEV:	119.3"	322.5"	489.1"	912.3"
0.058" SEISMIC DEFLECTION:	788.67	155.54	103.46	85.31
HORIZ. PLUS VERTICAL SEISMIC INERTIA:	499.79	429.39	512.76	723.14
TOTAL SEISMIC COMPRESSIVE STRESSES:	1288.46	584.93	616.22	808.45

3-D INPUT LOAD SECTION	INPUT 3-D UNIT LOAD DESCRIPTION	3-D STRESSES AT SECTION (psi)			
SECTION:		1	2	3	4
3-D NODES:		53-65	170-178	400-408	526-534
ELEV:		119.3"	322.5"	489.1"	912.3"
A	1000 lbs at nodes 563 through 569	85.43	37.94	34.94	55.23
B	500 lbs at 427&435, 1000 lbs at 428-434	89.88	39.92	36.76	0.00
C	500 lbs at 197&205, 1000 lbs at 198-204	97.64	43.37	0.00	0.00
D	500 lbs at 161&169, 1000 lbs at 162-168	89.85	0.00	0.00	0.00
	DESIRED COMPRESSIVE STRESSES (psi):	1288.46	584.93	616.22	808.45

3-D INPUT LOAD SECTION	LOAD TO BE APPLIED TO MATCH 2-D STRESSES	RESULTING STRESSES AT SECTION (psi)			
A	14637.9	1250.51	555.36	511.45	808.45
B	2850.2	256.17	113.78	104.77	0.00
C	-1941.7	-189.58	-84.21	0.00	0.00
D	-318.8	-28.64	0.00	0.00	0.00
	SUM:	1288.46	584.93	616.22	808.45

SEISFL.WK1

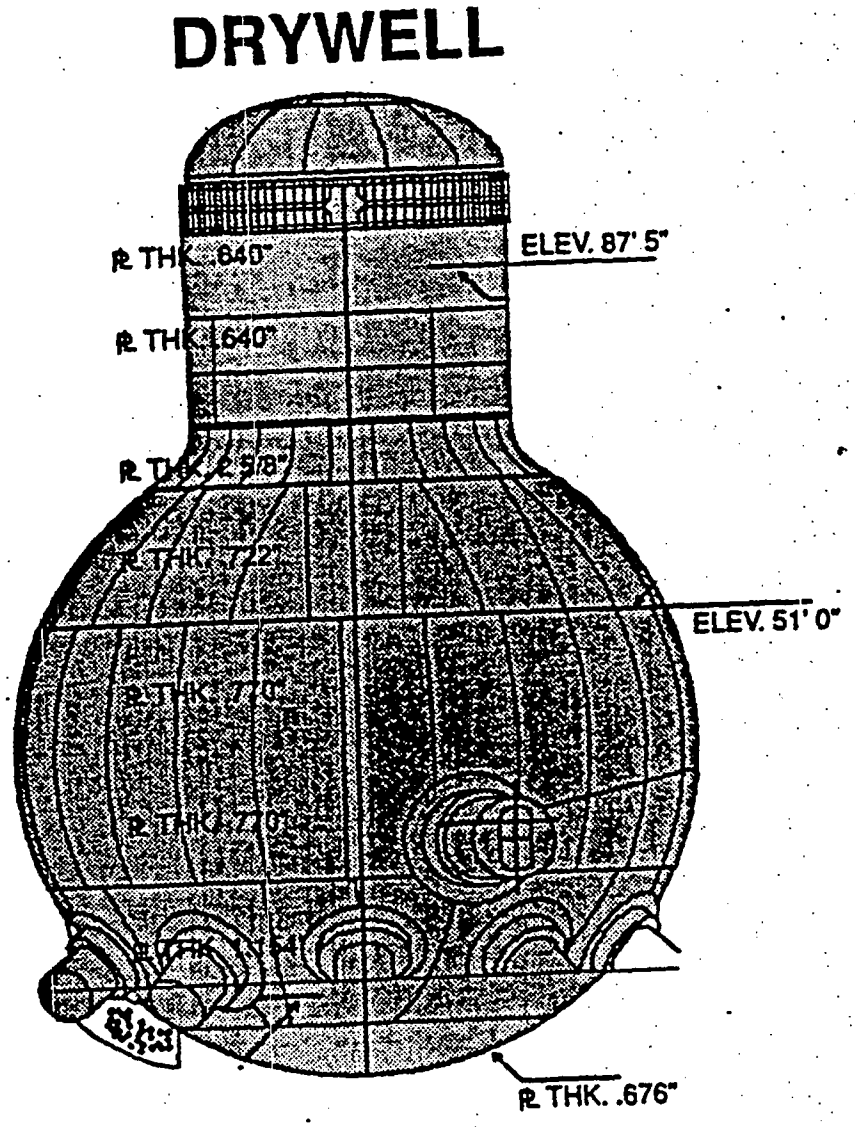

Figure 3-1. Oyster Creek Drywell Geometry

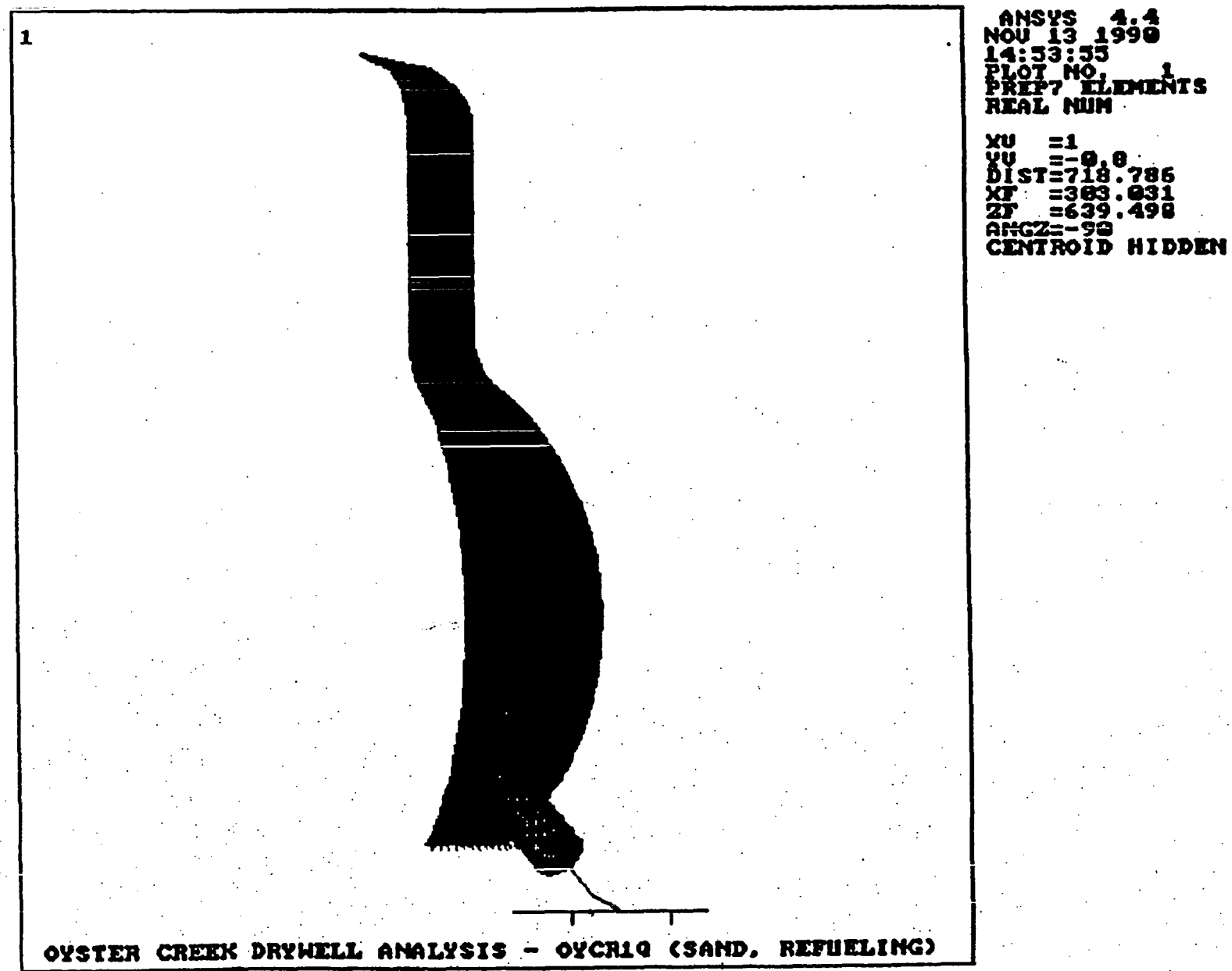

Figure 3-2 Oyster Creek Drywell 3-D Finite Element Model

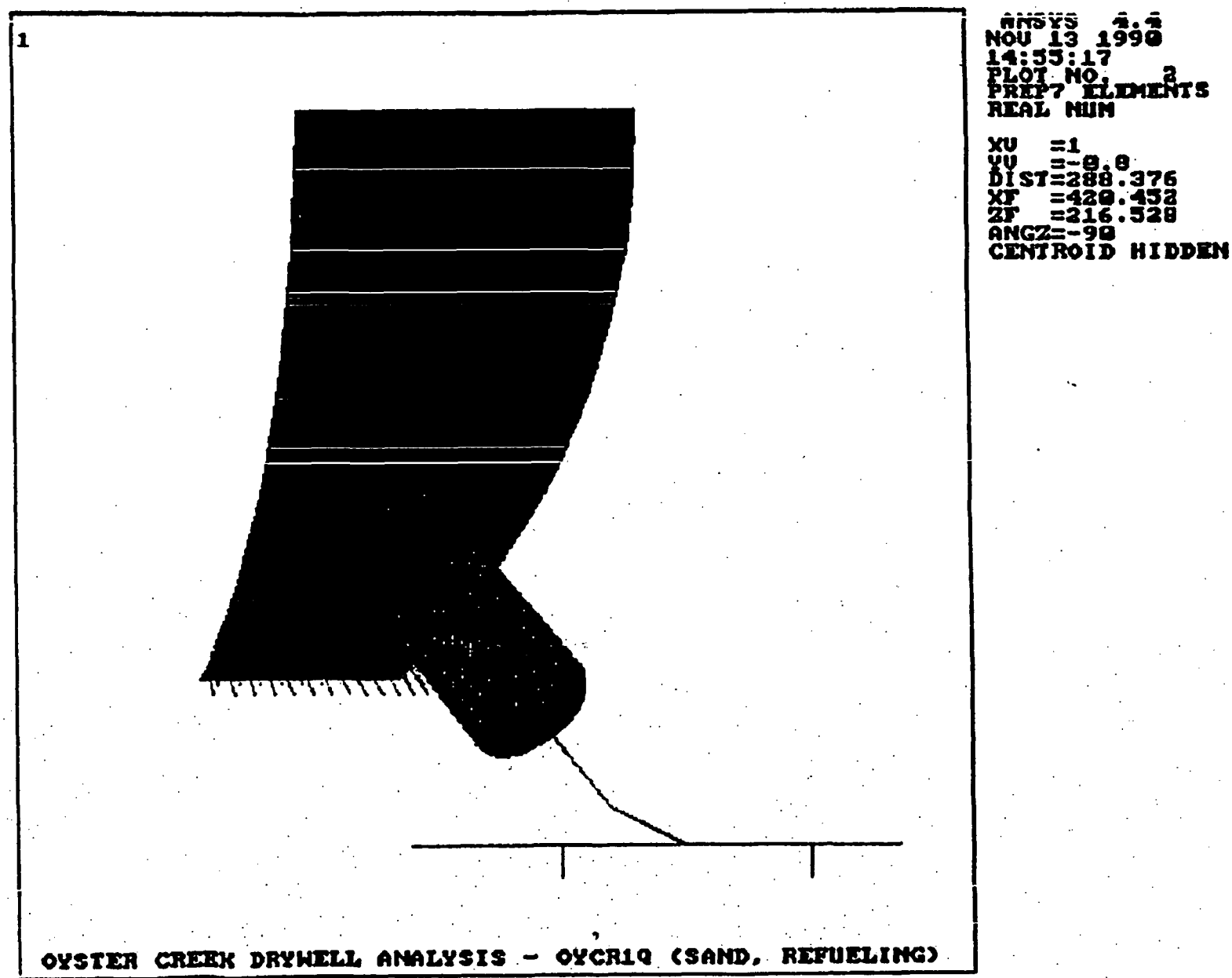

Figure 3-3. Closeup of Lower Drywell Section of FEM (Outside View)

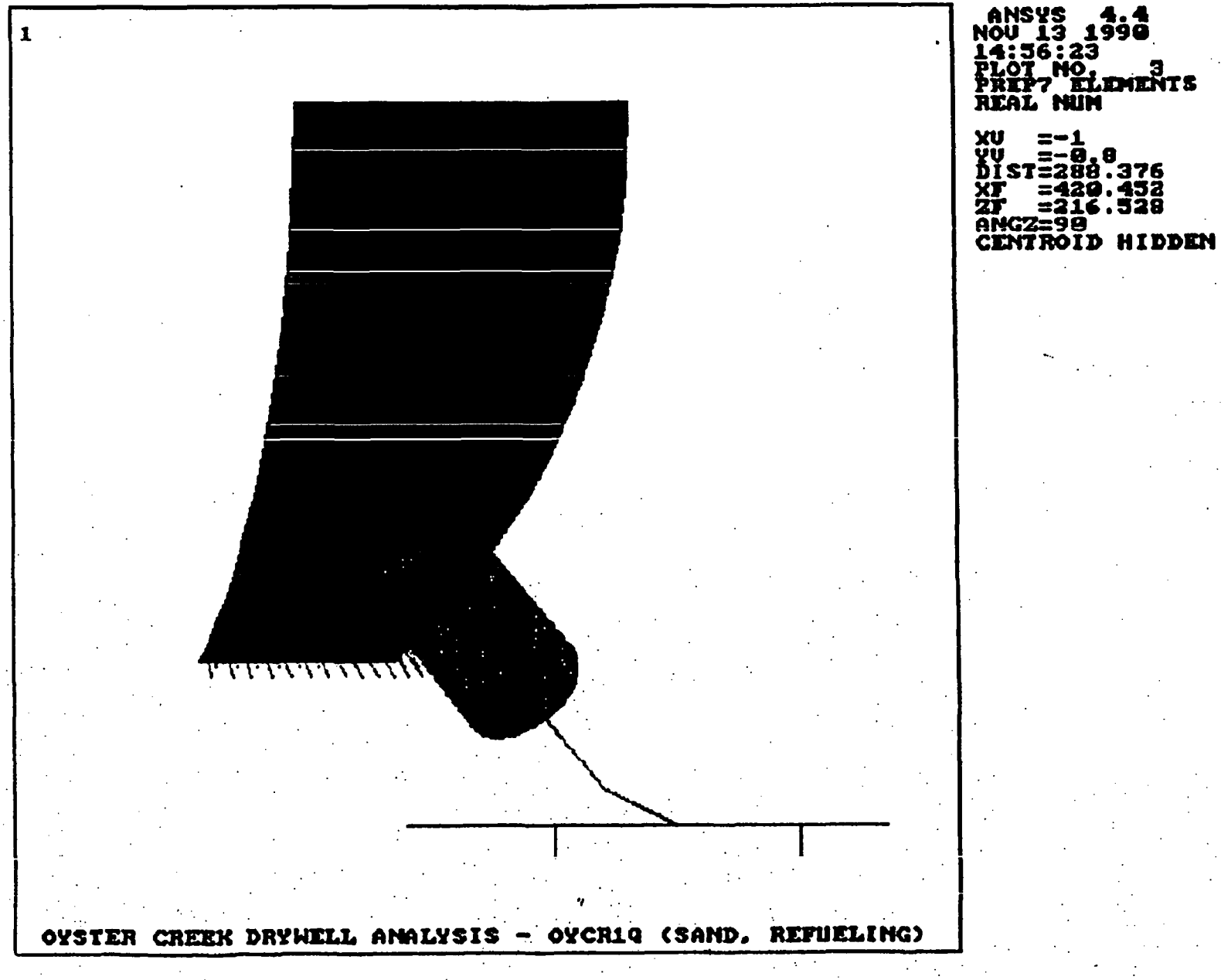

Figure 3-4 Closeup of Lower Drywell Section of FEM (Inside View)

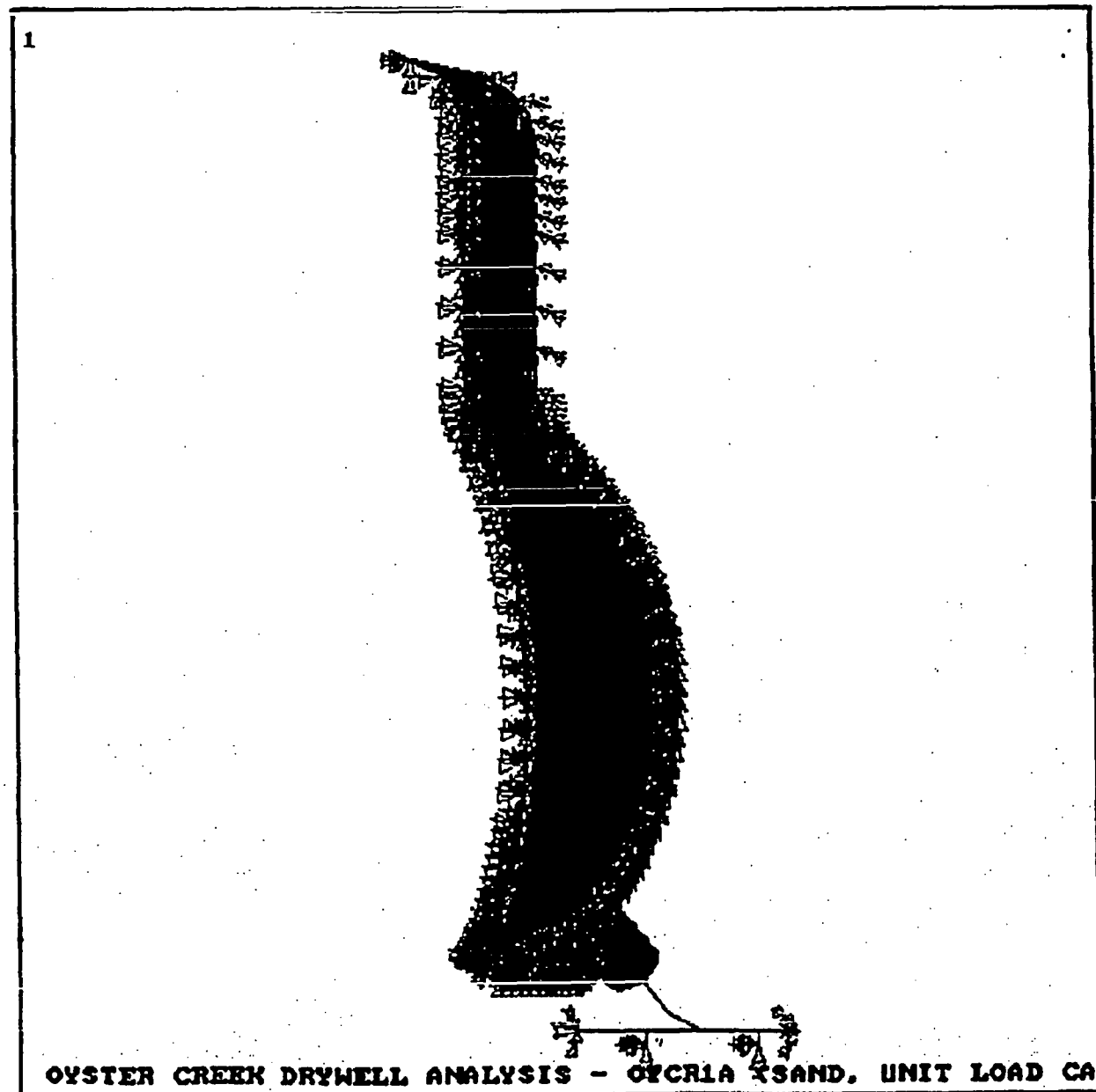

OYSTER CREEK DRYWELL ANALYSIS - OYCR1A XSAND, UNIT LOAD CASE)

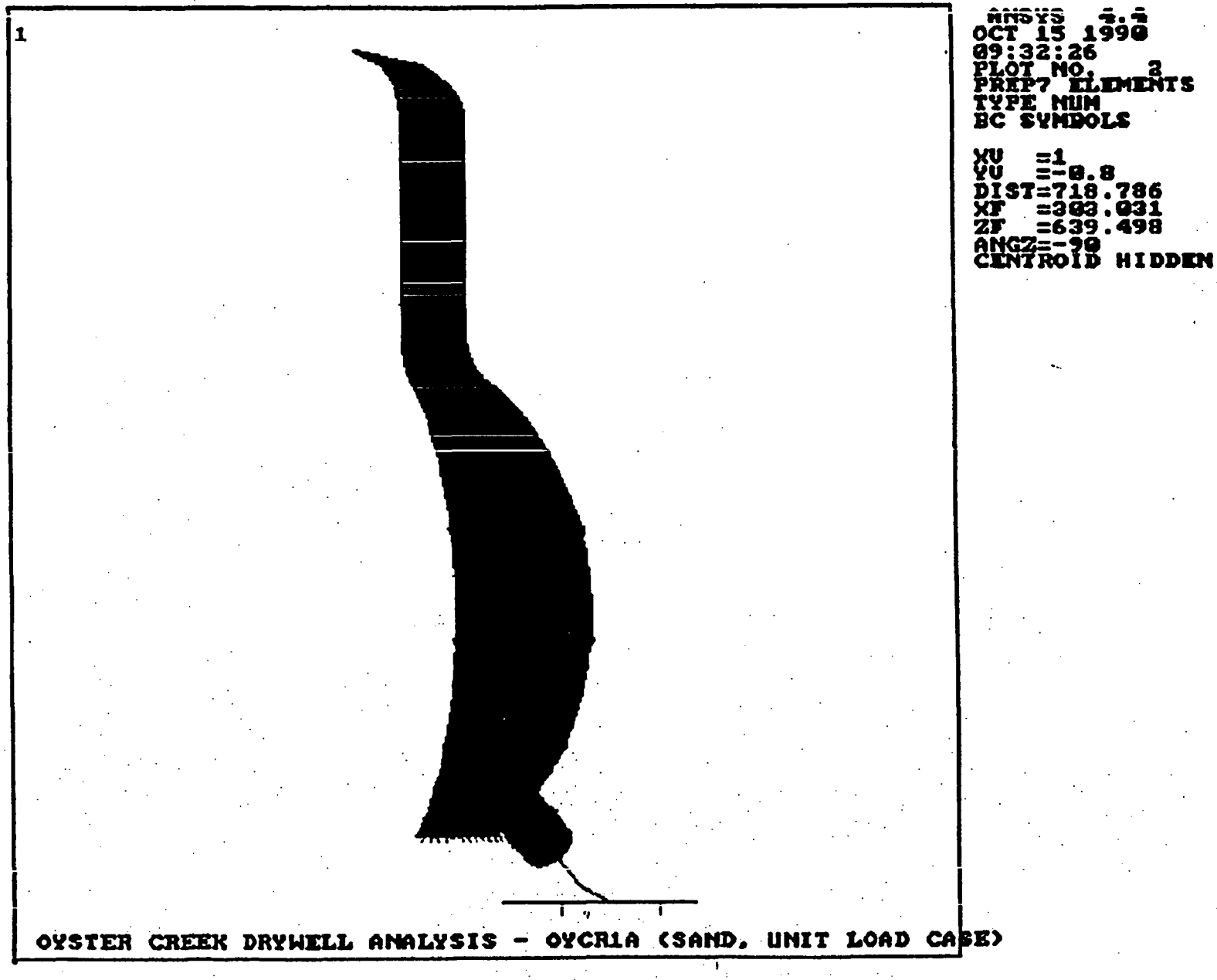

Figure 3-6 Application of Loading to Simulate Seismic Bending

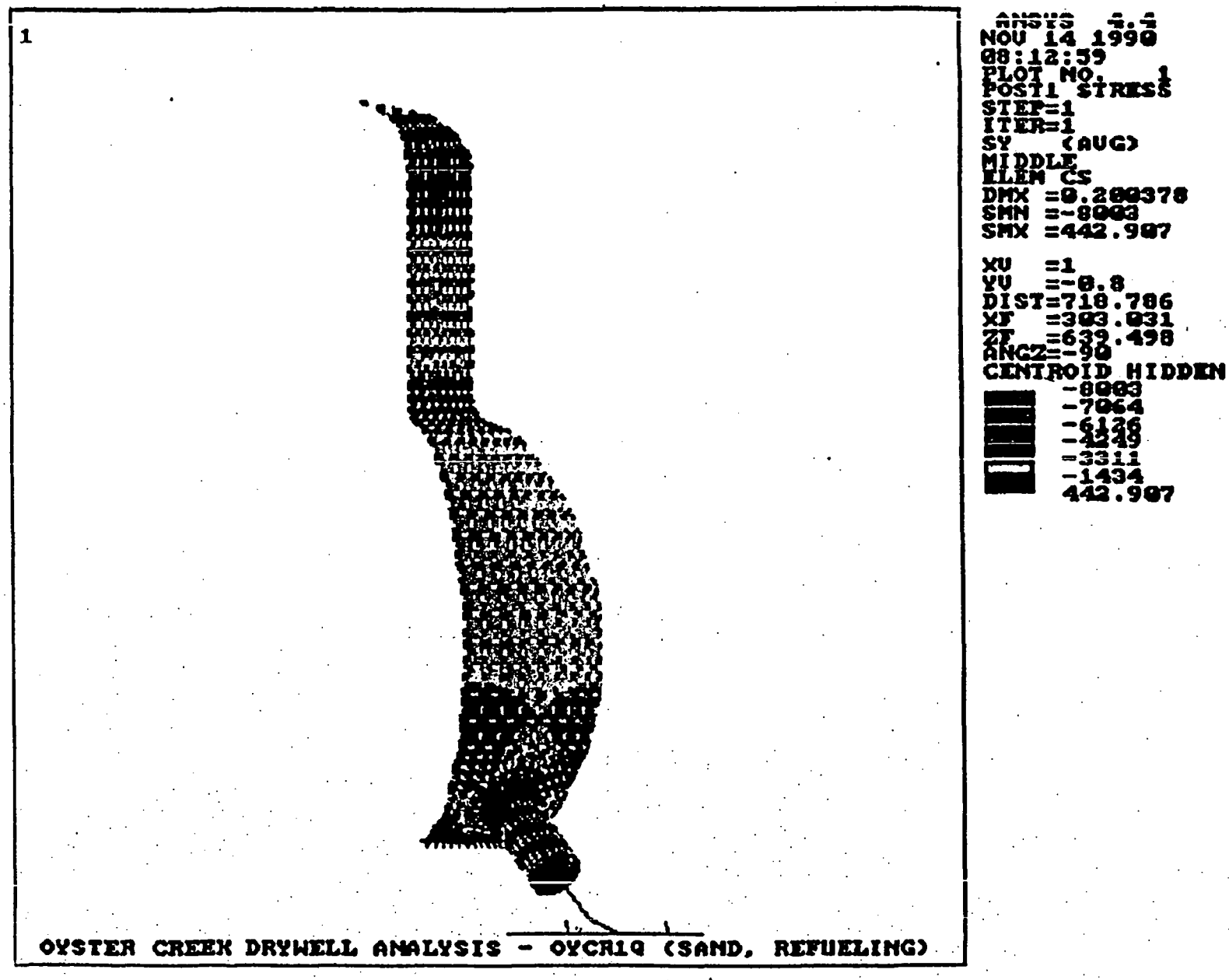

Figure 3-7 Meridional Stresses - Refueling Case

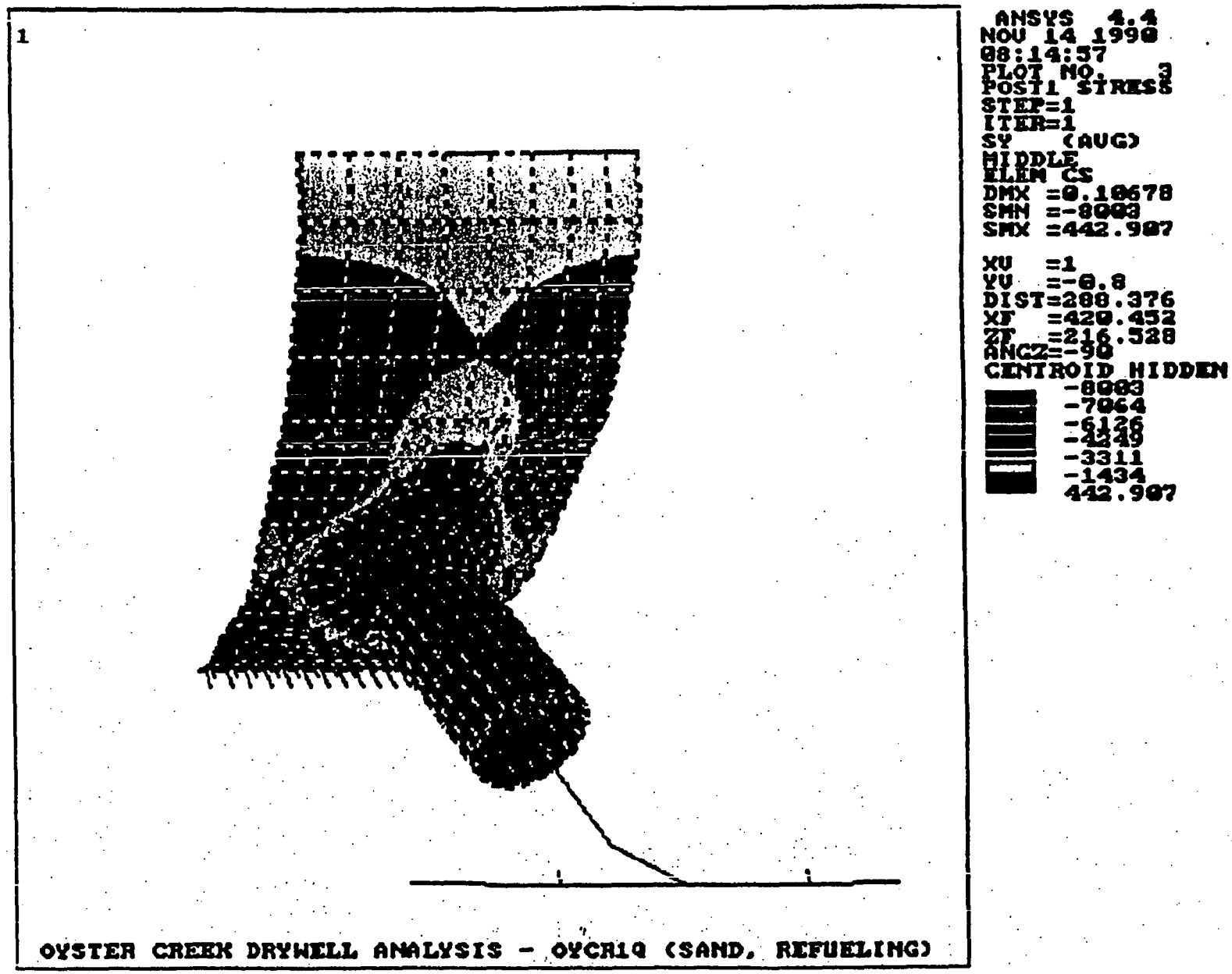

Figure 3-8 Lower Drywell Meridional Stresses - Refueling Case

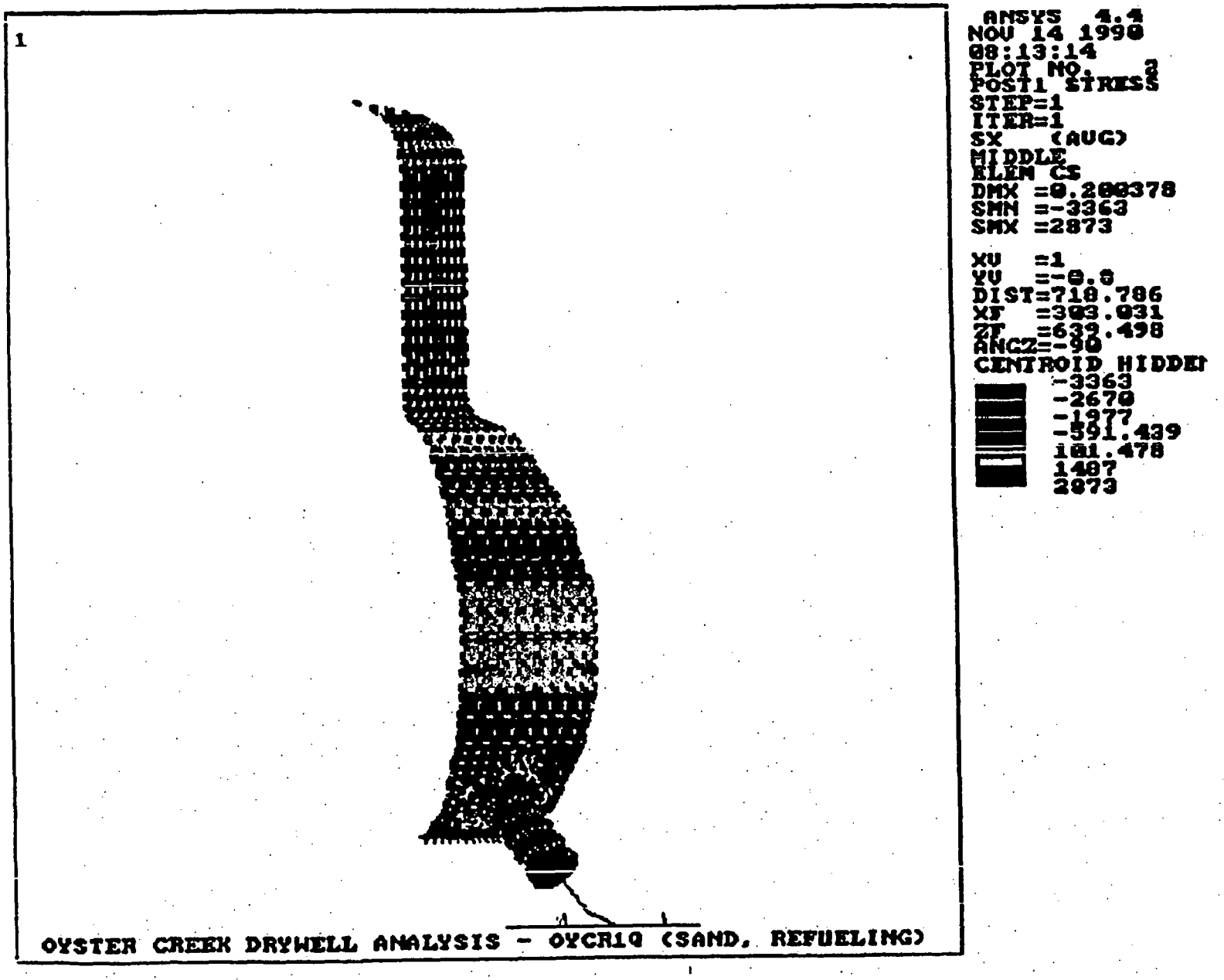

Figure 3-9 Circumferential Stresses - Refueling Case

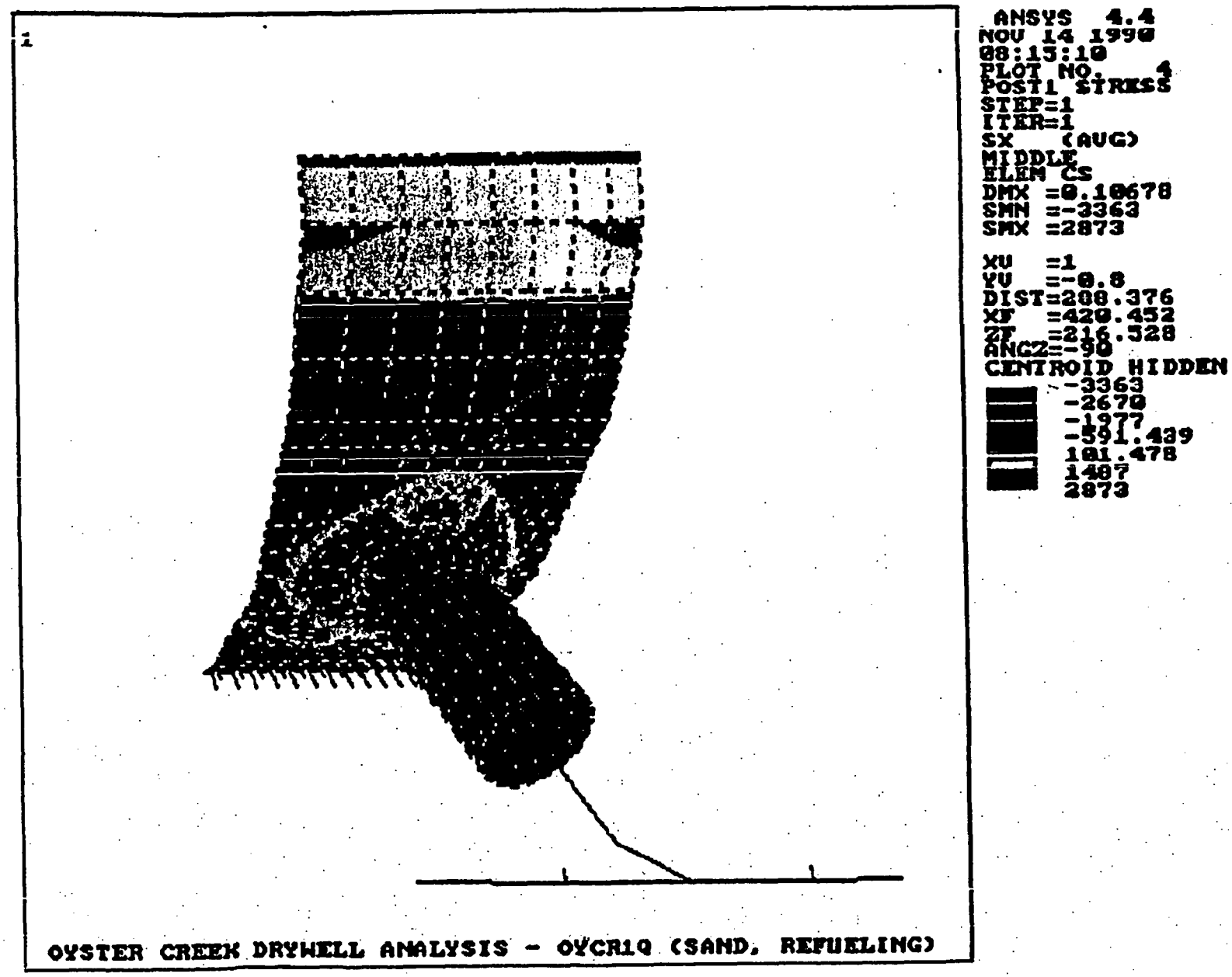

Figure 3-10. Lower Drywell Circumferential Stresses - Refueling Case

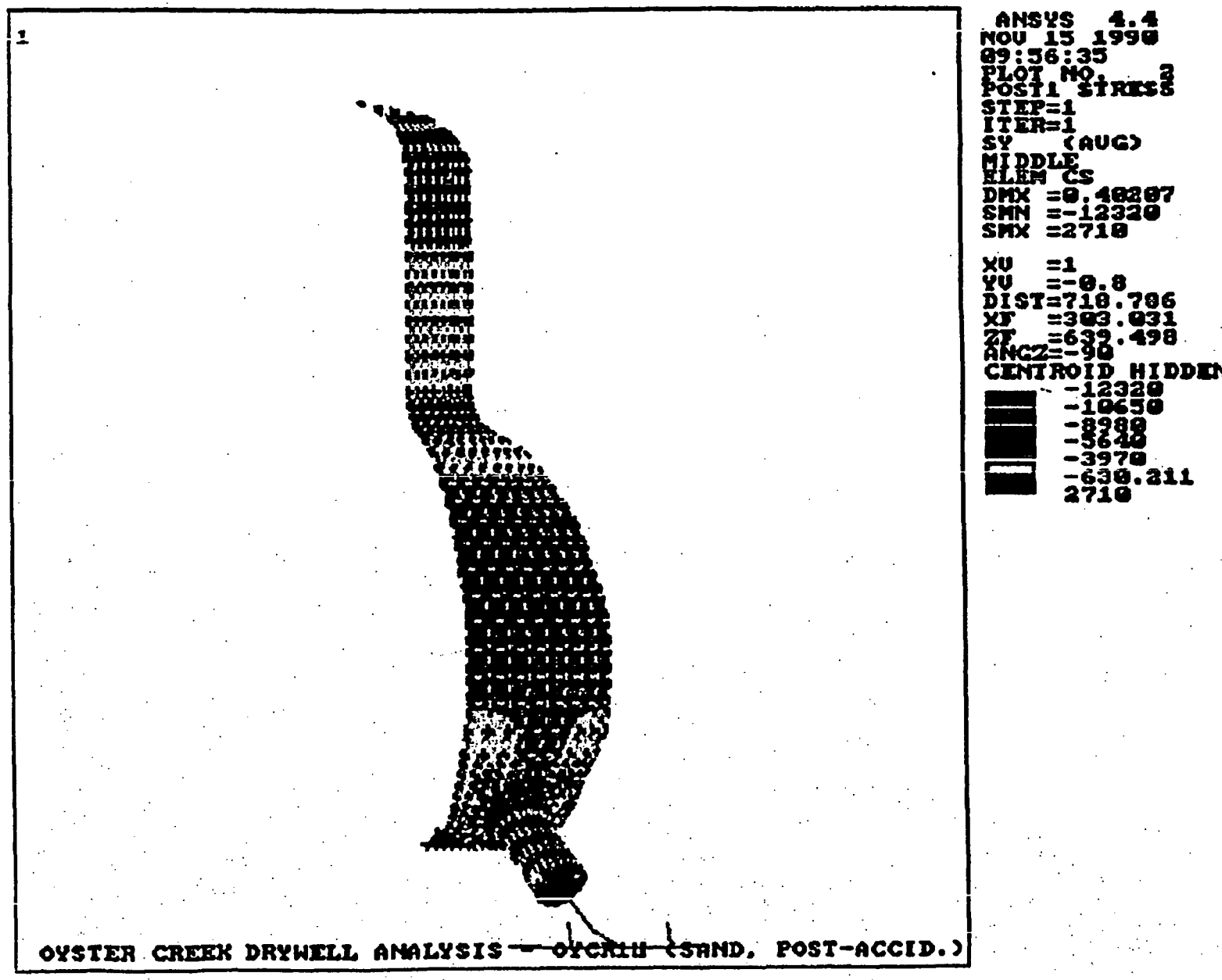

Figure 3-11 Meridional Stresses - Post-Accident Case

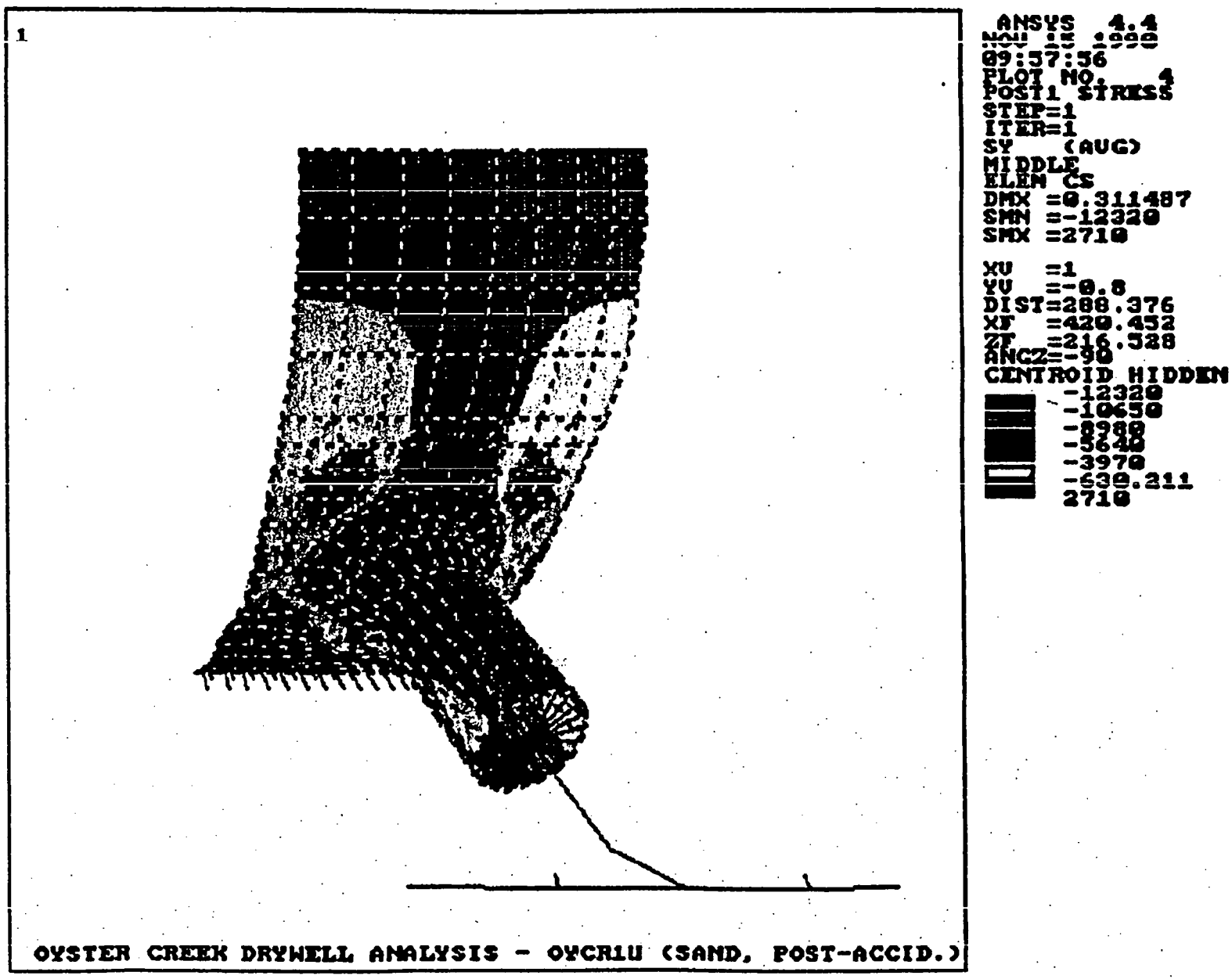

Figure 3-12 Lower Drywell Meridional Stresses - Post-Accident Case

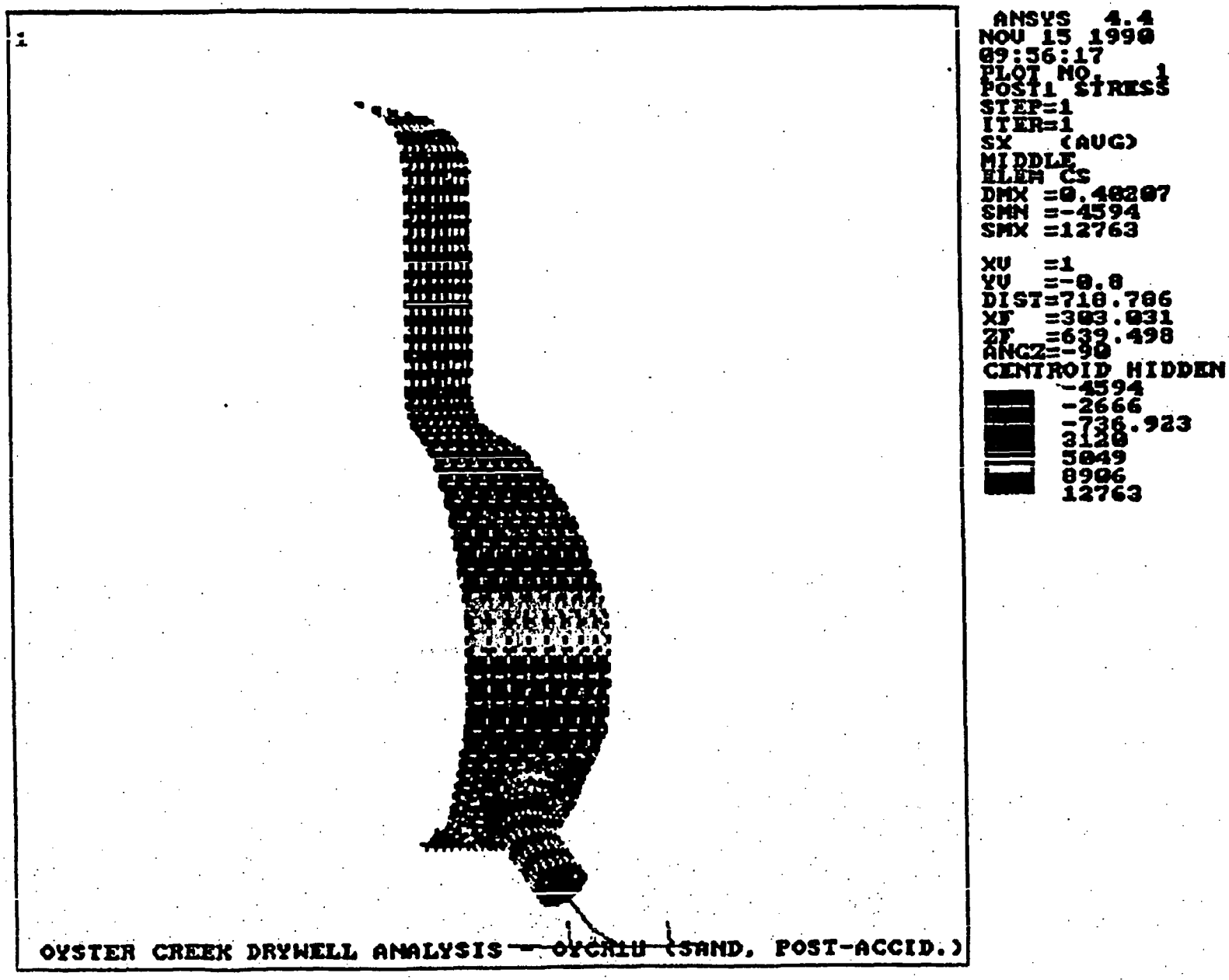

Figure 3.12 Circumferential Stresses - Post Accident Case

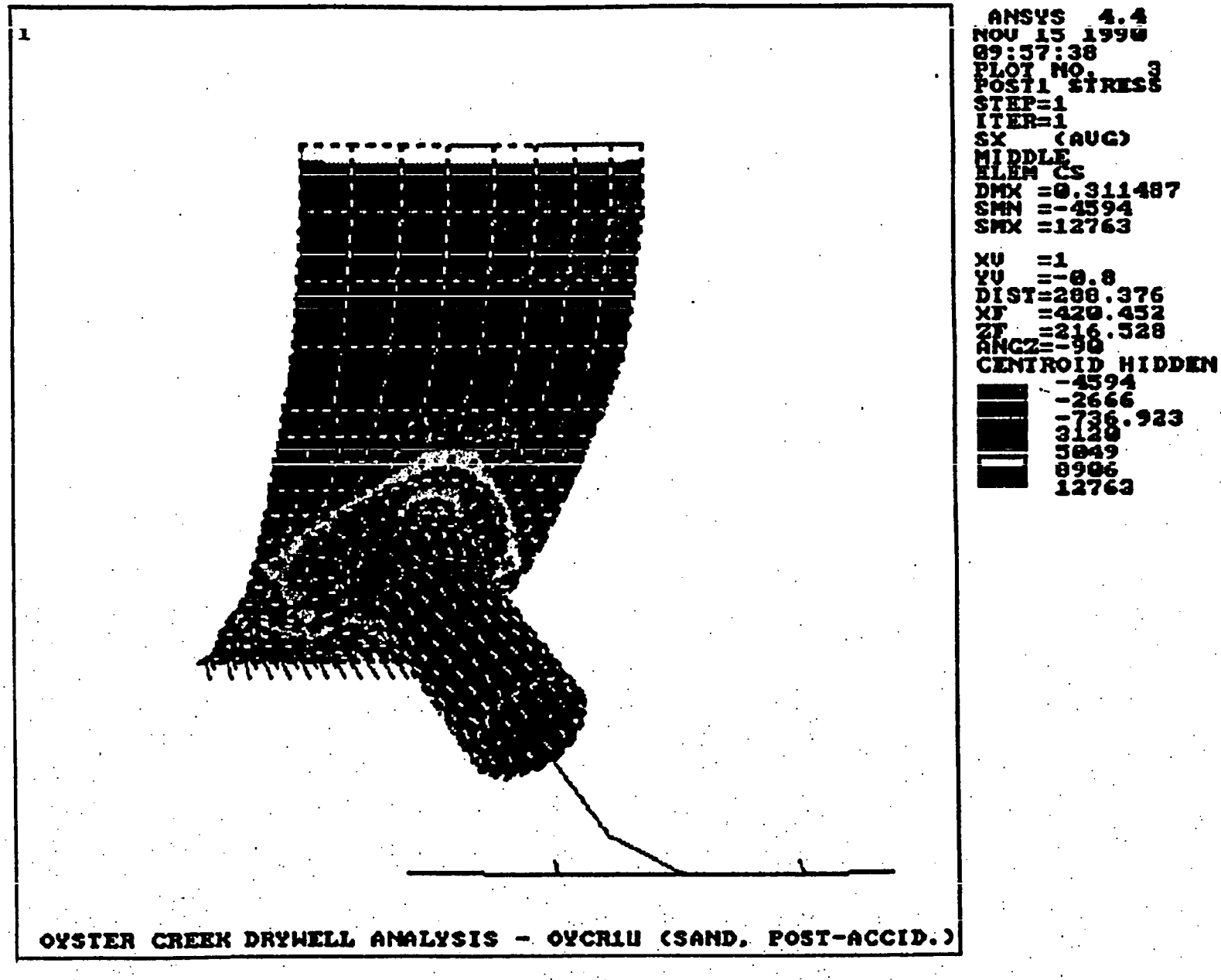

Figure 3-14. Lower Drywell Circumferential Stresses - Post-Accident Case

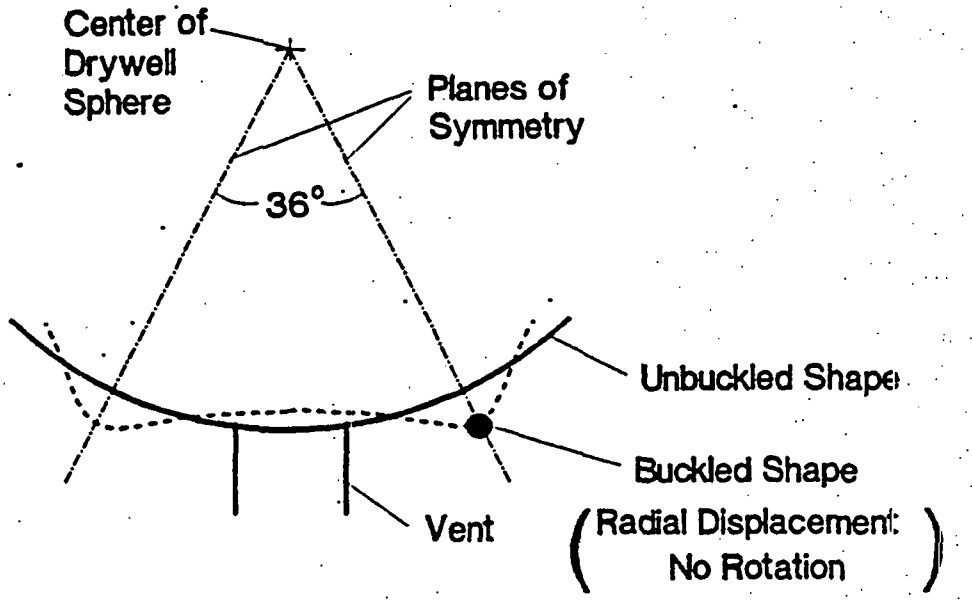

Symmetric Buckling of Drywell

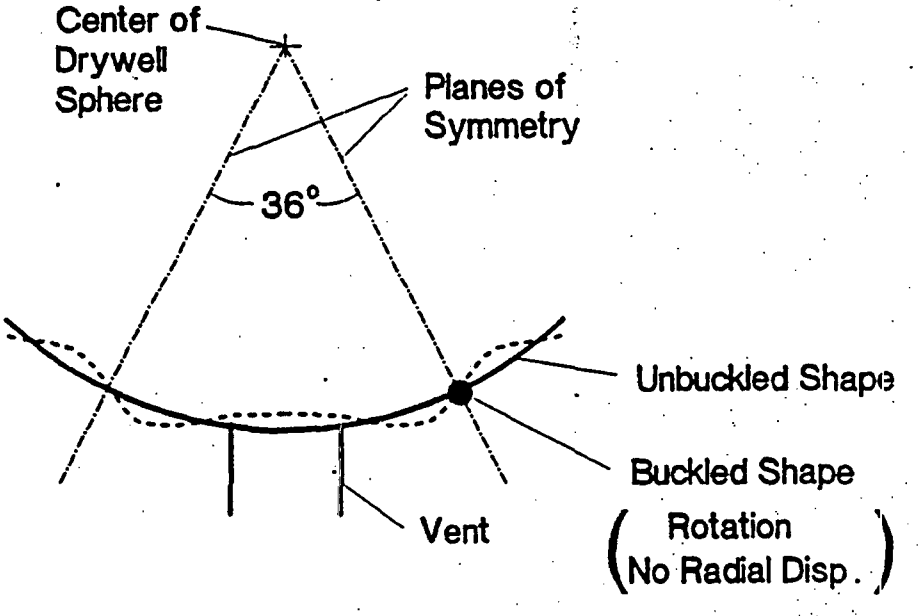

Anti-symmetric Buckling of Drywell

SYM.DRW

Figure 3-15. Symmetric and Anti-Symmetric Buckling Modes

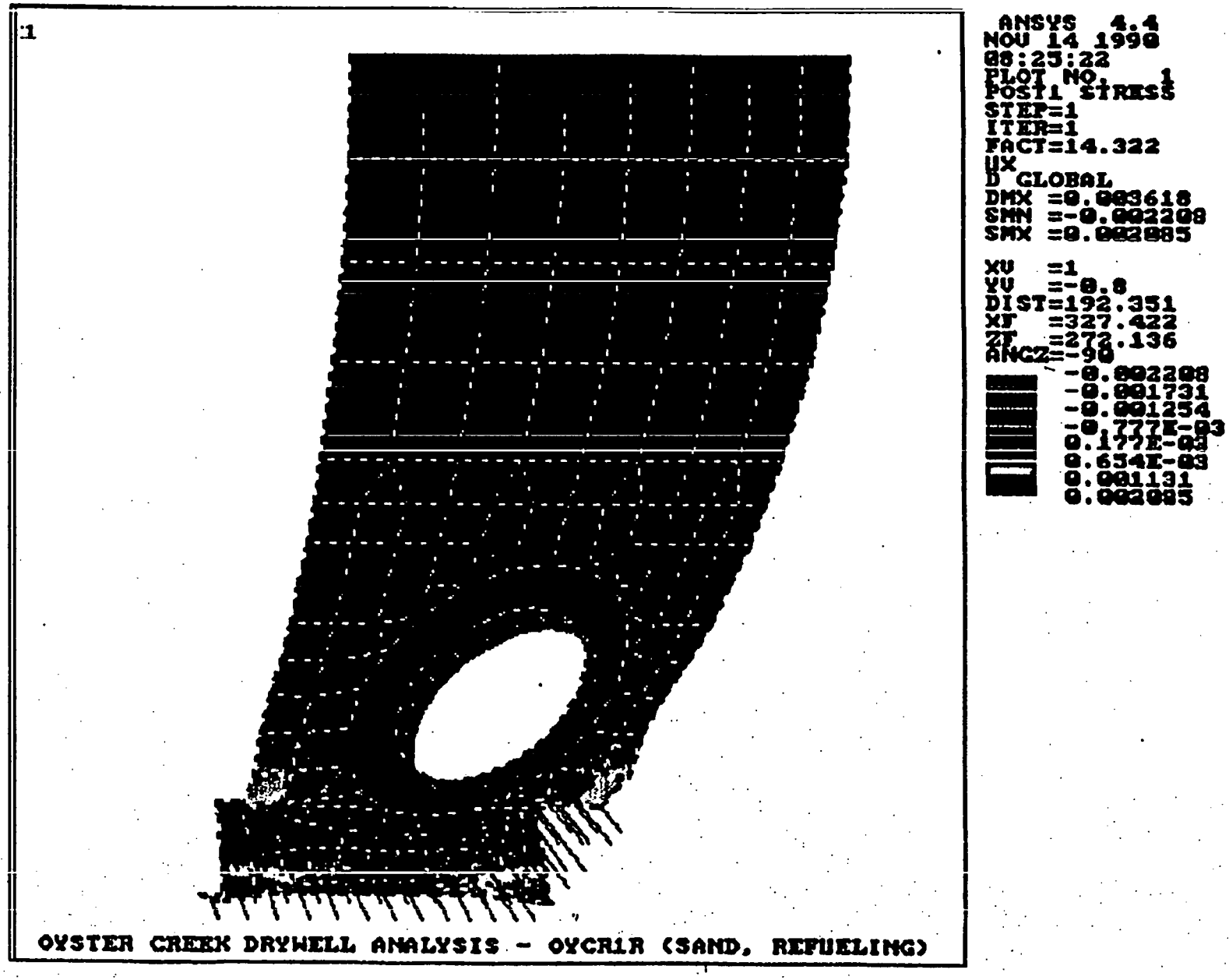

Figure 3-16 Symmetric Buckling Mode Shape - Refueling Case

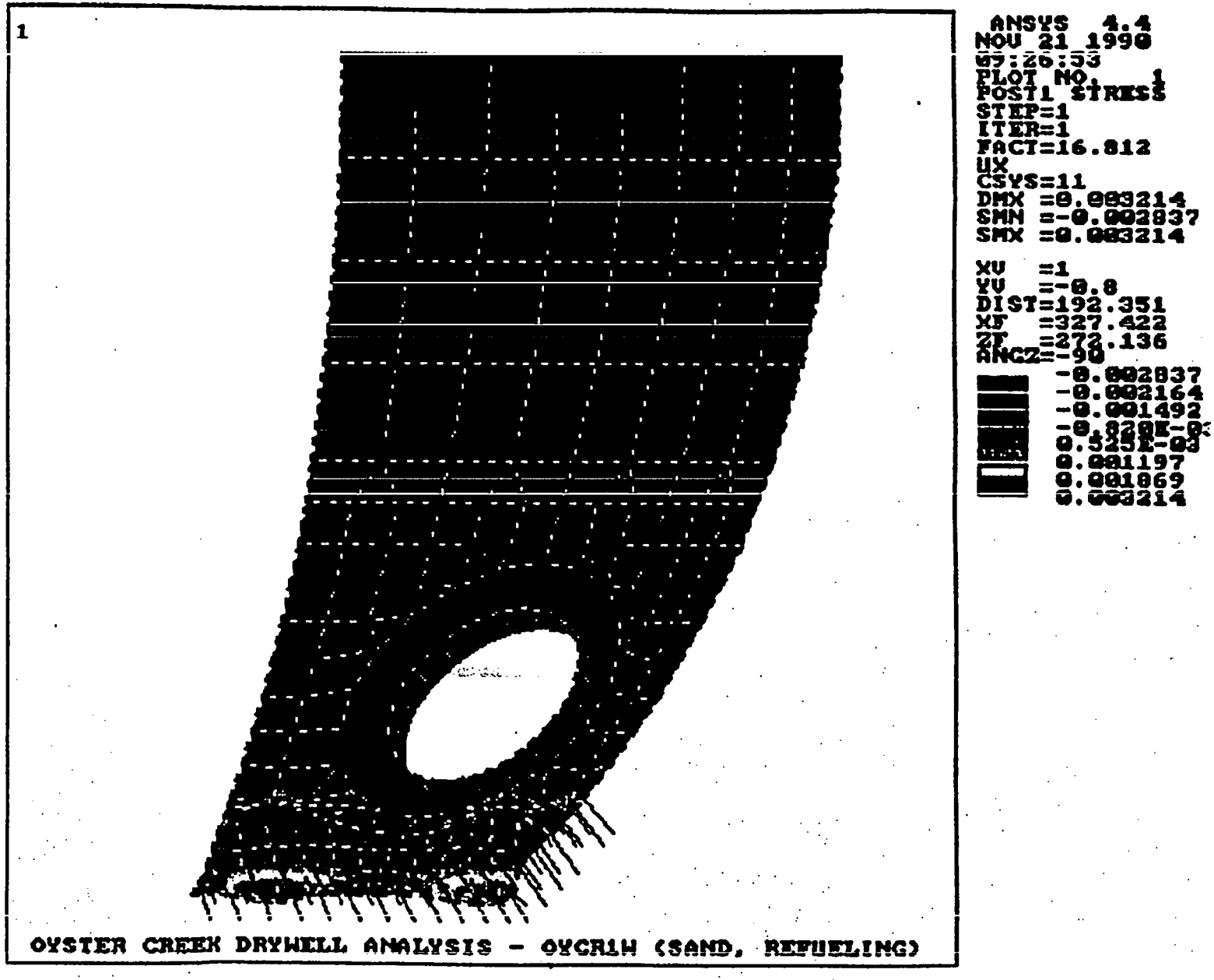

Figure 3-17 Anti-Symmetric Buckling Mode Shape - Refueling Case

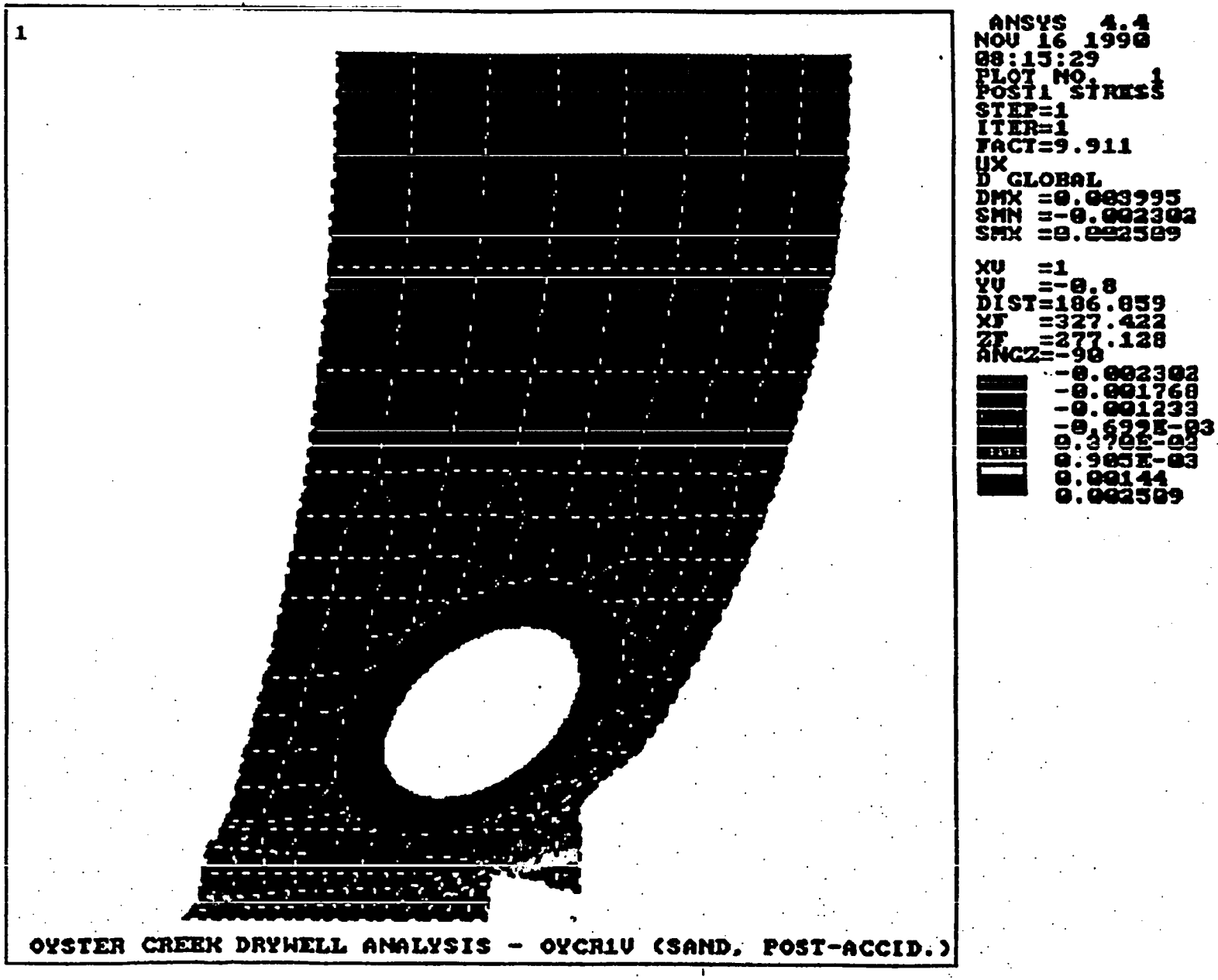

Figure 2.18 Buckling Mode Shape - Post Accident Case

4. ALLOWABLE BUCKLING STRESS EVALUATION

Applying the methodology described in Section 2 for the modification of the theoretical elastic buckling stress, the allowable compressive stresses are now calculated. Tables 4-1 and 4-2 summarize the calculation of the allowable buckling stresses for the Refueling and Post-Accident conditions, respectively. The modified capacity reduction factors are first calculated as described in sections 2.2 and 2.3. After reducing the theoretical instability stress by this reduction factor, the plasticity reduction factor is calculated and applied. The resulting inelastic buckling stresses are then divided by the factor of safety of 2.0 for the Refueling case and 1.67 for the Post-Accident case to obtain the final allowable compressive stresses.

The allowable compressive stress for the Refueling case is 10.44 ksi. Since the applied compressive stress is 7.10 ksi, there is a 47% margin. The allowable compressive stress for the Post-Accident, flooded case is 14.34 ksi. This results in a margin of 48% for the applied compressive stress of 9.69 ksi.

Table 4-1

Calculation of Allowable Buckling Stresses - Refueling Case

Parameter	Value
Theoretical Elastic Instability Stress, σ_{ie} (ksi)	101.65
Capacity Reduction Factor, α_i	0.207
Circumferential Stress, σ_c (ksi)	-0.28
Equivalent Pressure, p (psi)	0.000
"X" Parameter	0.000
ΔC	0.000
Modified Capacity Reduction Factor, $\alpha_{i,mod}$	0.207
Elastic Buckling Stress, $\sigma_e = \alpha_{i,mod}\,\sigma_{ie}$ (ksi)	21.04
Proportional Limit Ratio, $\Delta = \sigma_e/\sigma_y$	0.554
Plasticity Reduction Factor, η_i	0.993
Inelastic Buckling Stress, $\sigma_i = \eta_i\sigma_e$ (ksi)	20.89
Factor of Safety, FS	2.0
Allowable Compressive Stress, $\sigma_{all} = \sigma_i/FS$ (ksi)	10.44
Applied Compressive Meridional Stress, σ_m (ksi)	7.10
Margin = $[(\sigma_{all}/\sigma_m) - 1] \times 100\%$	47%

Table 4-2

Calculation of Allowable Buckling Stresses - Post-Accident Case

Parameter	Value
Theoretical Elastic Instability Stress, σ_{ie} (ksi)	96.06
Capacity Reduction Factor, α_i	0.207
Circumferential Stress, σ_c (ksi)	4.05
Equivalent Pressure, p (psi)	13.50
"X" Parameter	0.082
ΔC	0.069
Modified Capacity Reduction Factor, $\alpha_{i,mod}$	0.32
Elastic Buckling Stress, $\sigma_e = \alpha_{i,mod}\,\sigma_{ie}$ (ksi)	30.74
Proportional Limit Ratio, $\Delta = \sigma_e/\sigma_y$	0.809
Plasticity Reduction Factor, η_i	0.736
Inelastic Buckling Stress, $\sigma_i = \eta_i\sigma_e$ (ksi)	22.62
Factor of Safety, FS	1.67
Allowable Compressive Stress, $\sigma_{all} = \sigma_i/FS$ (ksi)	13.55
Applied Compressive Meridional Stress, σ_m (ksi)	9.69
Margin = $[(\sigma_{all}/\sigma_m) - 1] \times 100\%$	39.7%

5. SUMMARY AND CONCLUSIONS

The results of this buckling analysis for the refueling and post-accident load combinations are summarized on Table 5-1. The applied and allowable compressive meridional stresses shown in Table 5-1 are for the sandbed region which is the most limiting region in terms of buckling. This analysis demonstrates that the Oyster Creek drywell has adequate margin against buckling for an assumed sandbed shell thickness of 0.700 inch. This thickness is less than the 95% confidence projected thickness of 0.736 inches for the 14R outage.

Table 5-1

Buckling Analysis Summary

	Load Combination	
	Refueling	Post-Accident
Service Condition	Design	Level C
Factor of Safety Applied	2.00	1.67
Applied Compressive Meridional Stress (ksi)	7.10	9.69
Allowable Compressive Meridional Stress (ksi)	10.44	13.55
Buckling Margin	47%	40%

AN ASME SECTION VIII EVALUATION OF THE OYSTER CREEK DRYWELL FOR WITHOUT SAND CASE PART 2 STABILITY ANALYSIS

February 1991

prepared for

GPU Nuclear Corporation
Parsippany, New Jersey

prepared by

GE Nuclear Energy
San Jose, California

AN ASME SECTION VIII EVALUATION OF THE OYSTER CREEK DRYWELL FOR WITHOUT SAND CASE PART 2 STABILITY ANALYSIS

Prepared by: _____
C.D. Frederickson, Senior Engineer
Materials Monitoring &
Structural Analysis Services

Reviewed by: _____
H. S. Mehta, Principal Engineer
Materials Monitoring &
Structural Analysis Services

Approved by: _____
S. Ranganath, Manager
Materials Monitoring &
Structural Analysis Services

TABLE OF CONTENTS

	Page
1.. INTRODUCTION	1-1
1.1 General	1-1
1.2 Report Outline	1-1
1.3 References	1-2
2. BUCKLING ANALYSIS METHODOLOGY	2-1
2.1 Basic Approach	2-1
2.2 Determination of Capacity Reduction Factor	2-2
2.3 Modification of Capacity Reduction Factor for Hoop Stress	2-3
2.4 Determination of Plasticity Reduction Factor	2-5
2.5 References	2-5
3. FINITE ELEMENT MODELING AND ANALYSIS	3-1
3.1 Finite Element Buckling Analysis Methodology	3-1
3.2 Finite Element Model	3-2
3.3 Drywell Materials	3-3
3.4 Boundary Conditions	3-3
3.5 Loads	3-4
3.6 Stress Results	3-7
3.7 Theoretical Elastic Buckling Stress Results	3-9
3.8 References	3-10
4. ALLOWABLE BUCKLING STRESS EVALUATION	4-1
5. SUMMARY AND CONCLUSIONS	5-1

LIST OF TABLES

Table No.	Title	Page No.
3-1	Oyster Creek Drywell Shell Thicknesses	3-11
3-2	Cylinder Stiffener Locations and Section Properties	3-12
3-3	Material Properties for SA-212 Grade B Steel	3-12
3-4	Oyster Creek Drywell Load Combinations	3-13
3-5	Adjusted Weight Densities of Shell to Account for Compressible Material Weight	3-14
3-6	Oyster Creek Drywell Additional Weights - Refueling	3-15
3-7	Oyster Creek Drywell Additional Weights - Post-Accident	3-16
3-8	Hydrostatic Pressures for Post-Accident, Flooded Cond.	3-17
3-9	Meridional Seismic Stresses at Four Sections	3-18
3-10	Application of Loads to Match Seismic Stresses - Refueling Case	3-19
3-11	Application of Loads to Match Seismic Stresses - Post-Accident Case	3-20
4-1	Calculation of Allowable Buckling Stresses - Refueling	4-2
4-2	Calculation of Allowable Buckling Stresses - Post-Accident	4-3
5-1	Buckling Analysis Summary	5-2

LIST OF FIGURES

Figure No.	Title	Page No.
1-1	Drywell Configuration	1-3
2-1	Capacity Reduction Factors for Local Buckling of Stiffened and Unstiffened Spherical Shells	2-7
2-2	Experimental Data Showing Increase in Compressive Buckling Stress Due to Internal Pressure	2-8
2-3	Design Curve to Account for Increase in Compressive Buckling Stress due to Internal Pressure	2-9
2-4	Plasticity Reduction Factors for Inelastic Buckling	2-10
3-1	Oyster Creek Drywell Geometry	3-21
3-2	Oyster Creek Drywell 3-D Finite Element Model	3-22
3-3	Closeup of Lower Drywell Section of FEM (Outside View)	3-23
3-4	Closeup of Lower Drywell Section of FEM (Inside View)	3-24
3-5	Boundary Conditions of Finite Element Model	3-25
3-6	Application of Loading to Simulate Seismic Bending	3-26
3-7	Meridional Stresses - Refueling Case	3-27
3-8	Lower Drywell Meridional Stresses - Refueling Case	3-28

LIST OF FIGURES

Figure No.	Title	Page No.
3-9	Circumferential Stresses - Refueling Case	3-29
3-10	Lower Drywell Circumferential Stresses - Refueling Case	3-30
3-11	Meridional Stresses - Post-Accident Case	3-31
3-12	Lower Drywell Meridional Stresses - Post-Accident Case	3-32
3-13	Circumferential Stresses - Post-Accident Case	3-33
3-14	Lower Drywell Circumferential Stresses - Post-Accident Case	3-34
3-15	Symmetric and Asymmetric Buckling Modes	3-35
3-16	Symmetric Buckling Mode Shape - Refueling Case	3-36
3-17	Asymmetric Buckling Mode Shape - Refueling Case	3-37
3-18	Buckling Mode Shape - Post-Accident Case	3-38

1. INTRODUCTION

1.1 General

To address local wall thinning of the Oyster Creek drywell, GPUN has prepared a supplementary report to the Code stress report of record [1-1] which is divided into two parts. Part 1 includes all of the Code stress analysis results other than the buckling capability for the drywell shell [1-2]. Part 2 addresses the buckling capability of the drywell shell shown in Figure 1-1 [1-3]. The supplementary report for the degraded drywell is for the present configuration (with sand support in the lower sphere). One option which is being considered by GPUN to mitigate further corrosion in the sandbed region is to remove the sand. Reference 1-4 and this report evaluate the influence of removing the sand on the code stress analysis and buckling evaluation, respectively. Buckling of the entire drywell shell is considered in this analysis with the sandbed region being the area of primary concern.

1.2 Report Outline

Section 2 of this report outlines the methodology used in the buckling capability evaluation. Finite element modeling, analysis and results are described in section 3. Evaluation of the allowable compressive buckling stresses and comparisons with the calculated compressive stresses for the limiting load combinations are covered in section 4. Section 5 presents the summary of results and conclusions.

1.3 References

1-1 "Structural Design of the Pressure Suppression Containment Vessels," by Chicago Bridge & Iron Co.,Contract # 9-0971, 1965.

1-2 "An ASME Section VIII Evaluation of the Oyster Creek Drywell - Part 1 Stress Analysis," GE Report No. 9-1, DRF# 00664, November 1990, prepared for GPUN.

1-3 "An ASME Section VIII Evaluation of the Oyster Creek Drywell - Part 2 Stability Analysis," GE Report No. 9-2, DRF# 00664, November 1990, prepared for GPUN.

1-4 "An ASME Section VIII Evaluation of the Oyster Creek Drywell - Part 1 Stress Analysis," GE Report No. 9-3, DRF# 00664, February 1991, prepared for GPUN.

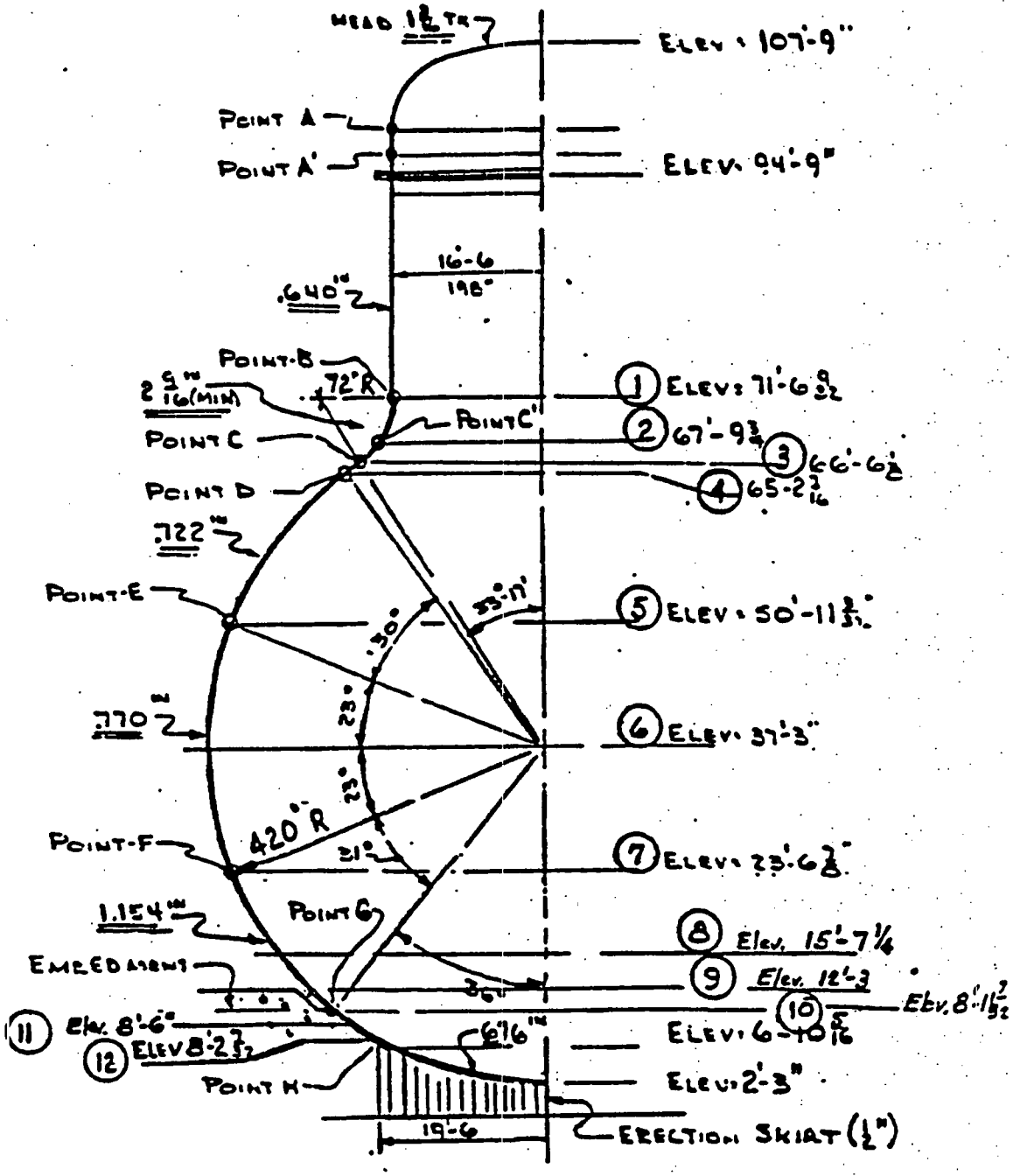

Figure 1-1 Drywell Configuration

2. BUCKLING ANALYSIS METHODOLOGY

2.1 Basic Approach

The basic approach used in the buckling evaluation follows the methodology outlined in the ASME Code Case N-284 [2-1 and 2-2]. Following the procedure of this Code Case, the allowable compressive stress is evaluated in three steps.

In the first step, a theoretical elastic buckling stress, σ_{ie}, is determined. This value may be calculated either by classical buckling equations or by finite element analysis. Since the drywell shell geometry is complex, a three dimensional finite element analysis approach is followed using the eigenvalue extraction technique. More details on the eigenvalue determination are given in Section 3.

In the second step, the theoretical elastic buckling stress is modified by the appropriate capacity and plasticity reduction factors. The capacity reduction factor, α_i, accounts for the difference between classical buckling theory and actual tested buckling stresses for fabricated shells. This difference is due to imperfections inherent in fabricated shells, not accounted for in classical buckling theory, which can cause significant reductions in the critical buckling stress. Thus, the elastic buckling stress for fabricated shells is given by the product of the theoretical elastic buckling stress and the capacity reduction factor, i.e., $\sigma_{ie}\alpha_i$. When the elastic buckling stress exceeds the proportional limit of the material, a plasticity reduction factor, η_i, is used to account for non-linear material behavior. The inelastic buckling stress for fabricated shells is given by $\eta_i\alpha_i\sigma_{ie}$.

In the final step, the allowable compressive stress is obtained by dividing the buckling stress calculated in the second step by the safety factor, FS:

$$\text{Allowable Compressive Stress} = \eta_i\alpha_i\sigma_{ie}/FS$$

In Reference 2-1, the safety factor for the Design and Level A & B service conditions is specified as 2.0. A safety factor of 1.67 is specified for Level C service conditions (such as the post-accident condition).

The determination of appropriate values for capacity and plasticity reduction factors is discussed next.

2.2 Determination of Capacity Reduction Factor

The capacity reduction factor, α_i, is used to account for reductions in actual buckling strength due to the existence of geometric imperfections. The capacity reduction factors given in Reference 2-1 are based on extensive data compiled by Miller [2-3]. The factors appropriate for a spherical shell geometry such as that of the drywell in the sandbed region, are shown in Figure 2-1 (Figure 1512-1 of Reference 2-1). The tail (flat) end of the curves are used for unstiffened shells. The curve marked 'Uniaxial compression' is applicable since the stress state in the sandbed region is compressive in the meridional direction but tensile in the circumferential direction. From this curve, α_i is determined to be 0.207.

The preceding value of the capacity reduction factor is very conservative for two reasons. First, it is based on the assumption that the spherical shell has a uniform thickness equal to the reduced thickness. However, the drywell shell has a greater thickness above the sandbed region which would reinforce the sandbed region. Second, it is assumed that the circumferential stress is zero. The tensile circumferential stress has the effect of rounding the shell and reducing the effect of imperfections introduced during the fabrication and construction phase. A modification of the α_i value to account for the presence of tensile circumferential stress is discussed in Subsection 2.3.

The capacity reduction factor values given in Reference 2-1 are applicable to shells which meet the tolerance requirements of NE-4220

of Section III [2-4]. Reference 2-5 compares the tolerance requirements of NE-4220 to the requirements to which the Oyster Creek drywell shell was fabricated. The comparison shows that the Oyster Creek drywell shell was erected to the tolerance requirements of NE-4220. Therefore, although the Oyster Creek drywell is not a Section III, NE vessel, it is justified to use the approach outlined in Code Case N-284.

2.3 Modification of Capacity Reduction Factor for Hoop Stress

The orthogonal tensile stress has the effect of rounding fabricated shells and reducing the effect of imperfections on the buckling strength. The Code Case N-284 [2-1 and 2-2] notes in the last paragraph of Article 1500 that, "The influence of internal pressure on a shell structure may reduce the initial imperfections and therefore higher values of capacity reduction factors may be acceptable. Justification for higher values of α_i must be given in the Design report."

The effect of hoop tensile stress on the buckling strength of cylinders has been extensivelly documented [2-6 through 2-11]. Since the methods used in accounting for the effect of tensile hoop stress for the cylinders and spheres are similar, the test data and the methods for the cylinders are first reviewed. Harris, et al [2-6] presented a comprehensive set of test data, including those from References 2-7 and 2-8, which clearly showed that internal pressure in the form of hoop tension, increases the axial buckling stress of cylinders. Figure 2-2 shows a plot of the test data showing the increase in buckling stress as a function of nondimensional pressure. This increase in buckling capacity is accounted for by defining a separate reduction factor, α_p. The capacity reduction factor α_i can then be modified as follows:

$$\alpha_{i,mod} = \alpha_i + \alpha_p$$

The buckling stress in uniaxial compression for a cylinder or a sphere of uniform thickness with no internal pressure is given by the following:

$$S_c = (0.605)(\alpha_i)Et/R$$
$$= (0.605)(0.207)\ Et/R$$

Where, 0.605 is a constant, 0.207 is the capacity reduction factor, α_i, and E,t and R are Young's Modulus, wall thickness and radius, respectively. In the presence of a tensile stress such as that produced by an internal pressure, the buckling stress is given as follows:

$$S_{c,mod} = (0.605)(\alpha_i + \alpha_p)Et/R$$
$$= (0.605)(0.207 + \alpha_p)Et/R$$
$$= [(0.605)(0.207) + \Delta C]\ Et/R$$

Where ΔC is $\alpha_p/0.605$ and is given for cylindrical geometries in the graphical form in Figure 2-3. As can be seen in Figure 2-3, ΔC is a function of the parameter $X=(p/4E)(2R/t)^2$, where ,p, is the internal pressure. Miller [2-12] gives the following equation that fits the graphical relationship between X and ΔC shown in Figure 2-3:

$$\Delta C = \alpha_p/0.605 = 1.25/(5+1/X)$$

The preceding approach pertains to cylinders. Along the similar lines, Miller [2-13] has developed an approach for spheres as described next.

The non-dimensional parameter X is essentially $(\sigma_\theta/E)(R/t)$. Since in the case of a sphere, the hoop stress is one-half of that in the cylinder, the parameter X is redefined for spheres as follows:

$$X_{(sphere)} = (p/8E)(2R/t)^2$$

When the tensile stress magnitude, S, is known, the equivalent internal pressure can be calculated using the expression:

$$p = 2tS/R$$

Based on a review of spherical shell buckling data [2-14, 2-15], Miller [2-13] proposed the following equation for ΔC:

$$\Delta C_{(sphere)} = 1.06/(3.24 + 1/X)$$

The modified capacity reduction factor, $\alpha_{i,mod}$, for the drywell geometry was obtained as follows:

$$\alpha_{i,mod} = 0.207 + \Delta C_{(sphere)}/0.605$$

2.4 Determination of Plasticity Reduction Factor

When the elastic buckling stress exceeds the proportional limit of the material, a plasticity reduction factor, η_i, is used to account for the non-linear material behavior. The inelastic buckling stress for fabricated shells is given by $\eta_i \alpha_i \sigma_{ie}$. Reference 2-2 gives the mathematical expressions shown below [Article -1611 (a)] to calculate the plasticity reduction factor for the meridional direction elastic buckling stress. Δ is equal to $\alpha_i \sigma_{ie}/\sigma_y$ and σ_y is the material yield strength. Figure 2-4 shows the relationship in graphical form.

$$\begin{aligned} \eta_i &= 1.0 && \text{if } \Delta \le 0.55 \\ &= (0.45/\Delta) + 0.18 && \text{if } 0.55 < \Delta \le 1.6 \\ &= 1.31/(1+1.15\Delta) && \text{if } 1.6 < \Delta \le 6.25 \\ &= 1/\Delta && \text{if } \Delta > 6.25 \end{aligned}$$

2.5 References

2-1 ASME Boiler and Pressure Vessel Code Case N-284, "Metal Containment Shell Buckling Design Methods, Section III, Division 1, Class MC", Approved August 25, 1980.

2-2 Letter (1985) from C.D. Miller to P. Raju; Subject: Recommended Revisions to ASME Code Case N-284.

2-3 Miller, C.D., "Commentary on the Metal Containment Shell Buckling Design Methods of the ASME Boiler and Pressure Vessel Code," December 1979.

2-4 ASME Boiler & Pressure Vessel Code, Section III, Nuclear Power Plant Components.

2-5 "Justification for Use of Section III, Subsection NE, Guidance in Evaluating the Oyster Creek Drywell," Appendix A to letter dated December 21, 1990 from H.S. Mehta of GE to S.C. Tumminelli of GPUN.

2-6 Harris, L.A., et al, "The Stability of Thin-Walled Unstiffened Circular Cylinders Under Axial Compression Including the Effects of Internal Pressure," Journal of the Aeronautical Sciences, Vol. 24, No. 8 (August 1957), pp. 587-596.

2-7 Lo, H., Crate, H., and Schwartz, E.B., "Buckling of Thin-Walled Cylinder Under Axial Compression and Internal Pressure," NACA TN 2021, January 1950.

2-8 Fung, Y.C., and Sechler, E.E., "Buckling of Thin-Walled Circular Cylinders Under Axial Compression and Internal Pressure," Journal of the Aeronautical Sciences, Vol. 24, No. 5, pp. 351-356, May 1957.

2-9 Baker, E.H., et al., "Shell Analysis Manual," NASA, CR-912 (April 1968).

2-10 Bushnell, D., "Computerized Buckling Analysis of Shells," Kluwer Academic Publishers, 1989 (Chapter 5).

2-11 Johnson, B.G., "Guide to Stability Design Criteria for Metal Structures," Third Edition (1976), John Wiley & Sons.

2-12 Miller, C.D., "Effects of Internal Pressure on Axial Compression Strength of Cylinders," CBI Technical Report No. 022891, February 1991.

2-13 Miller, C.D., "Evaluation of Stability Analysis Methods Used for the Oyster Creek Drywell," CBI Technical Report Prepared for GPU Nuclear Corporation, September 1991.

2-14 Odland, J., "Theoretical and Experimental Buckling Loads of Imperfect Spherical Shell Segments," Journal of Ship Research, Vol. 25, No.3, September 1981, pp. 201-218.

2-15 Yao, J.C., "Buckling of a Truncated Hemisphere Under Axial Tension," AIAA Journal, Vol. 1, No. 10, October 1963, pp. 2316-2319.

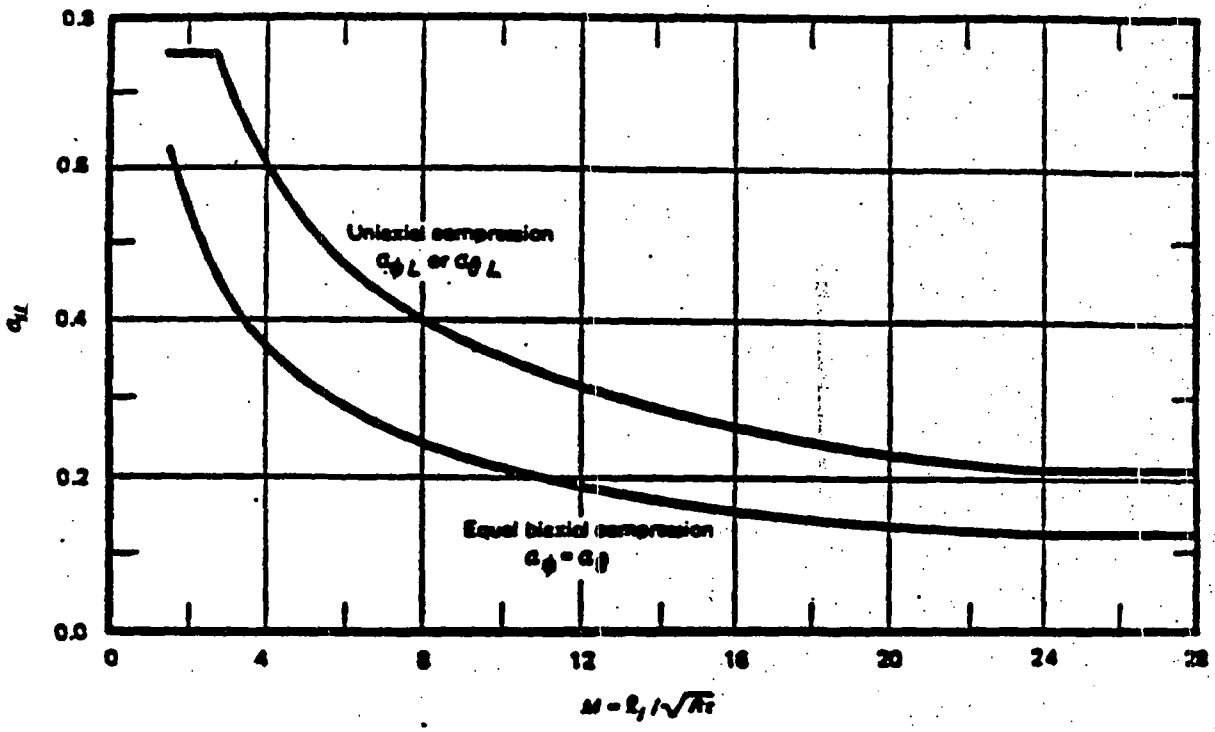

Figure 2-1 Capacity Reduction Factors for Local Buckling of Stiffened and Unstiffened Spherical Shells

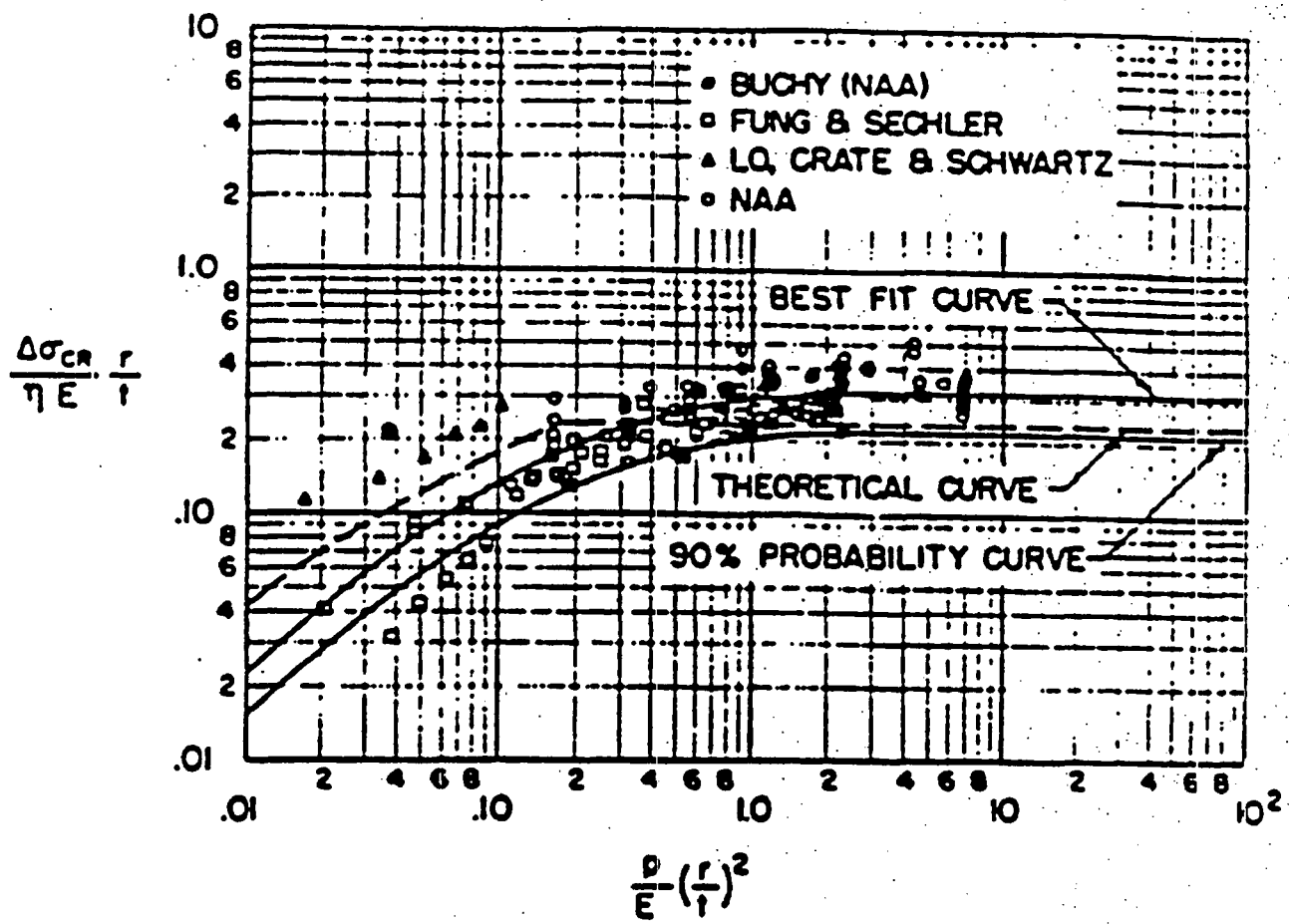

Figure 2-2 Experimental Data Showing Increase in Compressive Buckling Stress Due to Internal Pressure (Reference 2-6)

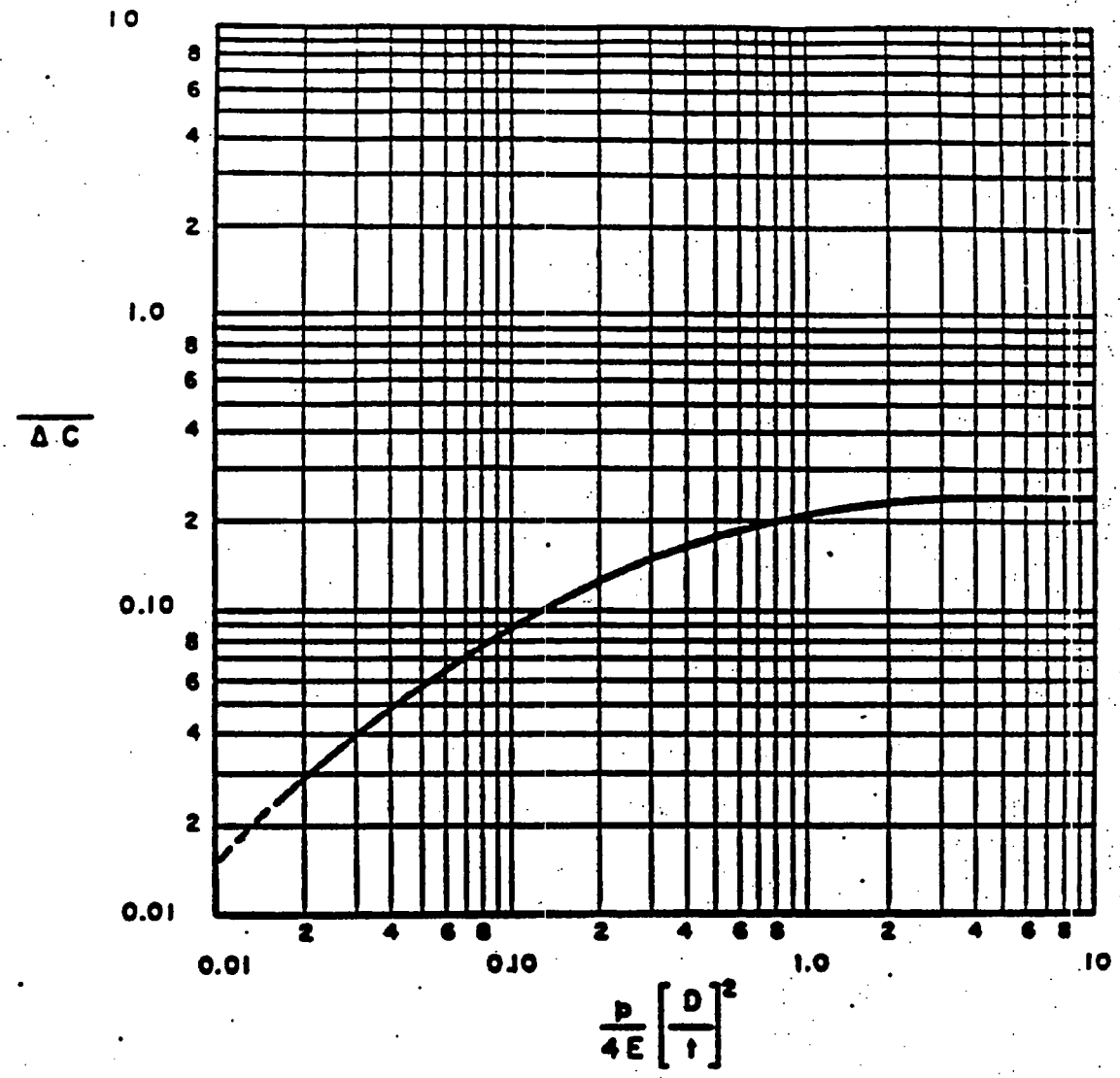

Figure 2-3 Design Curve to Account for Increase in Compressive Buckling Stress Due to Internal Pressure (Reference 2-11)

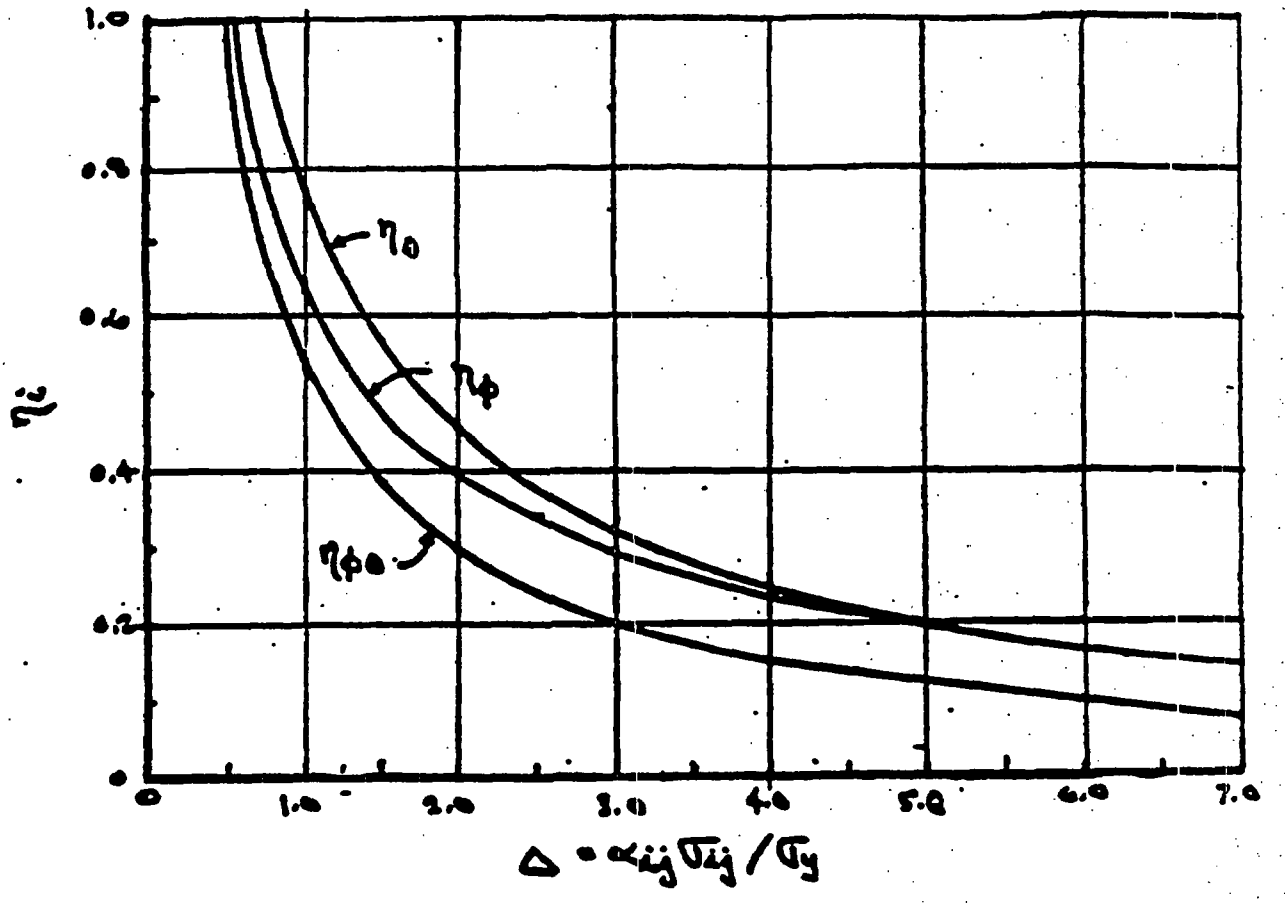

Figure 2-4 Plasticity Reduction Factors for Inelastic Buckling

3. FINITE ELEMENT MODELING AND ANALYSIS

3.1 Finite Element Buckling Analysis Methodology

This evaluation of the Oyster Creek Drywell buckling capability uses the Finite Element Analysis (FEA) program ANSYS [Reference 3-1]. The ANSYS program uses a two step eigenvalue formulation procedure to perform linear elastic buckling analysis. The first step is a static analysis of the structure with all anticipated loads applied. The structural stiffness matrix, [K], the stress stiffness matrix, [S], and the applied stresses, σ_{ap}, are developed and saved from this static analysis. A buckling pass is then run to solve for the eigenvalue or load factor, λ, for which elastic buckling is predicted using the equation:

$$([K] + \lambda [S]) \{u\} = 0$$

where: λ is the eigenvalue or load factor.
$\{u\}$ is the eigenvector representing the buckled shape of the structure.

This load factor is a multiplier for the applied stress state at which the onset of elastic buckling will theoretically occur. All applied loads (pressures, forces, gravity, etc...) are scaled equally. For example, a load factor of 4 would indicate that the structure would buckle for a load condition four times that defined in the stress pass. The critical stress, σ_{cr}, at a certain location of the structure is thus calculated as:

$$\sigma_{cr} = \lambda \sigma_{ap}$$

This theoretical elastic buckling stress is then modified by the capacity and plasticity reduction factors to determine the predicted buckling stress of the fabricated structure as discussed in Section 2. This stress is further reduced by a factor of safety to determine the allowable compressive stress.

3.2 Finite Element Model

The Oyster Creek drywell has been previously analyzed using a simplified axisymmetric model to evaluate the buckling capability in the sandbed region [Reference 3-2]. This type of analysis conservatively neglects the vents and reinforcements around the vents which significantly increase the stiffness of the shell near the sandbed region. In order to more accurately determine the buckling capability of the drywell, a three dimensional finite element model is developed.

The geometry of the Oyster Creek drywell is shown in Figure 3-1. Taking advantage of symmetry of the drywell with 10 vents, a 36° section is modeled. Figure 3-2 illustrates the finite element model of the drywell. This model includes the drywell shell from the base of the sandbed region to the top of the elliptical head and the vent and vent header. The torus is not included in this model because the bellows provide a very flexible connection which does not allow significant structural interaction between the drywell and torus.

Figure 3-3 shows a more detailed view of the lower section of the drywell model. The various colors on Figures 3-2 and 3-3 represent the different shell thicknesses of the drywell and vent. Nominal or as-designed thicknesses, summarized in Table 3-1, are used for the drywell shell for all regions other than the sandbed region. The sandbed region shown in blue in Figure 3-3 is considered to have a thickness of 0.736 inch. This is the 95% confidence projected thickness to outage 14R. Figure 3-4 shows the view from the inside of the drywell with the gussets and the vent jet deflector.

The drywell and vent shell are modeled using the 3-dimensional plastic quadrilateral shell (STIF43) element. Although this element has plastic capabilities, this analysis is conducted using only elastic behavior. This element type was chosen over the elastic quadrilateral shell (STIF63) element because it is better suited for modeling curved surfaces.

At a distance of 76 inches from the drywell shell, the vent is simplified using beam elements. The transition from shell to beam elements is made by extending rigid beam elements from a node along the centerline of the vent radially outward to each of the shell nodes of the vent. ANSYS STIF4 beam elements are then connected to this centerline node to model the axial and bending stiffness of the vent and header. Spring (STIF14) elements are used to model the vertical header supports inside the torus. ANSYS STIF4 beam elements are also used to model the stiffeners in the cylindrical region of the upper drywell. The section properties of these stiffeners are summarized in Table 3-2.

3.3 Drywell Materials

The drywell shell is fabricated from SA-212, Grade B high tensile strength carbon-silicon steel plates for boilers and other pressure vessels ordered to SA-300 specifications. The mechanical properties for this material at room temperature are shown in Table 3-3. These are the properties used in the finite element analysis. For the perforated vent jet deflector, the material properties were modified to account for the reduction in stiffness due to the perforations.

3.4 Boundary Conditions

Symmetric boundary conditions are defined for both edges of the 36° drywell model for the static stress analysis as shown on Figure 3-5. This allows the nodes at this boundary to expand radially outward from the drywell centerline and vertically, but not in the circumferential direction. Rotations are also fixed in two directions to prevent the boundary from rotating out of the plane of symmetry. Nodes at the bottom edge of the drywell are fixed in all directions to simulate the fixity of the shell within the concrete foundation. Nodes at the end of the header support spring elements are also fixed.

3.5 Loads

The loads are applied to the drywell finite element model in the manner which most accurately represents the actual loads anticipated on the drywell. Details on the application of loads are discussed in the following paragraphs.

3.5.1 Load Combinations

All load combinations to be considered on the drywell are summarized on Table 3-4. The most limiting load combinations in terms of possible buckling are those which cause the most compressive stresses in the sandbed region. Many of the design basis load combinations include high internal pressures which would create tensile stresses in the shell and help prevent buckling. The most severe design load combination identified for the buckling analysis of the drywell is the refueling condition (Case IV). This load combination consists of the following loads:

Dead weight of vessel, penetrations, compressible material, equipment supports and welding pads.
Live loads of welding pads and equipment door
Weight of refueling water
External Pressure of 2 psig
Seismic inertia and deflection loads for unflooded condition

The normal operation condition with seismic is very similar to this condition, however, it will be less severe due to the absence of the refueling water and equipment door weight.
The most severe load combination for the emergency condition is for the post-accident (Case VI) load combination including:

Dead weight of vessel, penetrations, compressible material and equipment supports
Live load of personnel lock
Hydrostatic Pressure of Water for Drywell Flooded to 74'-6"
External Pressure of 2 psig
Seismic inertia and deflection loads for flooded condition

The application of these loads is described in more detail in the following sections.

3.5.2 Gravity Loads

The gravity loads include dead weight loads of the drywell shell, weight of the compressible material and penetrations and live loads. The drywell shell loads are imposed on the model by defining the weight density of the shell material and applying a vertical acceleration of 1.0 g to simulate gravity. The ANSYS program automatically distributes the loads consistent with the mass and acceleration. The compressible material weight of 10 lb/ft^2 is added by adjusting the weight density of the shell to also include the compressible material. The adjusted weight densities for the various shell thicknesses are summarized in Table 3-5. The compressible material is assumed to cover the entire drywell shell (not including the vent) up to the elevation of the flange.

The additional dead weights, penetration weights and live loads are applied as additional nodal masses to the model. As shown on Table 3-6 for the refueling case, the total additional mass is summed for each 5 foot elevation of the drywell. The total is then divided by 10 for the 36° section assuming that the mass is evenly distributed around the perimeter of the drywell. The resulting mass is then applied uniformly to a set of nodes at the desired elevation as shown on Table 3-6. These applied masses automatically impose gravity loads on the drywell model with the defined acceleration of 1g. The same method is used to apply the additional masses to the model for the post-accident case as summarized in Table 3-7.

3.5.3 Pressure Loads

The 2 psi external pressure load for the refueling case is applied to the external faces of all of the drywell and vent shell elements. The compressive axial stress at the transition from vent shell to beam elements is simulated by applying equivalent axial forces to the nodes of the shell elements.

Considering the post-accident case, the drywell is assumed to be flooded to elevation 74'-6" (894 inches). Using a water density of 62.3 lb/ft^3 (0.0361 lb/in^3), the pressure gradient versus elevation is calculated as shown in Table 3-8. The hydrostatic pressure at the bottom of the sandbed region is calculated to be 28.3 psi. According to the elevation of the element centerline, the appropriate pressures are applied to the inside surface of the shell elements.

3.5.4 Seismic Loads

Seismic stresses have been calculated for the Oyster Creek Drywell in Part 1 of this report, Reference 3-3. Meridional stresses are imposed on the drywell during a seismic event due to a 0.058" deflection of the reactor building and due to horizontal and vertical inertial loads on the drywell.

The meridional stresses due to a seismic event are imposed on the 3-D drywell model by applying downward forces at four elevations of the model (A: 23'-7",B: 37'-3",C: 50'-11" and D: 88'-9") as shown on Figure 3-6. Using this method, the meridional stresses calculated in Reference 3-3 are duplicated at four sections of the drywell including 1) the mid-elevation of the sandbed region, 2) 17.25° below the equator, 3) 5.75° above the equator and 4) just above the knuckle region. These four sections were chosen to most accurately represent the load distribution in the lower drywell while also providing a reasonably accurate stress distribution in the upper drywell.

To find the correct loads to match the seismic stresses, the total seismic stress (due to reactor building deflection and horizontal and vertical inertia) are obtained from Reference 3-3 at the four sections of interest. The four sections and the corresponding meridional stresses for the refueling and post-accident seismic cases are summarized in Table 3-9.

Unit loads are then applied to the 3-D model in separate load steps at each elevation shown in Figure 3-6. The resulting stresses at the four sections of interest are then averaged for each of the applied unit loads. By solving four equations with four unknowns, the correct loads are determined to match the stresses shown in Table 3-9 at the four sections. The calculation for the correct loads are shown on Tables 3-10 and 3-11 for the refueling and post-accident cases, respectively.

3.6 Stress Results

The resulting stresses for the two load combinations described in section 3.5 are summarized in this section.

3.6.1 Refueling Condition Stress Results

The resulting stress distributions for the refueling condition are shown in Figures 3-7 through 3-10. The red colors represent the most tensile stresses and the blue colors, the most compressive. Figures 3-7 and 3-8 show the meridional stresses for the entire drywell and lower drywell. The circumferential stresses for the same areas are shown on Figures 3-9 and 3-10. The resulting average meridional stress at the mid-elevation of the sandbed region was found to be;

$$\sigma_{Rm} = -7580 \text{ psi}$$

The circumferential stress averaged from the bottom to the top of the sandbed region is;

$$\sigma_{Rc} = 4490 \text{ psi}$$

3.6.2 Post-Accident Condition Stress Results

The application of all of the loads described for the post-accident condition results in the stress distributions shown in Figures 3-11 through 3-14. The red colors represent the most tensile stresses and the blue colors, the most compressive. Figures 3-11 and 3-12 show the meridional stresses for the entire drywell and lower drywell. The circumferential stresses for the same areas are shown on Figures 3-13 and 3-14. The resulting average meridional stress at mid-elevation of the sandbed region was found to be;

$$\sigma_{PAm} = -11960 \text{ psi}$$

The circumferential stress averaged from the bottom to the top of the sandbed region is;

$$\sigma_{PAc} = +20080 \text{ psi}$$

3.7 Theoretical Elastic Buckling Stress Results

After completion of the stress runs for the Refueling and Post-Accident load combinations, the eigenvalue buckling runs are made as described in Section 3.1. This analysis determines the theoretical elastic buckling loads and buckling mode shapes.

3.7.1 Refueling Condition Buckling Results

As shown on Figure 3-15, it is possible for the drywell to buckle in two different modes. In the case of symmetric buckling shown on Figure 3-15, each edge of the 36° drywell model experiences radial displacement with no rotation. This mode is simulated by applying symmetric boundary conditions to the 3-D model the same as used for the stress run. Using these boundary conditions for the refueling case, the critical load factor was found to be 7.67 with the critical buckling occurring in the sandbed region. The critical buckling mode shape is shown in Figure 3-16 for symmetric boundary conditions. The red color indicates sections of the shell which displace radially outward and the blue, those areas which displace inward.

The first four buckling modes were computed in this eigenvalue buckling analysis with no buckling modes found outside the sandbed region for a load factor as high as 9.94. Therefore, buckling is not a concern outside of the sandbed region.

It is also possible for the drywell to buckle in the asymmetric manner shown in Figure 3-15. For this mode, the edges of the 3-D model are allowed to rotate but are restrained from expanding radially. This case is considered by applying asymmetric boundary conditions at the edges of the 3-D model. With the two pass approach used by ANSYS, it is possible to study asymmetric buckling of the drywell when the stresses are found based on symmetric boundary conditions. The resulting load factor found using asymmetric boundary conditions is 10.13. The mode shape for this case is shown on Figure 3-17.

Because the load factor is lower for symmetric boundary conditions with the same applied stress, the symmetric buckling condition is more limiting. Multiplying the load factor of 7.67 by the average meridional stress from section 3.6.1, the theoretical elastic buckling stress is found to be;

$$\sigma_{Rie} = 7.67 \times (7580 \text{ psi}) = 58{,}100 \text{ psi}$$

3.7.2 Post-Accident Condition Buckling Results

Considering the post-accident case with symmetric boundary conditions, the load factor was calculated as 5.18. Multiplying this load factor by the applied stress from section 3.6.2 results in a theoretical elastic buckling stress of

$$\sigma_{PAie} = 5.18 \times (11960 \text{ psi}) = 61{,}950 \text{ psi}$$

The critical mode shape for this condition is shown in Figure 3-18. Again, the critical buckling mode is in the sandbed region.

3.8 References

3-1 DeSalvo, G.J., Ph.D, and Gorman, R.W., "ANSYS Engineering Analysis System User's Manual, Revision 4.4," Swanson Analysis Systems, Inc., May 1, 1989.

3-2 GPUN Specification SP-1302-53-044, Technical Specification for Primary Containment Analysis - Oyster Creek Nuclear Generating Station; Rev. 2, October 1990.

3-3 "An ASME Section VIII Evaluation of the Oyster Creek Drywell - Part 1 Stress Analysis," GE Report No. 9-1, DRF # 00664, November 1990, prepared for GPUN.

Table 3-1

Oyster Creek Drywell Shell Thicknesses

Section	Thickness (in.)
Sandbed Region	0.736 *
Lower Sphere	1.154
Mid Sphere	0.770
Upper Sphere	0.722
Knuckle	2.5625
Cylinder	0.640
Reinforcement Below Flange	1.250
Reinforcement Above Flange	1.500
Elliptical Head	1.1875
Ventline Reinforcement	2.875
Gussets	0.875
Vent Jet Deflector	2.500
Ventline Connection	2.500
Upper Ventline	0.4375
Lower Ventline	0.250

* 95% confidence projected thickness to 14R.

Table 3-2

Cylinder Stiffener Locations and Section Properties

Elevation (in)	Height (in)	Width (in)	Area (in^2)	Bending Inertia (in^4) Horizontal	Vertical
966.3	0.75	6.0	4.5	13.5	0.211
1019.8	0.75	6.0	4.5	13.5	0.211
1064.5	0.50	6.0	3.0	9.0	0.063
1113.0(1)	2.75 1.00	7.0 7.38	26.6	387.5	12.75
1131.0	1.0	12.0	12.0	144.0	1.000

(1) - This stiffener is made up of 2 beam sections, one 2.75x7" and one 1.0x7.375"

Table 3-3

Material Properties for SA-212 Grade B Steel

Material Property	Value
Young's Modulus	29.6×10^6 psi
Yield Strength	38000 psi
Poisson's Ratio	0.3
Density	0.283 lb/in^3

Table 3-4

Oyster Creek Drywell Load Combinations

CASE I - INITIAL TEST CONDITION
Deadweight + Design Pressure (62 psi) + Seismic (2 x DBE)

CASE II - FINAL TEST CONDITION
Deadweight + Design Pressure (35 psi) + Seismic (2 x DBE)

CASE III - NORMAL OPERATING CONDITION
Deadweight + Pressure (2 psi external) + Seismic (2 x DBE)

CASE IV - REFUELING CONDITION
Deadweight + Pressure (2 psi external) + Water Load + Seismic (2 x DBE)

CASE V - ACCIDENT CONDITION
Deadweight + Pressure(62 psi @ 175°F or 35 psi @ 281°F) + Seismic (2 x DBE)

CASE VI - POST ACCIDENT CONDITION
Deadweight + Water Load @ 74'6" + Seismic (2 x DBE)

Table 3-5

Adjusted Weight Densities of Shell to Account for Compressible Material Weight

Shell Thickness (in.)	Adjusted Weight Density (lb/in^3)
1.154	0.343
0.770	0.373
0.722	0.379
2.563	0.310
0.640	0.392
1.250	0.339

Table 3-6

Oyster Creek Drywell Additional Weights - Refueling Condition

ELEVATION (feet)	DEAD WEIGHT (lbf)	PENETR. WEIGHT (lbf)	& MISC. LOADS (lbf)	TOTAL LOAD (lbf)	5 FOOT RANGE LOAD	LOAD PER 36 DEG. (lbf)	# OF ELEMENTS	NODES OF APPLICATION	LOAD PER FULL NODE (lbf)	LOAD PER HALF NODE (lbf)
15.56	50000			50000						
16		168100		168100						
20		11200		11200						
** 15-20					229300	22930	6	116-119	3822	1911
22#	556000			556000						
** 21-25#					556000	55600	8	161-169	6950	3475
26		11100		11100						
30	64100	51500		115600						
30.25	105000		100000	205000						
** 26-30					331700	33170	8	179-187	4146	2073
31		16500		16500						
32		750		750						
33		15450		15450						
34		28050		28050						
35		1500		1500						
** 31-35					62250	6225	8	188-196	778	389
36		1550		1550						
40	41000	43350		84350						
** 36-40					85900	8590	8	197-205	1074	537
50#	1102000			1102000						
** 45-50#					1102000	110200	8	418-426	13775	6888
54		7850		7850						
** 51-55					7850	785	8	436-444	98	49
56	56400		24000	80400						
60	95200	700	20000	115900						
** 56-60					196300	19630	8	454-462	2454	1227
65	52000		20000	72000						
** 61-65					72000	7200	8	472-480	900	450
70		5750		5750						
** 66-70					5750	575	8	508-516	72	36
73		8850		8850						
** 71-75					8850	885	8	526-534	111	55
82.17	21650			21650						
** 81-85					21650	2165	8	553-561	271	135
87		1000		1000						
90		15000		15000						
** 86-90					16000	1600	8	571-579	200	100
93.75	20700			20700						
94.75#			698000	698000						
95.75	20100			20100						
** 91-96					738800	73880	8	589-597	9235	4618
TOTALS:	2184150	388200	862000	3434350	3434350	343435				

- LOAD TO BE APPLIED IN VERTICAL DIRECTION ONLY.
& - MISCELLANEOUS LOADS INCLUDE 698000 LB WATER WEIGHT AT 94.75 FT. ELEVATION 100000 LB EQUIPMENT DOOR WEIGHT AT 30.25 FT. ELEVATION AND WELD PAD LIVE LOADS OF 24000, 20000 AND 20000 AT 56, 60 AND 65 FT. ELEVATIONS

REFWGT.WK1

Table 3-7

Oyster Creek Drywell Additional Weights - Post-Accident Condition

ELEVATION (feet)	DEAD WEIGHT (lbf)	PENETR. WEIGHT (lbf)	& MISC. LOADS (lbf)	TOTAL LOAD (lbf)	5 FOOT RANGE LOAD	LOAD PER 36 DEG. (lbf)	# OF ELEMENTS	NODES OF APPLICATION	LOAD PER FULL NODE (lbf)	LOAD PER HALF NODE (lbf)
15.56	50000			50000						
16		168100		168100						
20		11200		11200						
** 15-20					229300	22930	6	116-119	3822	1911
22#	556000			556000						
** 21-25#					556000	55600	8	161-169	6950	3475
26		11100		11100						
30	64100	51500		115600						
30.25	105000			105000						
** 26-30					231700	23170	8	179-187	2896	1448
31		16500		16500						
32		750		750						
33		15450		15450						
34		28050		28050						
35		1500		1500						
** 31-35					62250	6225	8	188-196	778	389
36		1550		1550						
40	41000	43350		84350						
** 36-40					85900	8590	8	197-205	1074	537
50#	1102000			1102000						
** 45-50#					1102000	110200	8	418-426	13775	6888
54		7850		7850						
** 51-55					7850	785	8	436-444	98	49
56	56400			56400						
60	95200	700		95900						
** 56-60					152300	15230	8	454-462	1904	952
65	52000			52000						
** 61-65					52000	5200	8	472-480	650	325
70		5750		5750						
** 66-70					5750	575	8	508-516	72	36
73		8850		8850						
** 71-75					8850	885	8	526-534	111	55
82.17	21650			21650						
** 81-85					21650	2165	8	553-561	271	135
87		1000		1000						
90		15000		15000						
** 86-90					16000	1600	8	571-579	200	100
93.75	20700			20700						
95.75	20100			20100						
** 91-96					40800	4080	8	589-597	510	255
TOTALS:	2184150	388200	0	2572350	2572350	257235				

- LOAD TO BE APPLIED IN VERTICAL DIRECTION ONLY.
& - NO MISCELLANEOUS LOADS FOR THIS CONDITION.

FLOODWGT.W:1

Table 3-8

Hydrostatic Pressures for Post-Accident, Flooded Condition

WATER DENSITY: 62.32 lb/ft3
0.03606 lb/in3

FLOODED ELEV: 74.5 ft
894 inches

ELEMENTS ABOVE NODES	ANGLE ABOVE EQUATOR (degrees)	ELEVATION (inch)	DEPTH (inch)	PRESSURE (psi)	ELEMENTS
27	-53.32	110.2	783.8	28.3	1-12
40	-51.97	116.2	777.8	28.1	13-24
53	-50.62	122.4	771.6	27.8	25-36
66	-49.27	128.8	765.2	27.6	37-48
79	-47.50	137.3	756.7	27.3	49-51, 61-66 ,55-57
92	-46.20	143.9	750.1	27.1	52-54, 138-141 ,58-60
102	-44.35	153.4	740.6	26.7	142-147, 240-242, 257-259
108	-41.89	166.6	727.4	26.2	148-151, 243, 256
112	-39.43	180.2	713.8	25.7	152-155, 244, 255
116	-36.93	194.6	699.4	25.2	156-159, 245, 254
120	-34.40	209.7	684.3	24.7	160-165, 246, 253
124	-31.87	225.2	668.8	24.1	166-173, 247, 252
130	-29.33	241.3	652.7	23.5	174-183, 248-251
138	-26.80	257.6	636.4	23.0	184-195
148	-24.27	274.4	619.6	22.3	196-207
161	-20.13	302.5	591.5	21.3	208-215
170	-14.38	342.7	551.3	19.9	216-223
179	-8.63	384.0	510.0	18.4	224-231
188	-2.88	425.9	468.1	16.9	232-239
197	2.88	468.1	425.9	15.4	430-437
400	8.63	510.0	384.0	13.8	438-445
409	14.38	551.3	342.7	12.4	446-453
418	20.13	591.5	302.5	10.9	454-461
427	25.50	627.8	266.2	9.6	462-469
436	30.50	660.2	233.8	8.4	470-477
445	35.50	690.9	203.1	7.3	478-485
454	40.50	719.8	174.2	6.3	486-493
463	45.50	746.6	147.4	5.3	494-501
472	50.50	771.1	122.9	4.4	502-509
481	54.86	790.5	103.5	3.7	510-517
490	-	805.6	88.4	3.2	518-525
499	-	820.7	73.3	2.6	526-533
508	-	835.7	58.3	2.1	534-541
517	-	850.8	43.2	1.6	542-549
526	-	885.3	8.7	0.3	550-557
-	-	187.3	706.7	25.5	340-399 (Ventline)

FLOODP.WK1

Table 3-9

Meridional Seismic Stresses at Four Sections

Section	Elevation (inches)	2-D Shell Model Node	Meridional Stresses Refueling (psi)	Meridional Stresses Post-Accident (psi)
A) Middle of Sandbed	119	32	1258	1288
B) 17.25° Below Equator	323	302	295	585
C) 5.75° Above Equator	489	461	214	616
D) Above Knuckle	1037	1037	216	808

Table 3-10

Application of Loads to Match Seismic Stresses - Refueling Case

	2-D SEISMIC STRESSES AT SECTION (psi)			
SECTION:	1	2	3	4
2-D NODE:	32	302	461	1037
COMPRESSIVE STRESSES FROM 2-D ANALYSIS — ELEV:	119.3"	322.5"	489.1"	912.3"
0.058" SEISMIC DEFLECTION:	788.67	155.54	103.46	85.31
HORIZ. PLUS VERTICAL SEISMIC INERTIA:	469.55	139.44	110.13	130.21
TOTAL SEISMIC COMPRESSIVE STRESSES:	1258.22	294.98	213.59	215.52

3-D INPUT LOAD SECTION	INPUT 3-D UNIT LOAD DESCRIPTION	3-D STRESSES AT SECTION (psi)			
	SECTION:	1	2	3	4
	3-D NODES:	53-65	170-178	400-408	526-534
	ELEV:	119.3"	322.5"	489.1"	912.3"
A	1000 lbs at nodes 563 through 569	85.43	37.94	34.94	55.23
B	500 lbs at 427&435, 1000 lbs at 428-434	89.88	39.92	36.76	0.00
C	500 lbs at 197&205, 1000 lbs at 198-204	97.64	43.37	0.00	0.00
D	500 lbs at 161&169, 1000 lbs at 162-168	89.85	0.00	0.00	0.00
	DESIRED COMPRESSIVE STRESSES (psi):	1258.22	294.98	213.59	215.52

3-D INPUT LOAD SECTION	LOAD TO BE APPLIED TO MATCH 2-D STRESSES	RESULTING STRESSES AT SECTION (psi)			
A	3902.2	333.37	148.05	136.34	215.52
B	2101.4	188.87	83.89	77.25	0.00
C	1453.6	141.93	63.04	0.00	0.00
D	6611.6	594.05	0.00	0.00	0.00
	SUM:	1258.22	294.98	213.59	215.52

:SEISUNFL.WK1

Table 3-11

Application of Loads to Match Seismic Stresses - Post-Accident Case

COMPRESSIVE STRESSES FROM 2-D ANALYSIS	2-D SEISMIC STRESSES AT SECTION (psi)			
SECTION:	1	2	3	4
2-D NODE:	32	302	461	1037
ELEV:	119.3"	322.5"	489.1"	912.3"
0.058" SEISMIC DEFLECTION:	788.67	155.54	103.46	85.31
HORIZ. PLUS VERTICAL SEISMIC INERTIA:	499.79	429.39	512.76	723.14
TOTAL SEISMIC COMPRESSIVE STRESSES:	1288.46	584.93	616.22	808.45

3-D INPUT LOAD SECTION	INPUT 3-D UNIT LOAD DESCRIPTION	3-D STRESSES AT SECTION (psi)			
	SECTION:	1	2	3	4
	3-D NODES:	53-65	170-178	400-408	526-534
	ELEV:	119.3"	322.5"	489.1"	912.3"
A	1000 lbs at nodes 563 through 569	85.43	37.94	34.94	55.23
B	500 lbs at 427&435, 1000 lbs at 428-434	89.88	39.92	36.76	0.00
C	500 lbs at 197&205, 1000 lbs at 198-204	97.64	43.37	0.00	0.00
D	500 lbs at 161&169, 1000 lbs at 162-168	89.85	0.00	0.00	0.00
	DESIRED COMPRESSIVE STRESSES (psi):	1288.46	584.93	616.22	808.45

3-D INPUT LOAD SECTION	LOAD TO BE APPLIED TO MATCH 2-D STRESSES	RESULTING STRESSES AT SECTION (psi)			
A	14637.9	1250.51	555.36	511.45	808.45
B	2850.2	256.17	113.78	104.77	0.00
C	-1941.7	-189.58	-84.21	0.00	0.00
D	-318.8	-28.64	0.00	0.00	0.00
	SUM:	1288.46	584.93	616.22	808.45

SEISFL.WK1

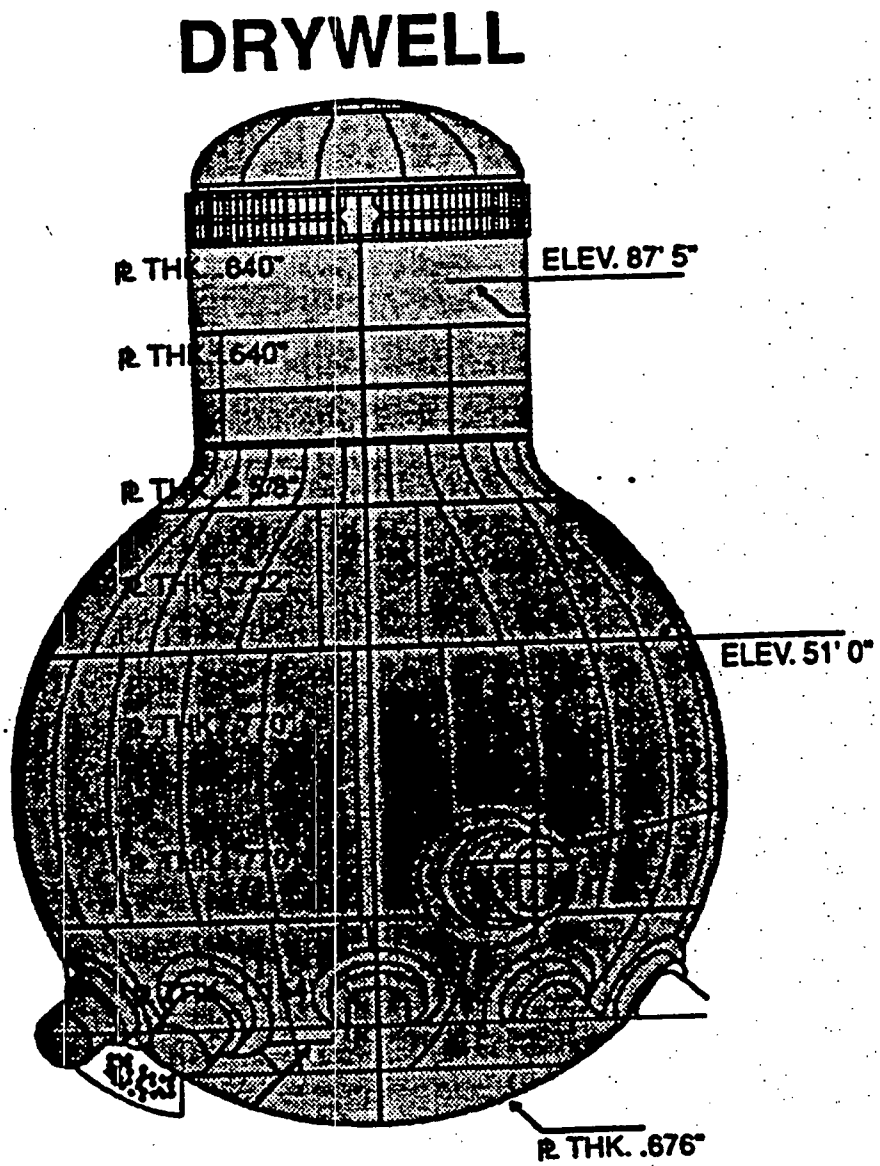

Figure 3-1. Oyster Creek Drywell Geometry

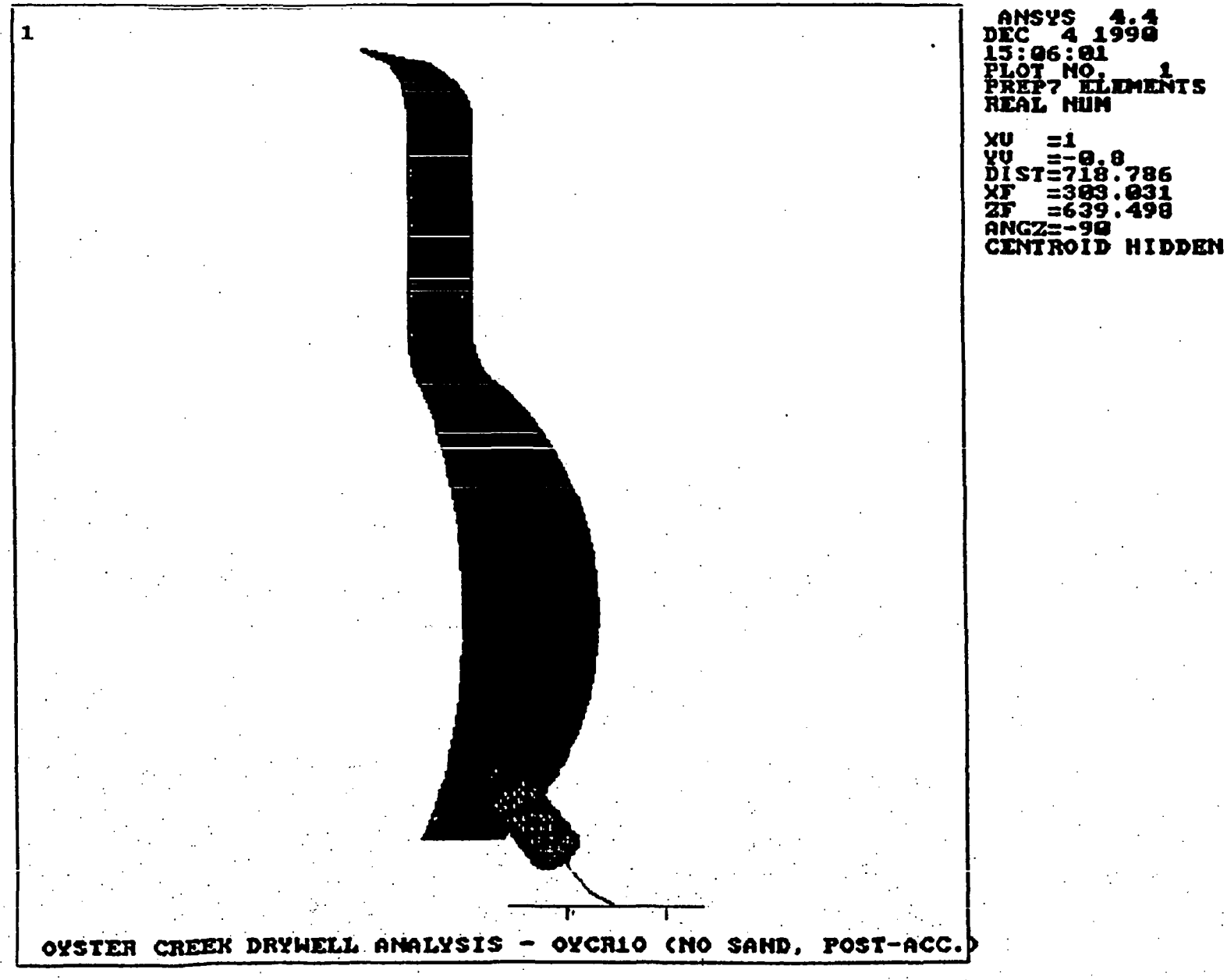

Figure 3-2. Oyster Creek Drywell 3-D Finite Element Model

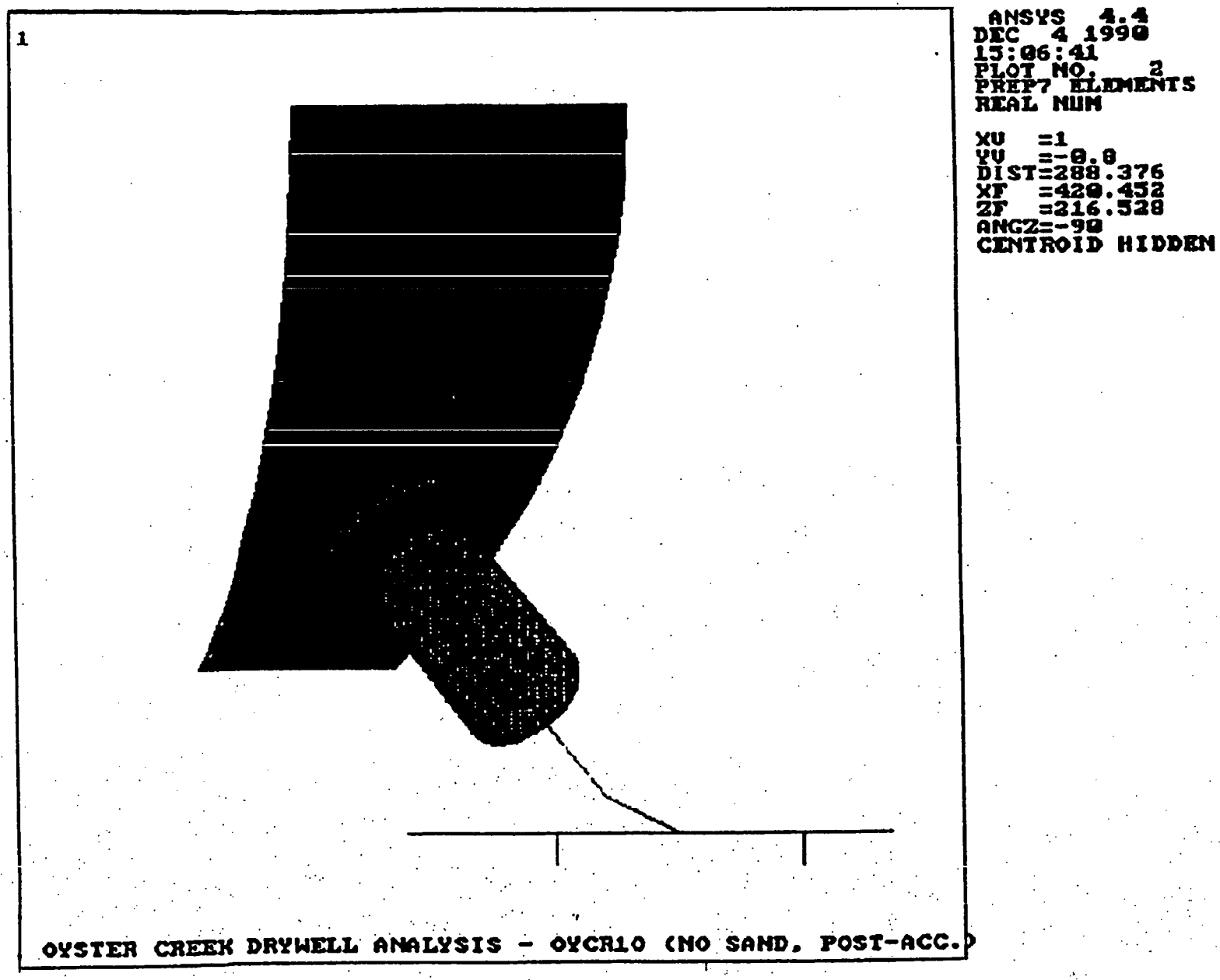

Figure 3-3. Closeup of Lower Drywell Section of FEM (Outside View)

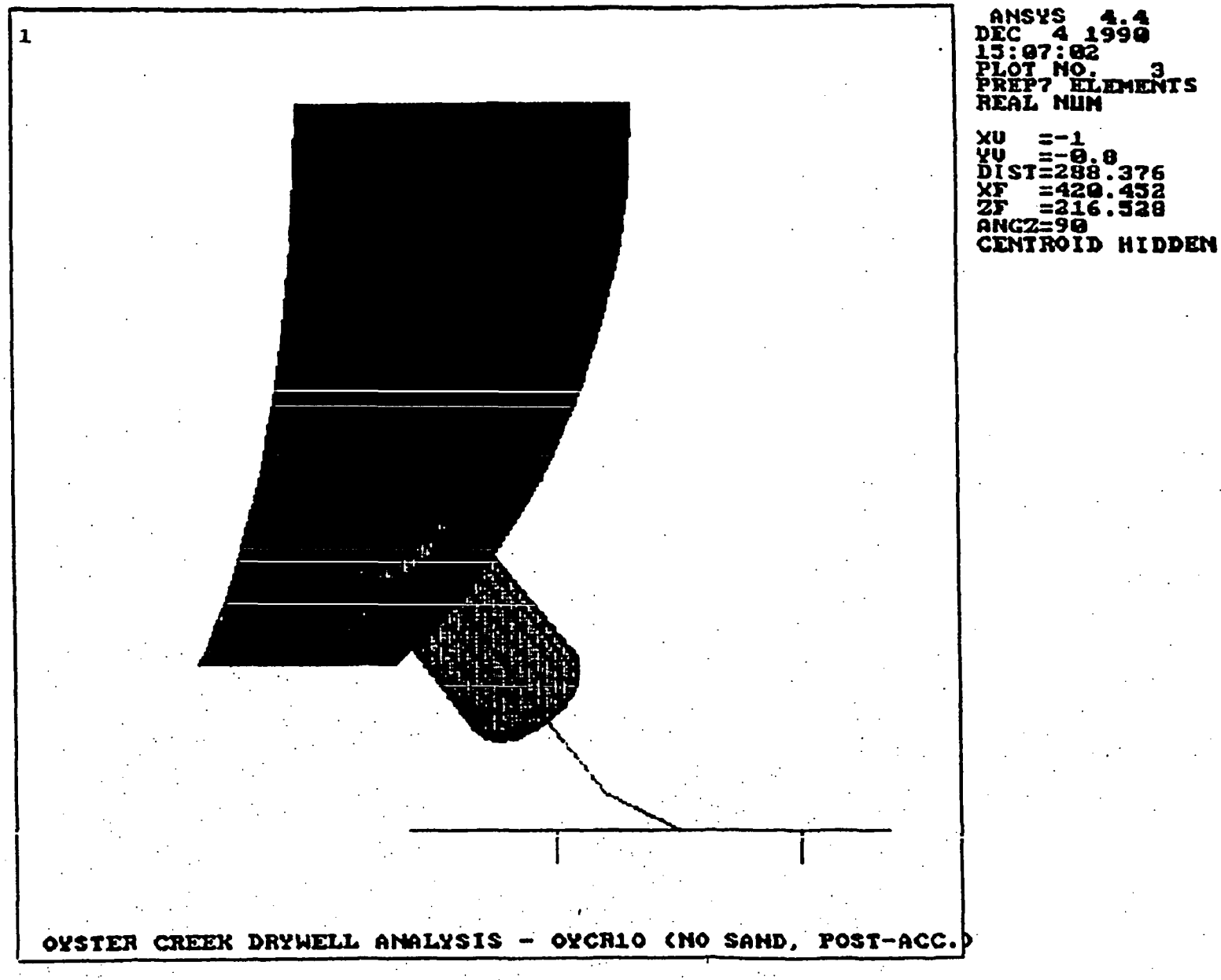

Figure 3-4. Closeup of Lower Drywell Section of FEM (Inside View)

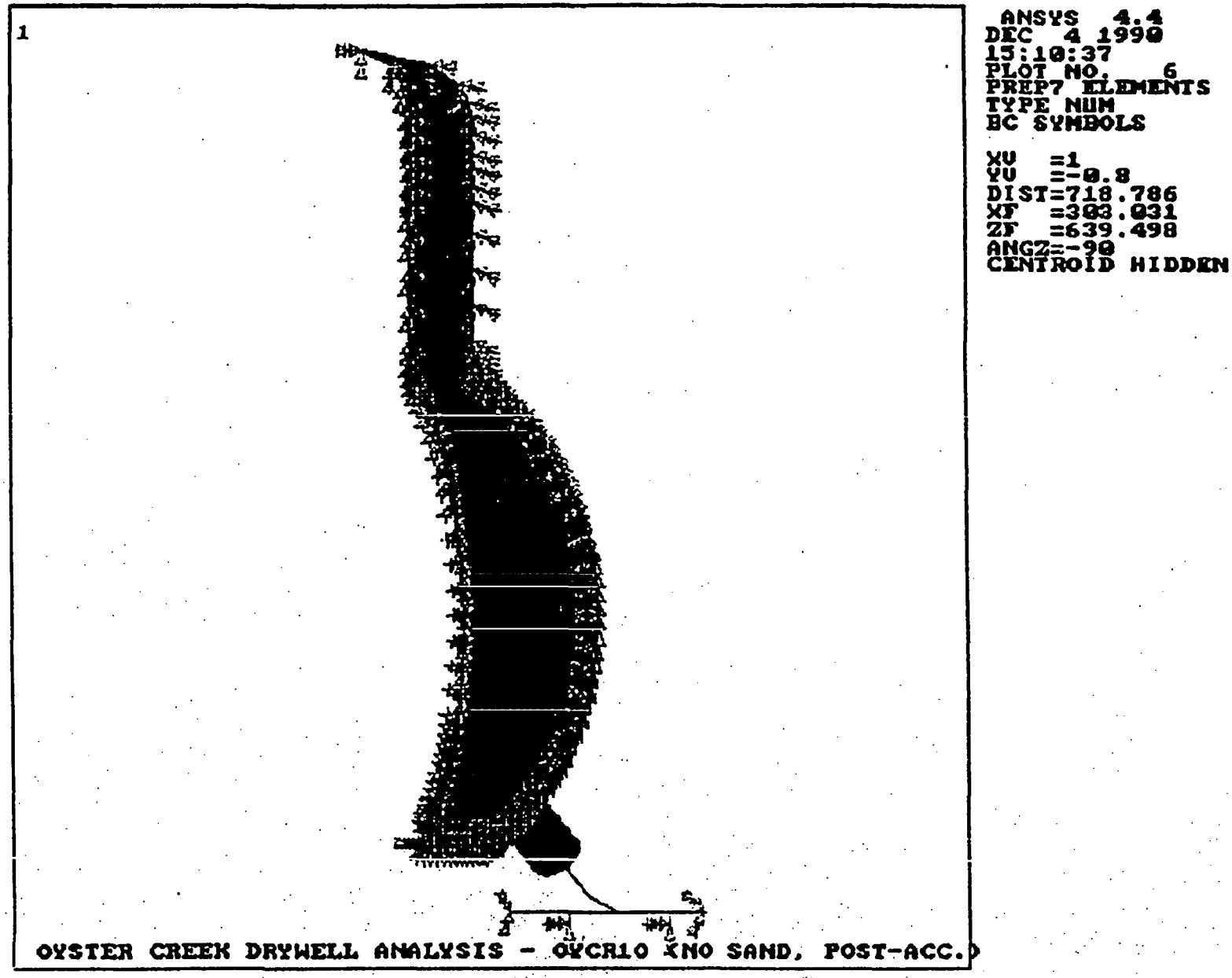

Figure 3-5. Boundary Conditions of Finite Element Model

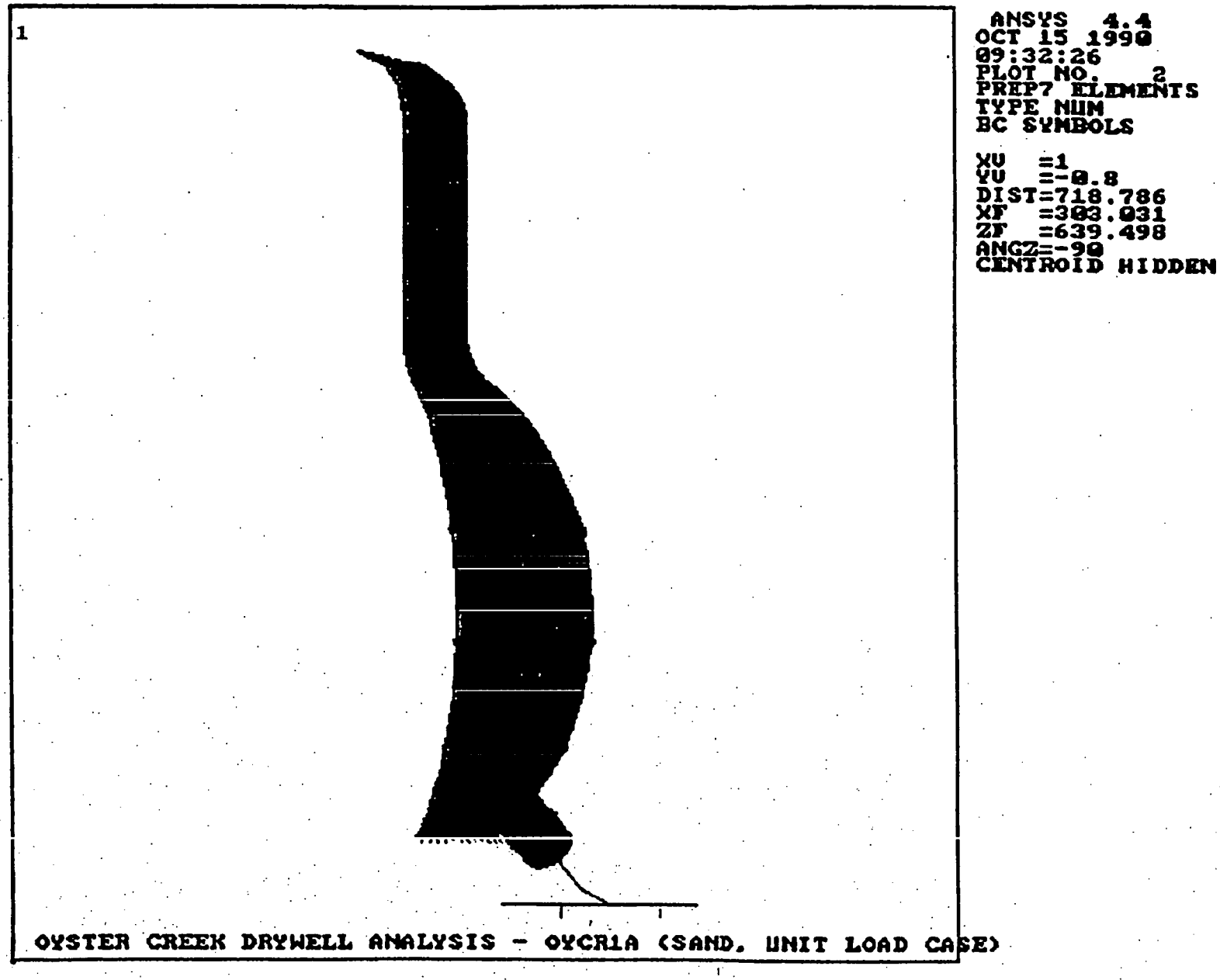

Figure 3-6. Application of Loading to Simulate Seismic Bending

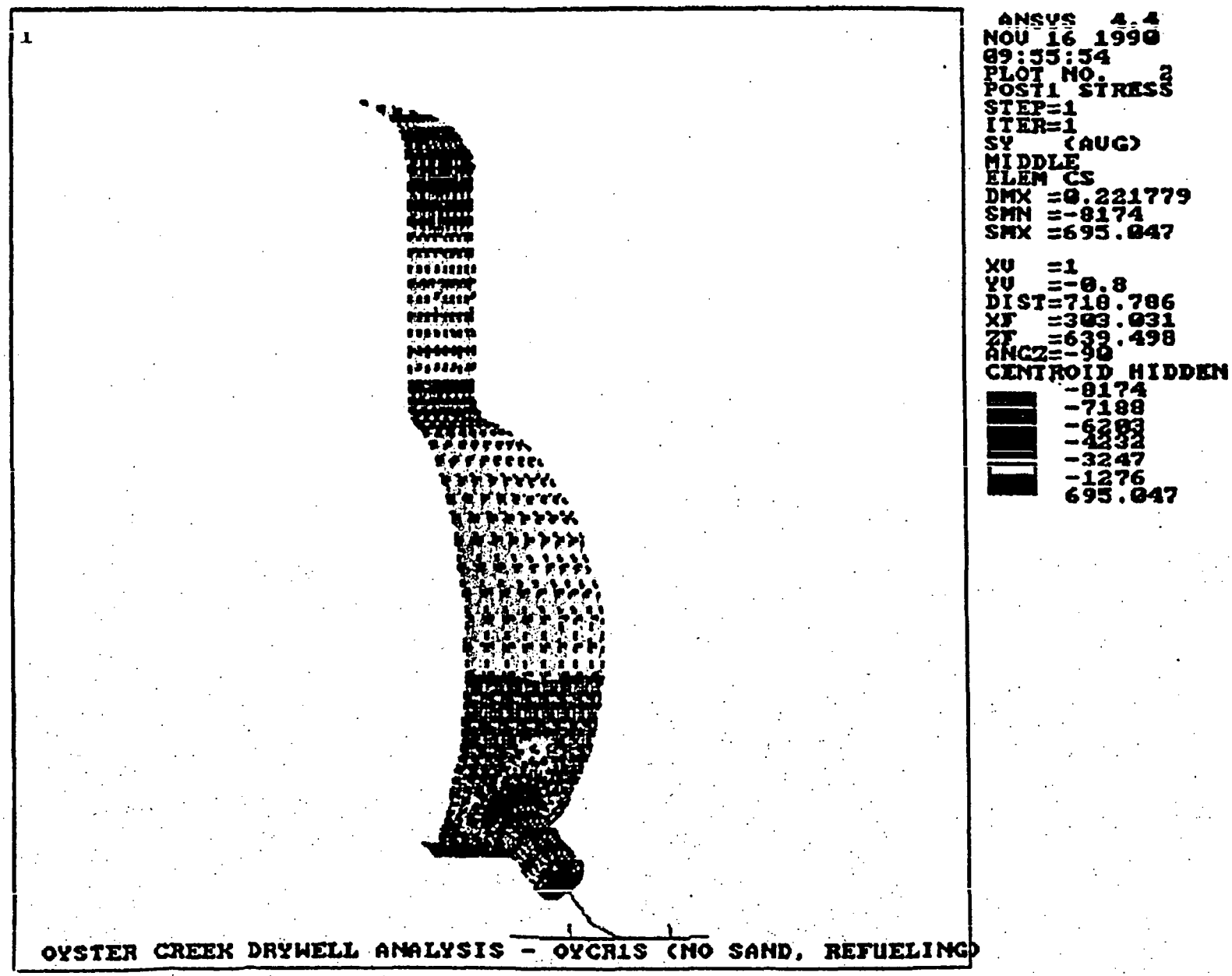

Figure 3-7. Meridional Stresses - Refueling Case

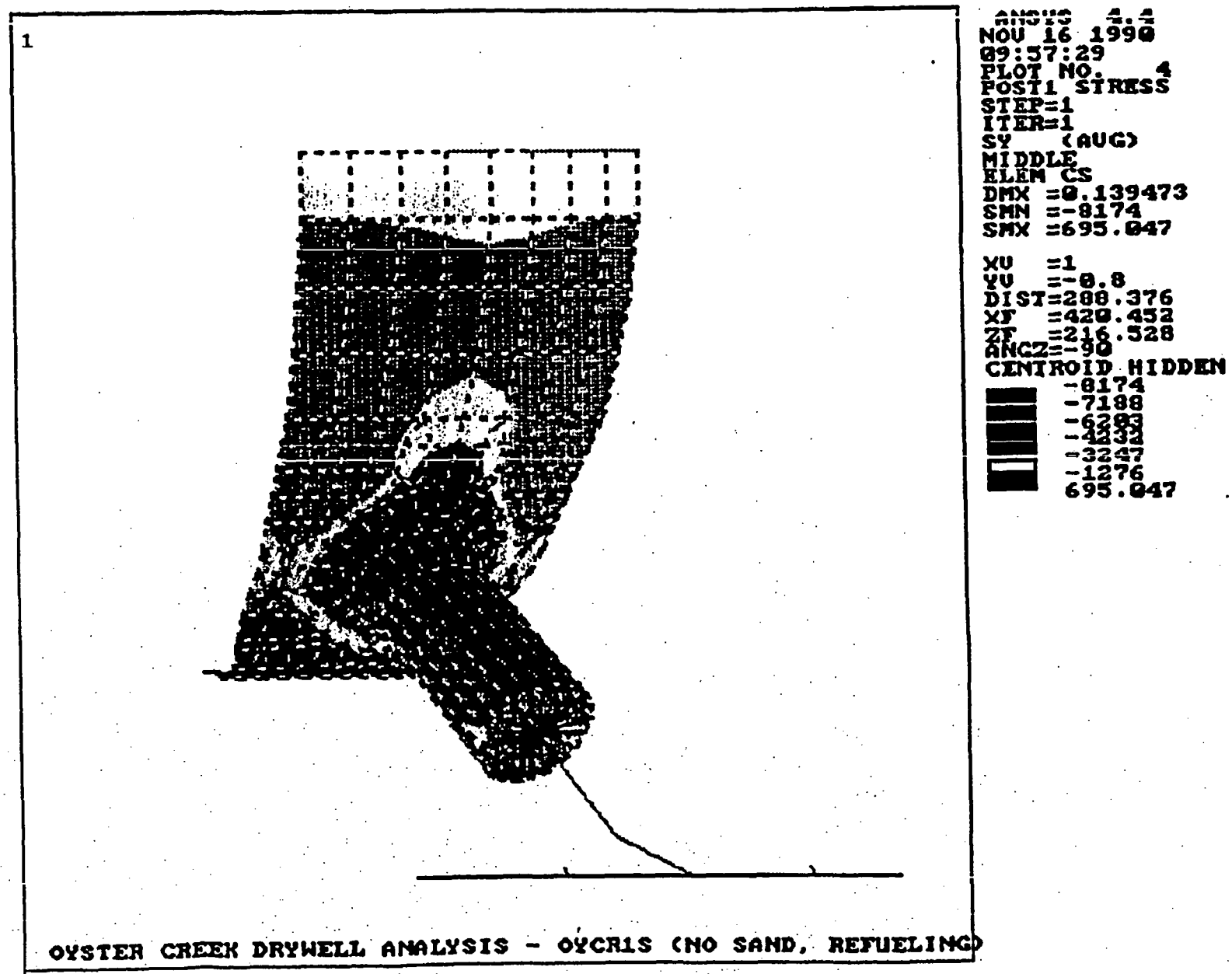

Figure 3-8 Lower Drywell Meridional Stresses - Refueling Case

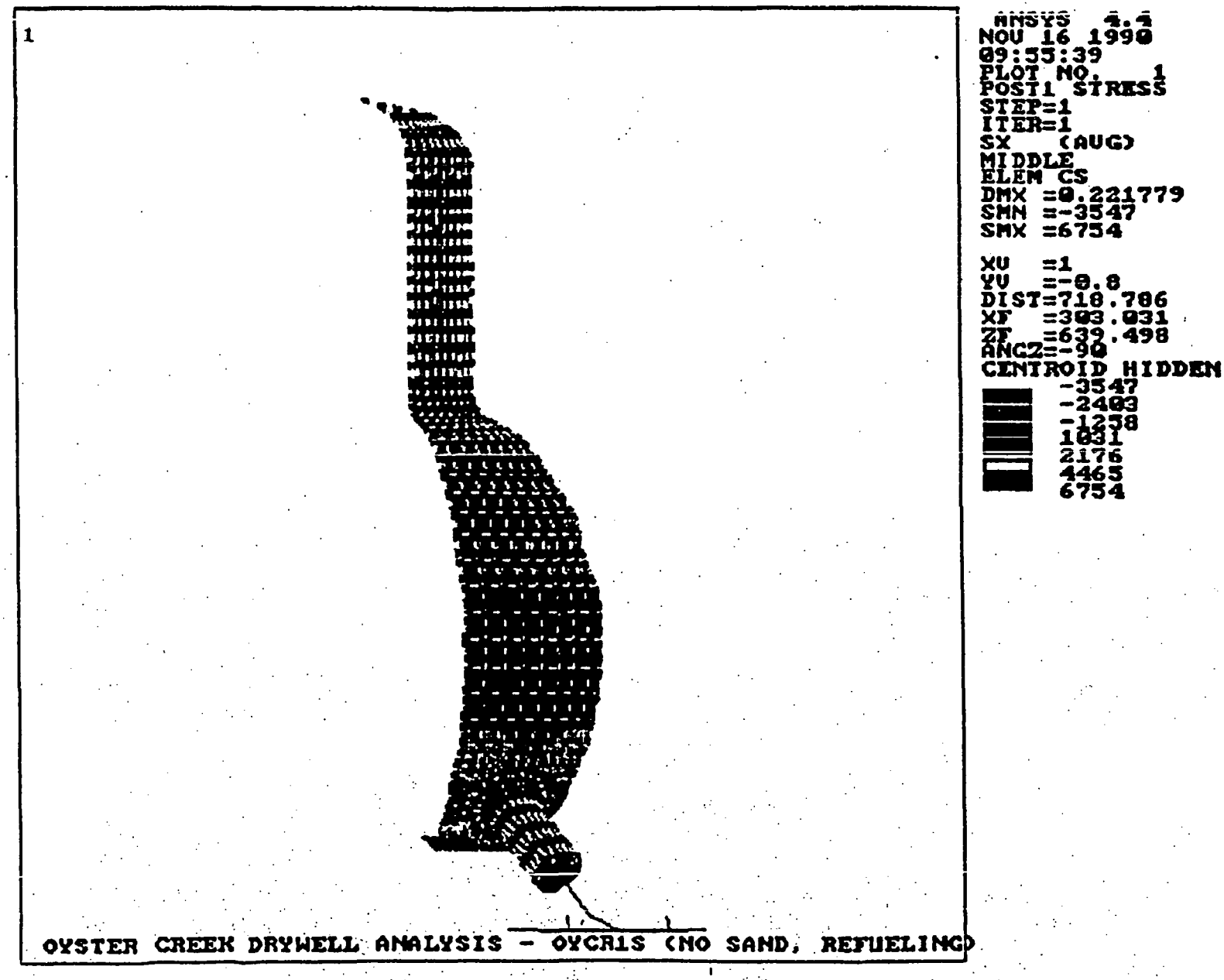

Figure 3-9. Circumferential Stresses - Refueling Case

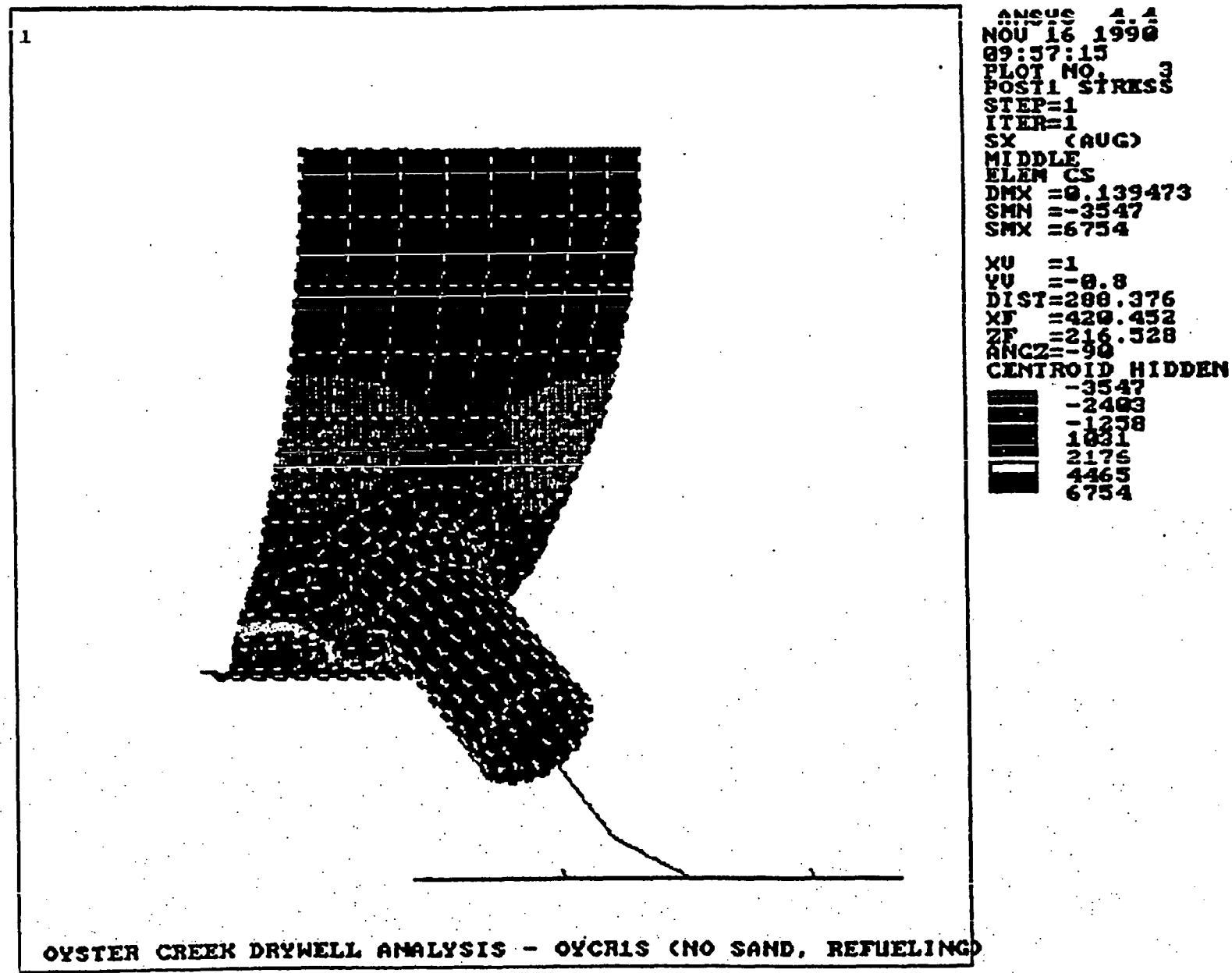

Figure 3-10. Lower Drywell Circumferential Stresses - Refueling Case

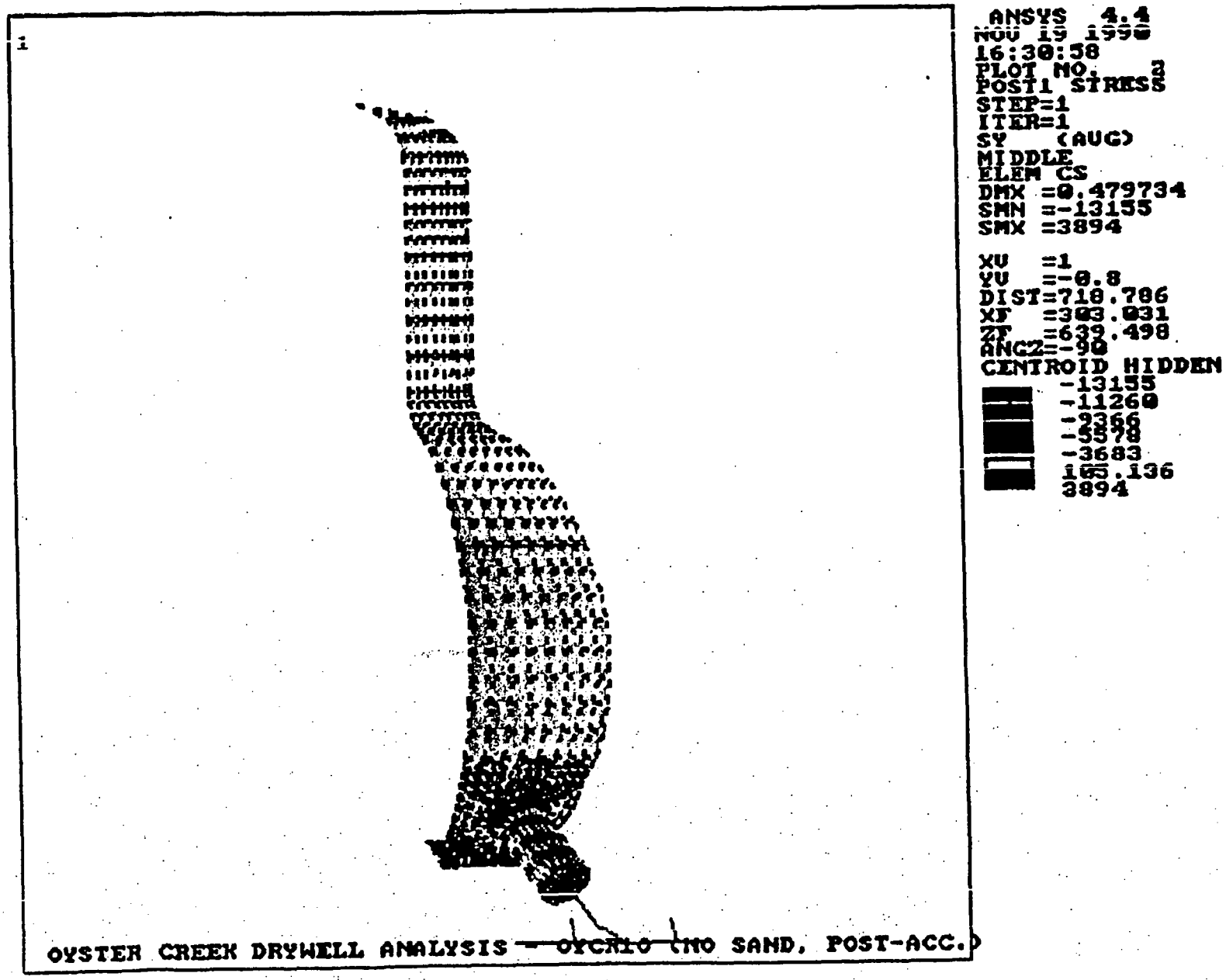

Figure 3-11 Meridional Stresses - Post-Accident Case

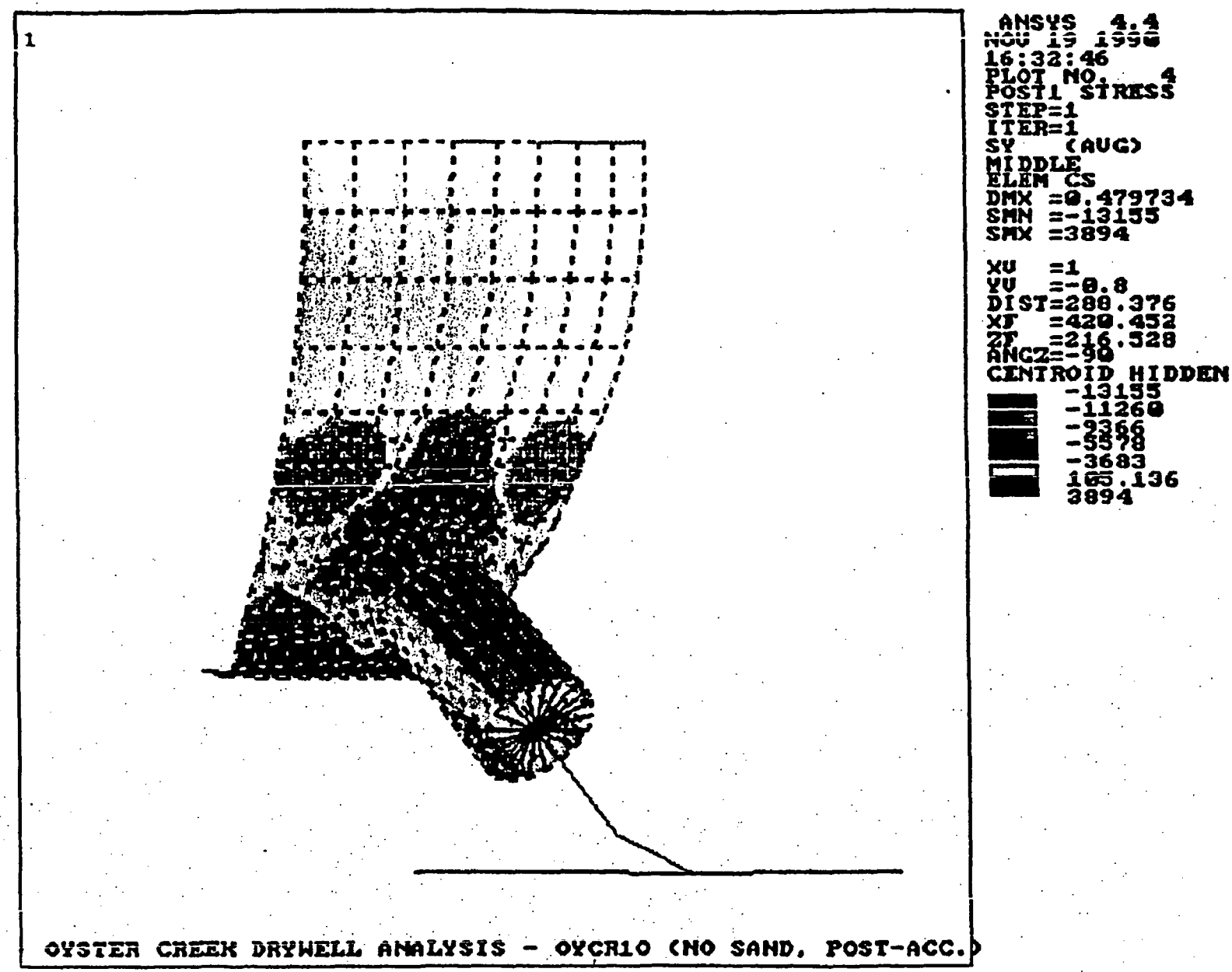

Figure 3-12. Lower Drywell Meridional Stresses - Post-Accident Case

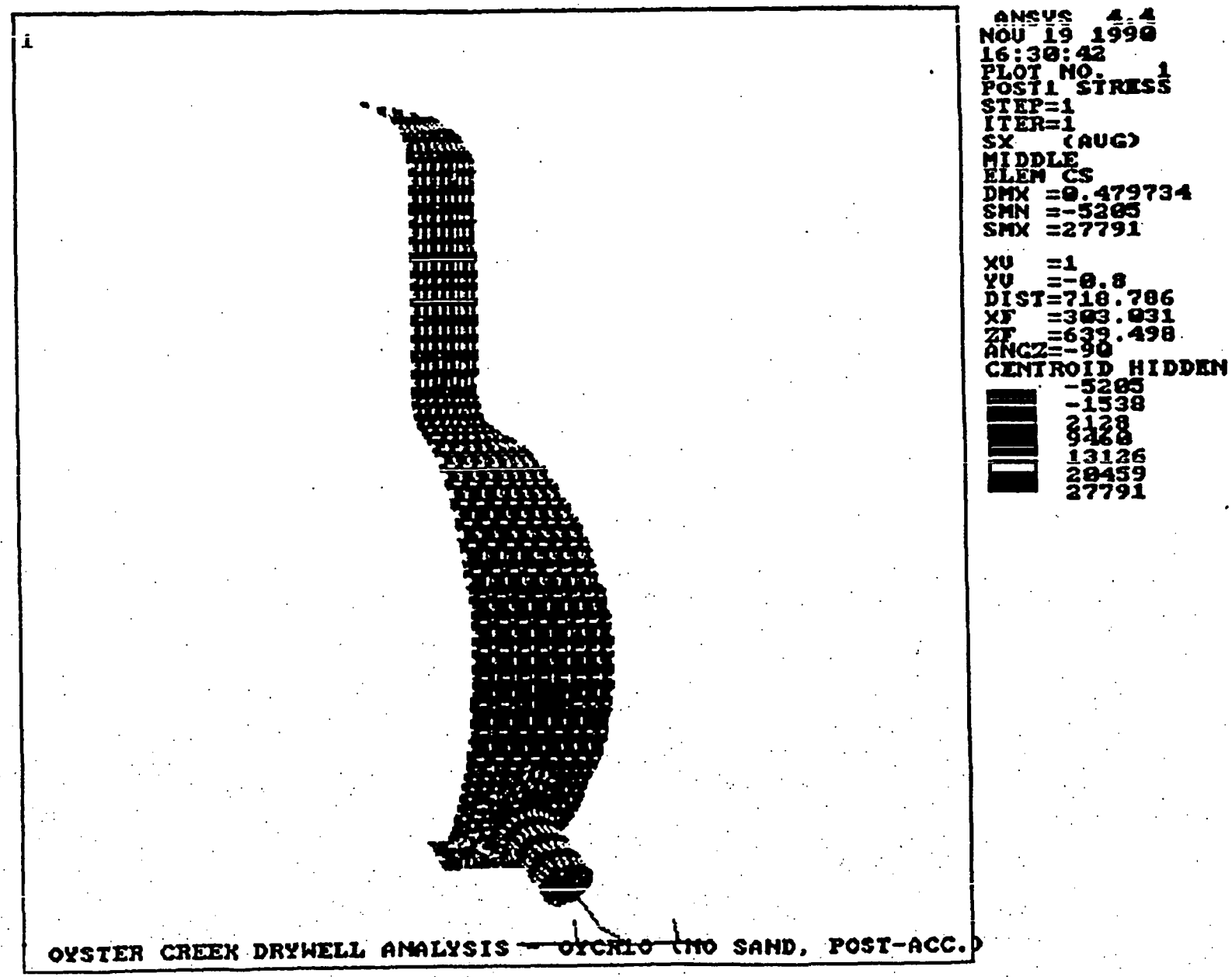

Figure 3-13. Circumferential Stresses - Post-Accident Case

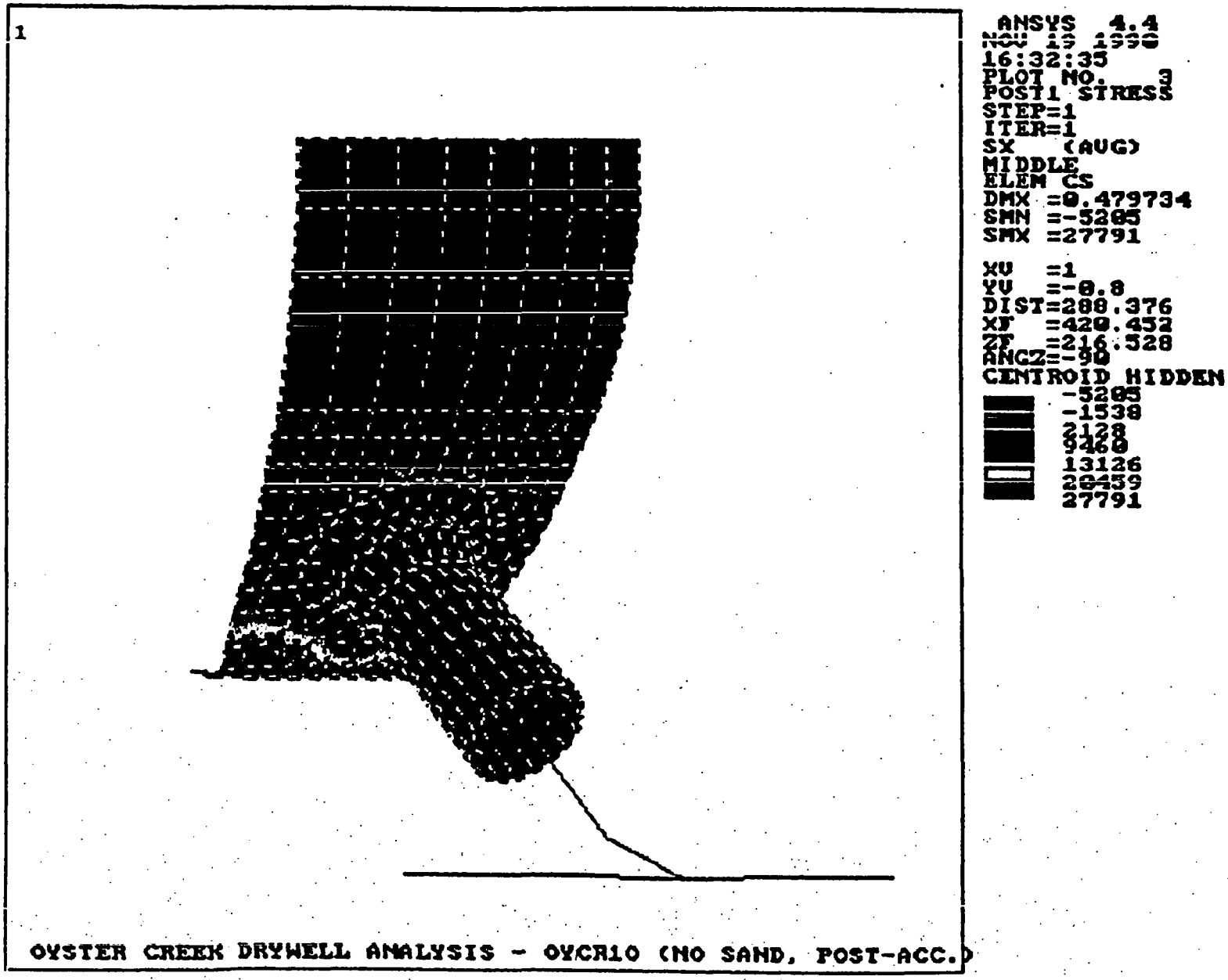

Figure 3-14. Lower Drywell Circumferential Stresses - Post-Accident Case

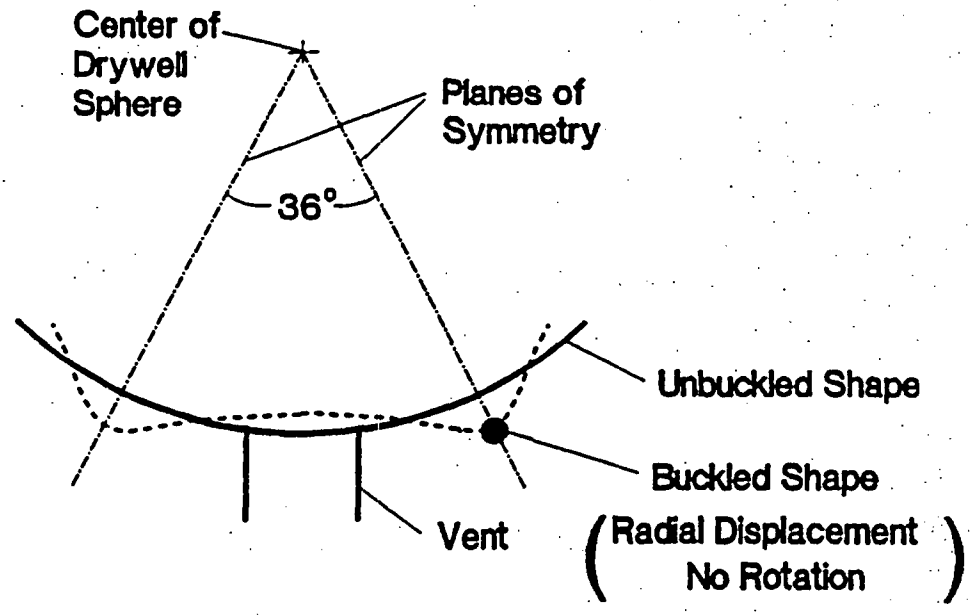

Symmetric Buckling of Drywell

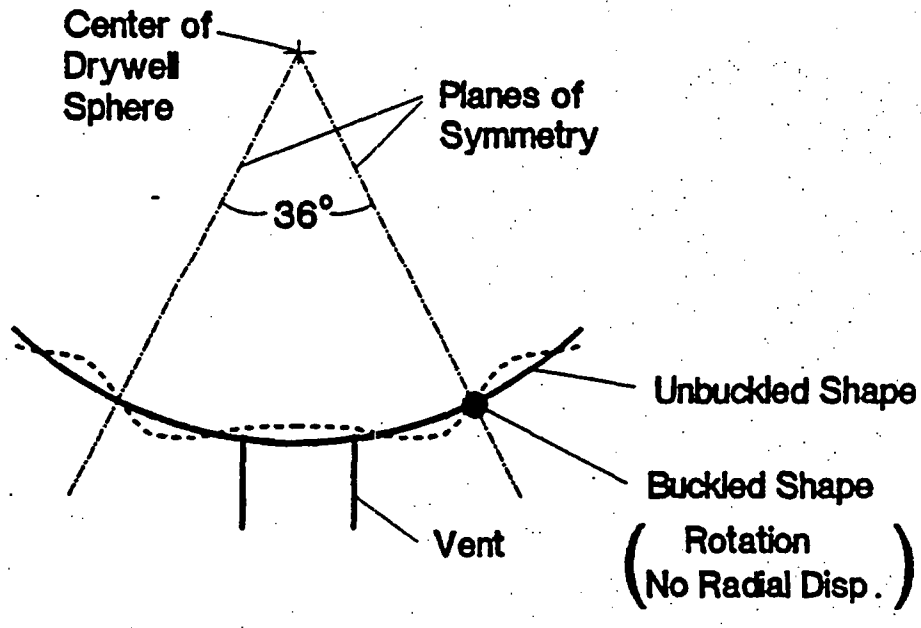

Asymmetric Buckling of Drywell

SYM.DRW

Figure 3-15. Symmetric and Asymmetric Buckling Modes

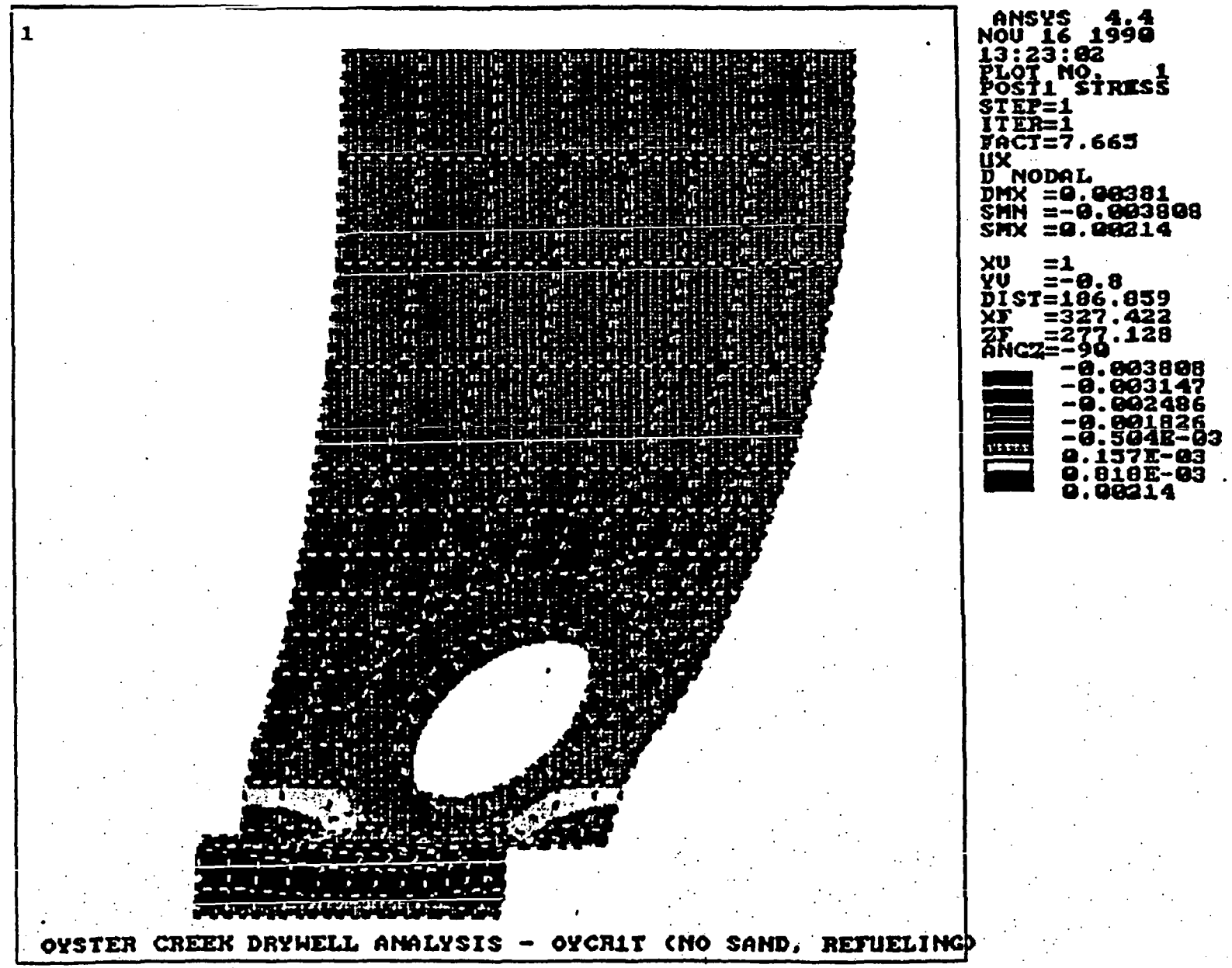

Figure 3-16. Symmetric Buckling Mode Shape - Refueling Case

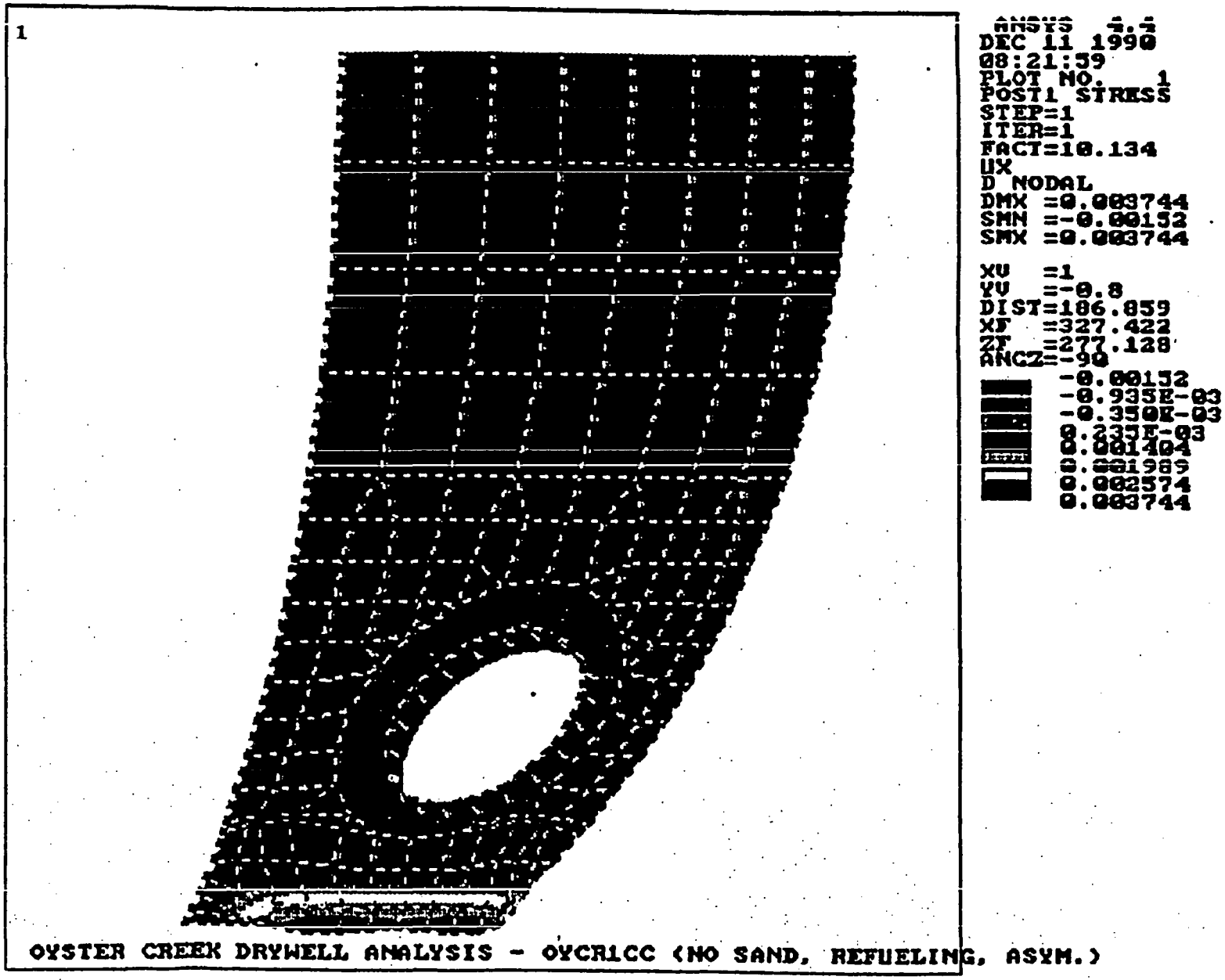

Figure 3-17. Asymmetric Buckling Mode Shape - Refueling Case

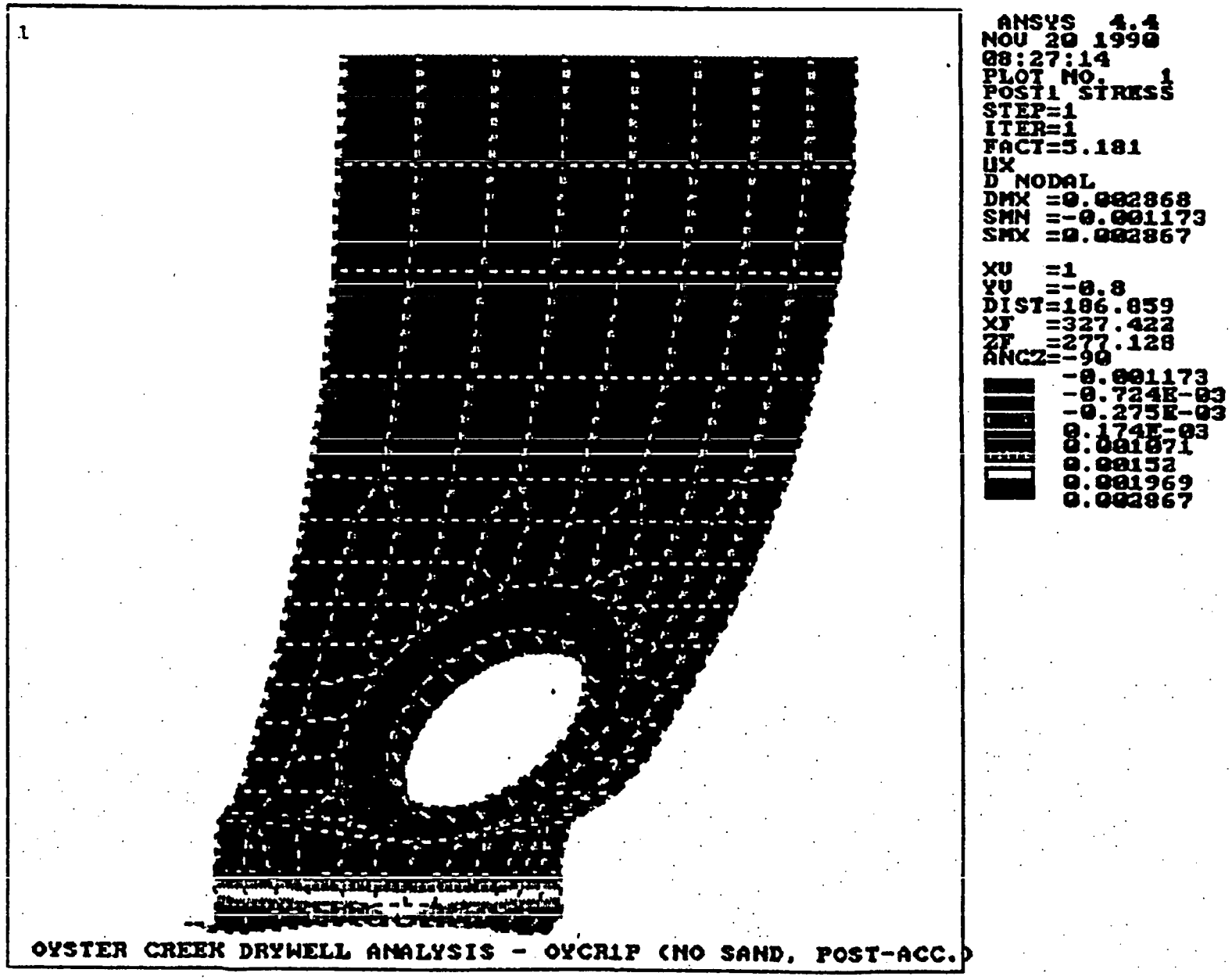

Figure 3-18. Buckling Mode Shape - Post Accident Case

4. ALLOWABLE BUCKLING STRESS EVALUATION

Applying the methodology described in Section 2 for the modification of the theoretical elastic buckling stress, the allowable compressive stresses are now calculated. Tables 4-1 and 4-2 summarize the calculation of the allowable buckling stresses for the Refueling and Post-Accident conditions, respectively. The modified capacity reduction factors are first calculated as described in sections 2.2 and 2.3. After reducing the theoretical instability stress by this reduction factor, the plasticity reduction factor is calculated and applied. The resulting inelastic buckling stresses are then divided by the factor of safety of 2.0 for the Refueling case and 1.67 for the Post-Accident case to obtain the final allowable compressive stresses.

The allowable compressive stress for the Refueling case is 10.65 ksi. Since the applied compressive stress is 7.58 ksi, there is a 41% margin. The allowable compressive stress for the Post-Accident, flooded case is 13.77 ksi. This results in a margin of 15% for the applied compressive stress of 11.96 ksi.

Table 4-1

Calculation of Allowable Buckling Stresses - Refueling Case

Parameter	Value
Theoretical Elastic Instability Stress, σ_{ie} (ksi)	58.10
Capacity Reduction Factor, α_i	0.207
Circumferential Stress, σ_c (ksi)	4.49
Equivalent Pressure, p (psi)	15.74
"X" Parameter	0.0865
ΔC	0.0716
Modified Capacity Reduction Factor, $\alpha_{i,mod}$	0.325
Elastic Buckling Stress, $\sigma_e = \alpha_{i,mod}\,\sigma_{ie}$ (ksi)	18.88
Proportional Limit Ratio, $\Delta = \sigma_e/\sigma_y$	0.497
Plasticity Reduction Factor, η_i	1.00
Inelastic Buckling Stress, $\sigma_i = \eta_i\sigma_e$ (ksi)	18.88
Factor of Safety, FS	2.0
Allowable Compressive Stress, $\sigma_{all} = \sigma_i/FS$ (ksi)	9.44
Applied Compressive Meridional Stress, σ_m (ksi)	7.58
Margin = $[(\sigma_{all}/\sigma_m) - 1] \times 100\%$	24.5%

Table 4-2

Calculation of Allowable Buckling Stresses - Post-Accident Case

Parameter	Value
Theoretical Elastic Instability Stress, σ_{ie} (ksi)	61.95
Capacity Reduction Factor, α_i	0.207
Circumferential Stress, σ_c (ksi)	20.08
Equivalent Pressure, p (psi)	70.38
"X" Parameter	0.387
ΔC	0.182
Modified Capacity Reduction Factor, $\alpha_{i,mod}$	0.508
Elastic Buckling Stress, $\sigma_e = \alpha_{i,mod}\ \sigma_{ie}$ (ksi)	31.47
Proportional Limit Ratio, $\Delta = \sigma_e/\sigma_y$	0.828
Plasticity Reduction Factor, η_i	0.724
Inelastic Buckling Stress, $\sigma_i = \eta_i\sigma_e$ (ksi)	22.78
Factor of Safety, FS	1.67
Allowable Compressive Stress, $\sigma_{all} = \sigma_i/FS$ (ksi)	13.64
Applied Compressive Meridional Stress, σ_m (ksi)	11.96
Margin = $[(\sigma_{all}/\sigma_m) - 1] \times 100\%$	14%

5. SUMMARY AND CONCLUSIONS

The results of this buckling analysis for the refueling and post-accident load combinations are summarized in Table 5-1. The applied and allowable compressive meridional stresses shown in Table 5-1 are for the sandbed region which is the most limiting region in terms of buckling. This analysis demonstrates that the Oyster Creek drywell has adequate margin against buckling with no sand support for an assumed sandbed shell thickness of 0.736 inch. This thickness is the 95% confidence projected thickness for the 14R outage.

Table 5-1

Buckling Analysis Summary

	Load Combination	
	Refueling	Post-Accident
Service Condition	Design	Level C
Factor of Safety Applied	2.00	1.67
Applied Compressive Meridional Stress (ksi)	7.58	11.96
Allowable Compressive Meridional Stress (ksi)	9.44	13.64
Buckling Margin	24.5%	14.0%